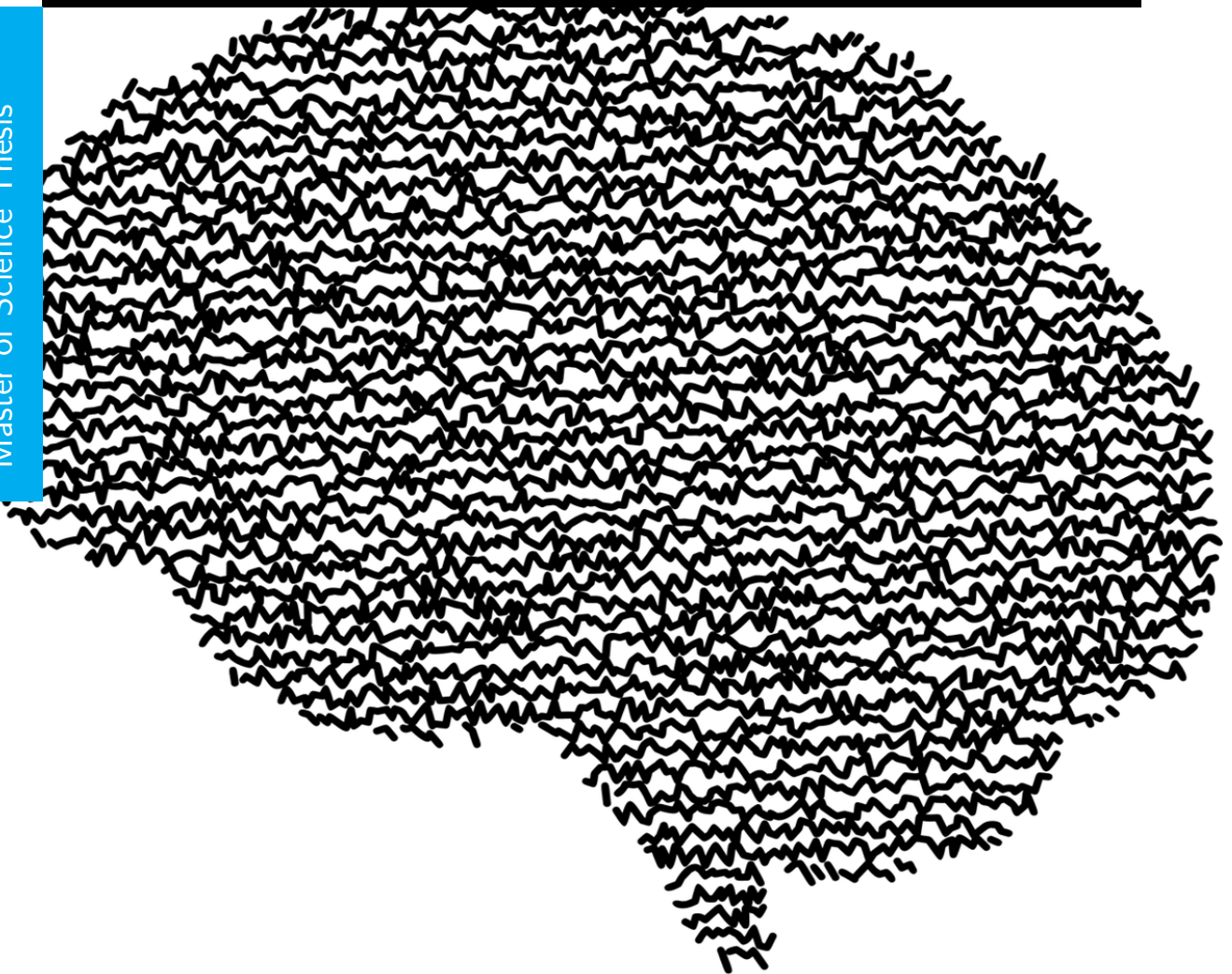


Assessing meditation through electroencephalographic data: a dynamical systems approach

F. van Engen

Master of Science Thesis



Assessing meditation through electroencephalographic data: a dynamical systems approach

MASTER OF SCIENCE THESIS

For the degree of Master of Science in Systems and Control at Delft
University of Technology

F. van Engen

December 15, 2022

Faculty of Mechanical, Maritime and Materials Engineering (3mE) · Delft University of
Technology

TNO innovation
for life

The work in this literature survey was supported by TNO (Nederlandse organisatie voor toegepast-natuurwetenschappelijk onderzoek). Their cooperation is hereby gratefully acknowledged.

 **TU Delft** Delft
University of
Technology

DCSC

Copyright © Delft Center for Systems and Control (DCSC)
All rights reserved.

DELFT UNIVERSITY OF TECHNOLOGY
DEPARTMENT OF
DELFT CENTER FOR SYSTEMS AND CONTROL (DCSC)

The undersigned hereby certify that they have read and recommend to the Faculty of
Mechanical, Maritime and Materials Engineering (3mE) for acceptance a thesis
entitled

ASSESSING MEDITATION THROUGH ELECTROENCEPHALOGRAPHIC DATA: A
DYNAMICAL SYSTEMS APPROACH

by

F. VAN ENGEN

in partial fulfillment of the requirements for the degree of
MASTER OF SCIENCE SYSTEMS AND CONTROL

Dated: December 15, 2022

Supervisor(s):

dr. ing. R. van de Plas

dr. S.D.G.M. Pequito

dr. A. Brouwer

Reader(s):

dr. ing. Y. Vardar

Abstract

Meditation is a contemplative practice that is believed to entail attentional and emotional regulation. One of the biggest challenges in developing personalized, accessible healthcare options with meditation is finding understandable features that signify whether someone is meditating. Specifically, there is no consensus on a feature resulting from the *electroencephalogram* (EEG) in the current body of literature on meditation.

In this thesis, I propose a dynamic systems analysis on EEG data to obtain a dynamic feature capable of distinguishing meditation from an eyes-closed resting baseline. I gathered the EEG data at TNO (Dutch Organisation for Applied Scientific Research) from twenty-two participants during a sixteen-minute loving-kindness meditation and two two-minute baselines. The proposed methodology characterizes temporal and spatial characteristics of the EEG simultaneously by approximating the EEG dynamics with a linear model on short time windows. I assess changes among three features: the frequency and magnitude of the oscillatory dynamics and the corresponding active electrodes.

The analysis can identify changes in EEG dynamics for each individual. Across all participants, regions associated with vision and language processing were active throughout the experiment. Notably, attention-related regions were more involved during meditation than rest. Moreover, the results show a shift in active regions throughout the meditation and the baselines for several participants.

Moreover, the thesis investigates the sensitivity of the analytical approach to changes in the electrode subset used for the analysis. For each participant, I constructed a subset of electrodes that were most involved in the changing EEG dynamics. The personalized subset was most sensitive to changes between meditation and rest, compared to other subsets based on commercial wearable EEG headsets. Finally, I compare the findings of the dynamic systems approach to a conventional analytical approach, and the participants' emotional ratings inquired in subjective questionnaires. Unfortunately, from the current data, there appears to be no relationship between the proposed features and the conventional measures or the subjective questionnaires.

Table of Contents

| | |
|--|-----------|
| Acknowledgements | v |
| 1 Introduction | 1 |
| 2 Preliminaries | 5 |
| 2-1 Neural basis of the EEG | 5 |
| 2-2 Spectral bandwidth analysis | 7 |
| 2-3 Eigendecomposition and stability analysis | 10 |
| 3 Methodology | 13 |
| 3-1 Dynamic systems analysis | 13 |
| 3-2 Experiment protocol | 14 |
| 3-3 Data processing steps | 16 |
| 3-4 Evaluation metrics | 16 |
| 4 Results | 19 |
| 4-1 Problem definition | 19 |
| 4-2 Assessing stationarity of the residuals for different window sizes | 19 |
| 4-3 Assessing the dynamic features | 20 |
| 4-3-1 Eigenvalues: magnitude and frequency | 20 |
| 4-3-2 Eigenvectors | 26 |
| 4-4 Dynamic system analysis using a subset of the sensors | 30 |
| 4-5 Alpha power analysis | 32 |
| 4-6 SAM questionnaire | 33 |
| 5 Conclusions & discussion | 35 |

| | |
|--|-----------|
| A Eigenvalue-eigenvector decomposition | 37 |
| A-1 Eigenvalue distribution test results | 37 |
| A-2 Eigenvectors | 43 |
| B Subsets of electrodes | 55 |
| B-1 Personalized subset | 55 |
| B-2 Wearable EEG subsets | 57 |
| Bibliography | 61 |
| Glossary | 65 |
| List of Acronyms | 65 |

Acknowledgements

I want to thank my daily supervisor Sérgio Pequito for his advice and guidance while writing this thesis. Our meetings helped me maintain structure and focus throughout the past months. In addition, I would like to thank Anne-Marie Brouwer and her team at TNO (Nederlandse Organisatie voor Toegepast Natuurwetenschappelijk Onderzoek; English: Dutch Organisation for Applied Scientific Research) for the opportunity to gain valuable experience in designing and conducting an experiment with participants. Finally, a word of thanks to Raf van de Plas for being my thesis advisor and supervisor and Yasemin Vardar for being part of my graduate committee.

Delft, University of Technology
December 15, 2022

F. van Engen

Chapter 1

Introduction

Meditation is a contemplative practice that involves monitoring and regulating attention and emotion [1]. Meditation originates from religious and philosophical systems, such as Buddhism and Christianity [2]. Over the past two decades, there has been considerable interest in the neural basis of meditative practices [3]. An increasing body of research suggests that meditation is associated with improved mental health by reducing feelings of anxiety and depression and helping patients deal with chronic pain or illness [4, 5]. Increased evidence and acceptance have led to the secularization of meditation and increased accessibility through the development of meditation apps, instruction videos, and online courses. Despite the popularity of meditation, it is still unknown what factors make meditation effective.

One of the biggest challenges in assessing effective meditation is finding a feature that signifies whether someone is meditating. Studies going back to the 1970s have used the *electroencephalogram* (EEG) to quantify changes in neural activity [6]. EEG is a non-invasive neuroscientific measure that records voltage fluctuations over time with electrodes on different locations on the scalp [7]. The potential differences relative to a reference provide an objective method to judge what conditions affect neural activity during meditation. Thus, the EEG can quantify changes in neural activity.

Some commercial devices claim to monitor meditation with only a few EEG sensors built into a headset. Figure 1-1 shows one example, the Muse headset [8]. The device provides the user with real-time feedback through auditory stimuli and develops a personalized meditation schedule on an app on the user's phone. Wearable devices like Muse are more accessible than professional EEG systems and easier to use. In addition, the app provides an understandable interface that could help individuals identify what factors increase the effectiveness of their meditation and thus contribute to their mental health. However, it is unknown how the device assesses the efficacy of a particular meditation session.

A common approach to characterize EEG signals is with *spectral bandwidth analysis*. Spectral bandwidth analysis expresses the power of one signal contributed by different frequencies. Section 2-2 explains spectral bandwidth analysis in more detail. Studies quantify changes between states with the difference in the average power contributed by frequencies in a

particular bandwidth. For example, several studies propose that the power of the EEG signal increases during meditation compared to rest in the frequency range 8 to 12 Hz, referred to as the *alpha* bandwidth [6, 9, 10, 11]. Generally, increased power in the alpha bandwidth is associated with a relaxed state. However, other research reports contradicting results, such as a decrease in alpha power, an increase in the *theta* bandwidth power, 4 to 8 Hz, or no systematic change during meditation [6, 9].

Spectral bandwidth analysis considers the signal of each EEG electrode separately. Due to varying results per electrode, studies usually compute the average power per bandwidth of particular regions or across all electrodes to examine a participant's state. A few studies looked at the electrode-specific effects of meditation. Most notably, Dunn *et al.* [12] found that the alpha power in parietal electrodes was higher during mindfulness meditation compared to a concentration exercise and rest. Figure 1-2 shows the location of the parietal lobe in the brain. While some studies corroborate that meditation increases parietal alpha power, other studies find that alpha power increases in the occipital region or reduces in the parietal or occipital region [11]. Consequently, there seems to be no consensus on a feature that distinguishes meditation from rest resulting from spectral analysis.

Other neuroimaging methods can identify active brain areas during meditation, such as *functional magnetic resonance imaging* (fMRI) and *positron emission tomography* (PET). fMRI and PET scans generally have a better spatial resolution than EEG, meaning they can identify areas of interest more precisely. In a meta-analysis of 78 functional neuroimaging studies, Fox *et al.* [14] found that several areas were activated consistently across different types of meditation. Moreover, they identified areas specific to the most common meditation types. For example, during loving-kindness meditation, areas linked to sensory processing and bodily awareness (somatosensory cortices and insula) were active. However, fMRI and PET scans are not as widely accessible as EEG and are limited in temporal resolution. Generally, studies can consider only one or a few scans during meditation per participant.



Figure 1-1: The Muse headband [8].

Dynamic systems analysis is a method that assesses both spatial and temporal characteristics of neural activity by locally approximating the dynamics as a linear system. Two studies applied dynamic systems analysis to *electrocochleography* (ECoG) data [15, 16]. ECoG electrodes are placed directly on the cortex rather than on the scalp as EEG electrodes. ECoG recordings have better spatial resolution than EEG and typically measure higher voltages than EEG, around several hundreds of microvolts compared to several tens the EEG records [17, 18]. Because the human skull acts as a low-pass filter, ECoG can record more high-frequency neural activity, up to 10 kHz [17]. The downside of ECoG measurements is that the electrodes have to be placed on the subject's cortex, making it an invasive measure.

Solovey *et al.* [15] applied dynamic system analysis to characterize differences between the conscious and unconscious brain. They provided a novel measure to distinguish the neural activity of four monkeys before, during and after anesthesia. The research study by Ashourvan *et al.* [16] monitored 21 subjects during 94 seizures with ECoG recordings. They were able to characterize the spatiotemporal dynamics of seizures subject-specifically. Works [15] and [16] provide evidence that dynamic system analysis can identify features that characterize loss of consciousness and seizures based on neural data.

Proposed study In the current body of literature on meditation, there has yet to be a consensus on a feature signifying meditation. Currently, there is no objective measure to tell whether someone is in a meditative state. The lack of understanding limits the development of meditation as an accessible, low-cost, personalized healthcare option. Several studies aim to identify either temporal or spatial characteristics of the EEG, but in the context of meditation, very few assess both simultaneously.

Accordingly, I propose a dynamic systems approach to assess changes in EEG data during a meditation session compared to eyes-closed, resting baseline measurements. Section 2-3

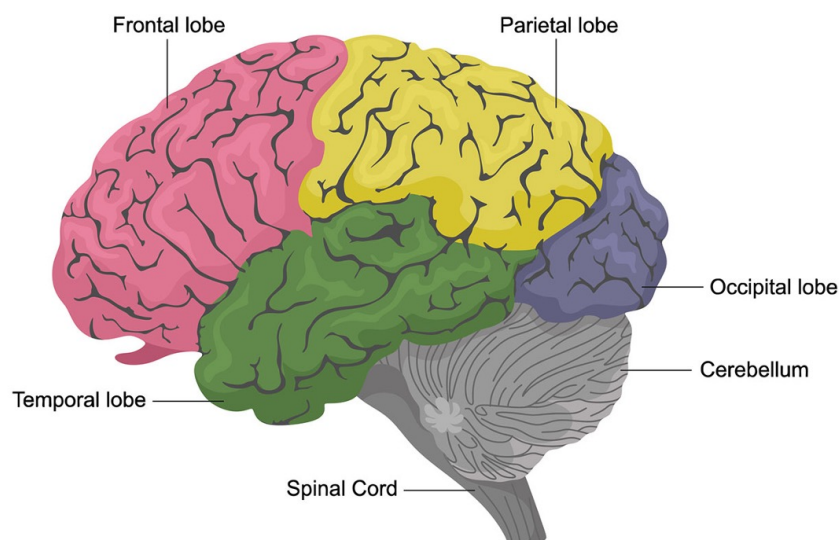


Figure 1-2: The human brain divided into four regions, or lobes: lobes: frontal, parietal, temporal and occipital [13].

further explains dynamic systems analysis. Dynamical systems analysis successfully identified characteristic features for both loss of consciousness and seizures on ECoG data. EEG cannot capture the same high-frequency spectrum as ECoG but based on the literature, the range of interest lies in the theta and alpha bandwidth (4-12 Hz), which the EEG can capture well. Since the method was successful for processes related to consciousness, a dynamical systems approach could provide features for distinguishing meditation. By extension, a model that captures spatiotemporal changes during meditation could help to obtain knowledge about the neural mechanisms underlying meditation.

In this thesis, I seek to explore the hypothesis that a dynamic feature distinguishes meditation from a resting baseline. I gathered an EEG dataset for this thesis at TNO in the context of a broader mental state monitoring experiment. In the experiment, twenty-two participants performed a sixteen-minute audio-guided loving-kindness meditation. Before and after the meditation, I asked the participants to rate their current emotions and recorded a two-minute eyes-closed resting baseline.

During analysis, I model the EEG data as a linear system on short time windows and compute three features for each window that result from the dynamic system model, discussed in Section 3-1. Next, I assess the differences in the feature distributions during meditation compared to the baselines to validate the hypothesis. Additionally, I explore the sensitivity of the analysis to using different subsets of electrodes rather than the complete set. I explore using a personalized headset and a subset of electrodes based on available wearable EEGs. The EEG in this experiment uses a saline solution between the electrodes and the scalp, whereas wearable EEGs usually use a dry technology. Therefore, the analysis serves as a theoretical experiment to investigate the impact of the locations of the EEG electrodes.

Contributions The experimental work presented in this thesis provides the first application of dynamic systems analysis on EEG data in the context of meditation. The approach combines the analysis of temporal and spatial characteristics of EEG signals. The analysis shows that the EEG dynamics change for every participant in the experiment conducted for this thesis. Furthermore, it identifies the most active regions corresponding to the changing dynamics, both subject-specific and across all participants. Finally, shifts in the active regions may suggest changing neural dynamics underlying meditation.

Outline thesis Chapter 2 provides background information on the concepts discussed in this thesis. It explains the workings of the EEG and the challenges when working with EEG signals. Furthermore, it highlights the conventionally applied spectral bandwidth analysis. Finally, it introduces eigenvalue-eigenvector decomposition and stability analysis. Chapter 3 discusses the protocol of the experiment at TNO. Moreover, it explains the dynamical systems approach, the data processing steps, and the evaluation metrics of the analysis.

In Chapter 4, I first show the results of a stationarity analysis to choose the appropriate model parameters for the linear model. Second, it discusses the results of the dynamic systems analysis. In addition, I discuss the scenario in which only a subset of the sensors is available, such as the Muse headset or a personalized subset, and display the corresponding results. Finally, the chapter shows the results of the subjective questionnaires the participants answered before and after meditation. To conclude, Chapter 5 discusses the results, evaluates the study, and provides recommendations for future studies following this thesis.

Chapter 2

Preliminaries

To quantify changes in the human mind that meditation brings about, we can use an *electroencephalogram* (EEG) to measure the voltage fluctuations at different locations on the scalp [7]. This chapter provides background information on important concepts discussed in this thesis. Section 2-1 explains how the EEG can capture part of the neural activity. Section 2-2 describes a conventional method to analyze the EEG data, the *spectral bandwidth analysis*. Finally, Section 2-3 provides a more elaborate explanation of the *eigendecomposition* and *stability analysis* of a linear system.

2-1 Neural basis of the EEG

Electric activity in the neuron *Neurons*, electrically excitable cells, can transmit electrochemical signals in the brain. Neurons transmit sensory inputs to the brain, carry signals within the central nervous system, or send a message to target cells, such as muscles or glands. To pass from one neuron to the next, the signal has to pass the *synapse*, a structure that allows for the transmission of signals via chemical signaling or directly as an electrical signal. Chemical signaling occurs through specific chemicals called *neurotransmitters*.

The neuron's structure can roughly be divided into three parts: the *dendrites*, the *cell body*, and the *axon* (see Figure 2-1). The dendrites receive signals from other neurons. If the sum of input signals that lead to a change in the electrical potential reaches a certain threshold, the cell body is triggered to send an impulse along the axon: the *action potential*. The neuron's resting *membrane potential*, the difference in potential between the inside and outside of the cell, is typically -70 mV. The resting membrane potential differs per type of neuron, and can lie between -80 and -40 mV. The threshold is usually -55 mV, and the action potential typically causes the membrane potential to increase to $+30$ mV. The action potential causes a brief local current lasting about 1-10 ms [7]. The action potential is a local trigger, propagating throughout the axon by activating other local triggers, *i.e.* other action potentials.

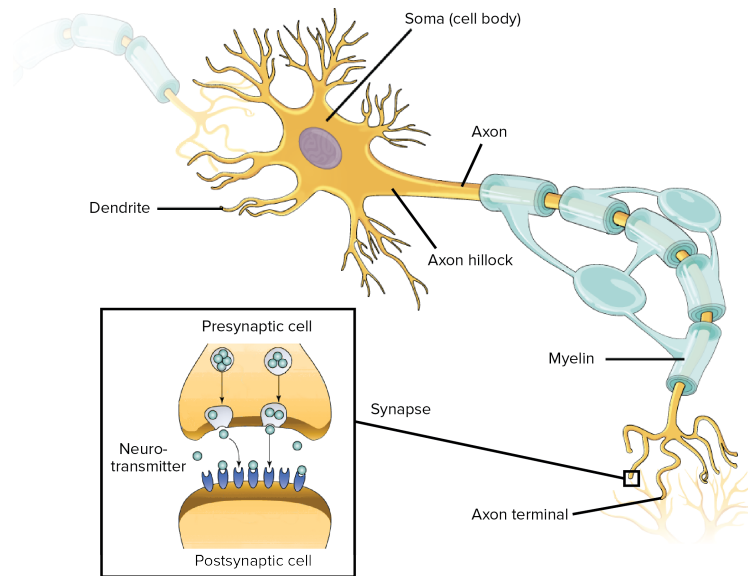


Figure 2-1: Structure of a neuron [19].

The action potential can propagate until it reaches the ends of the axon, the *axon terminals*. The axon terminals can release neurotransmitters in the case of chemical signaling or pass the electric signal directly to another neuron. When a neurotransmitter binds to a receptor on the dendrites of another neuron, it can trigger a response, the *postsynaptic potential*. The postsynaptic potential depolarizes the neuron receiving the neurotransmitter, making it more likely to fire an action potential. Postsynaptic potentials typically last longer than action potentials, lasting about 50-200 ms [7].

EEG measurements The EEG only captures the neural activity when the potential field is large enough [7]. Since the postsynaptic potential lasts longer than the action potential, the probability that multiple postsynaptic potentials happen synchronously is higher. Specifically, neurons called *pyramidal cells* often behave similarly simultaneously. Moreover, their dendrites lie parallelly, orienting their potential field in the same direction such that the sum of their potentials does not cancel each other out. Contrarily, action potentials can go in many directions relative to the surface of the cortex and are not synchronized. Postsynaptic potentials of the pyramidal cells usually have a greater potential field and are considered the main contributor to the EEG [7].

During the postsynaptic potential, the pyramidal cell has two oppositely charged poles separated by some distance, a *dipole*, emitting an electric field in almost every direction (see Figure 2-2). We model many neighboring dipole sources as one dipole that can be oriented in any direction. The electrical field causes currents to flow through the surrounding conductive medium, such as the brain tissue and the scalp. This effect is called *volume conduction*. The dipoles express the direction and the strength of the current flow. The polarity of the dipoles can vary, and the conductivity of the biological tissue between the dipole and each electrode is not uniform either. The voltage fluctuations measured at any electrode on the scalp are a weighted sum of activities generated by many neural sources, known as *spatial smearing*. As a consequence, the spatial resolution of EEG is limited [7].

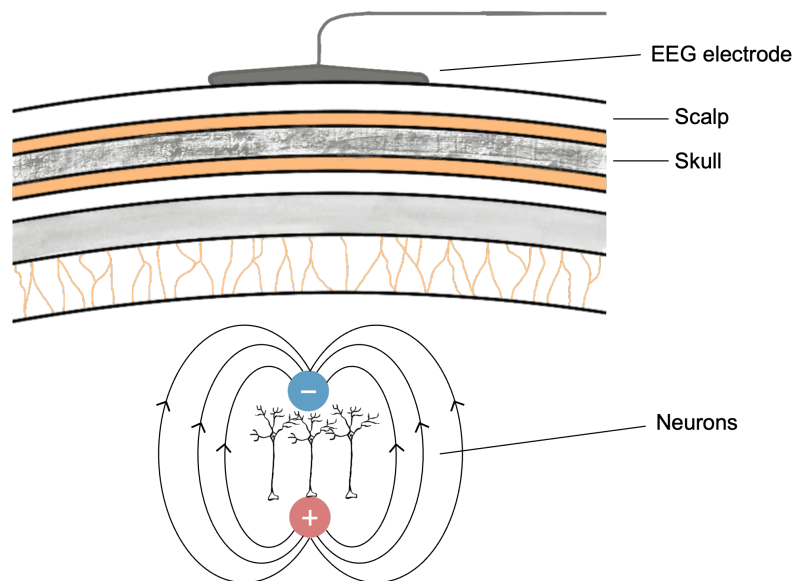


Figure 2-2: We model a group of neurons that behave similarly simultaneously as one dipole that causes currents to flow through the surrounding conducting medium.

On the other hand, the temporal resolution of EEG measurements is very high, making it possible to capture fast dynamics of processes in the brain (such as cognitive, motor and emotional processes). Furthermore, EEG is a non-invasive measure, meaning that we place the sensors on the outside of the head. EEG measurements do not require patients to have electrodes implanted surgically. However, having the electrodes on the scalp rather than on the brain introduces larger spatial smearing and more data processing challenges. Despite these limitations, EEG is one of the most accessible and used mechanisms to quantify neural activity.

2-2 Spectral bandwidth analysis

Spectral bandwidth analysis is one of the first and most frequently used methods to quantify changes in EEG measurements in studies monitoring meditation [9]. An EEG recording expresses the voltage potential of one channel compared to some reference for multiple points in time. Spectral estimation transforms the signal from the time domain to the frequency domain, expressing the signal's power distribution as a function of the frequency. By comparing the power contributed by different frequencies, the spectral analysis characterizes the EEG signals in the frequency domain.

Fourier Transform The basis for the spectral estimation is the Fourier Transform. It characterizes a time-series signal in the frequency domain by expressing the signal as a composition of oscillations with different frequencies. For a discrete signal, we use the *Discrete-Time Fourier Transform* (DTFT). Define the frequency as $\omega \in \mathbb{R}$ in radians per

second and sampling time T in seconds, then the DTFT is defined as [20]:

$$X(e^{j\omega T}) = \sum_{k=-\infty}^{\infty} x(k)e^{-j\omega kT}. \quad (2-1)$$

The DTFT exists only for signals for which the sum in Equation 2-1 converges. The condition is met when the signal $x(k)$ is absolutely summable: $\|x\|_1 < \infty$.

Note that to compute this signal transform, we need the signal to be defined on the time interval $(-\infty, \infty)$. In practise, we only have a finite number of data samples. Therefore, we use the *Discrete Fourier Transform* (DFT). Let $x(k)$ be the signal in volt for time step $k \in \mathbb{Z} = 0, 1, \dots, N-1$, where N is the total number of samples. $\omega_n = 2\pi n/(NT)$ in radians per second for $n \in \mathbb{Z} = 0, 1, \dots, N-1$ and $T \in \mathbb{R}$ is the sampling time in seconds. The *Discrete Fourier Transform* (DFT) of $x(k)$ is given by [20]:

$$X_N(\omega_n) = \sum_{k=0}^{N-1} x(k)e^{-j\omega_n kT}. \quad (2-2)$$

The DFT transforms a time sequence of N samples into a sequence of complex numbers at N different frequency points.

Power spectrum estimation To display the frequency content for a signal, the power-spectral density function, or the *power spectrum* is used. The spectrum can be thought of as the distribution of the signal's energy over the whole frequency band. For discrete signals with a finite number of samples, we can estimate the power spectrum with a *periodogram*. Let $\omega_n = 2\pi n/(NT)$ in radians per second for $n \in \mathbb{Z} = 0, 1, \dots, N-1$, with N is the total number of samples and $T \in \mathbb{R}$ is the sampling time in seconds. Then the periodogram is defined by the following [7, 20]:

$$\hat{\Phi}_N^x(\omega_n) = \frac{1}{N} |X_N(\omega_n)|^2. \quad (2-3)$$

To reduce the periodogram's variance, a well-known method is Welch's [21]. *Welch's method* divides the data samples into data segments. First, the periodogram of each windowed data segment is calculated. Then, the final spectral estimate is the average of each periodogram. Welch's method reduces the variance of the spectral estimate, assuming the variance of the spectral content of the signal is less in a shorter time window.

The lower variance comes at the expense of decreasing the *frequency resolution*. The frequency resolution is the fineness of detail that we can distinguish in a periodogram. For a sequence of N samples the DFT defines frequency values at points $2\pi n/(NT)$, $n \in \mathbb{Z} = 0, 1, \dots, N-1$. In between these points there is no information available. Therefore, the frequency resolution of the periodogram is defined as $NT/(2\pi)$. Thus, the reduced variance means that we will lose detail in the frequency spectrum.

Spectral bandwidth analysis In the power spectrum, we can recognize peaks around specific frequencies. In the context of EEG measurements, it is common to divide the frequency bandwidth into several bandwidths: *delta* (1-4 Hz), *theta* (4-8 Hz), *alpha* (8-12 Hz), *beta* (12-30 Hz) and *gamma* (>30 Hz). However, the exact definitions of the bandwidths differ per study [6, 9]. In early EEG studies, specific characteristics were attributed to peaks in the different bandwidths, as shown in Figure 2-3. The most prominent peak in the spectrum roughly indicates in what state someone is. For example, the spectrum of the EEG in Figure 2-3 shows a peak in the alpha bandwidth, suggesting the person is in a relaxed state. The person was sitting in a chair with their eyes closed so we could classify their state as relaxed. More recent studies still adhere to these bandwidths by comparing the average power across a bandwidth during different states. We can compute the average power of the frequency points within a bandwidth for a discrete-time signal.

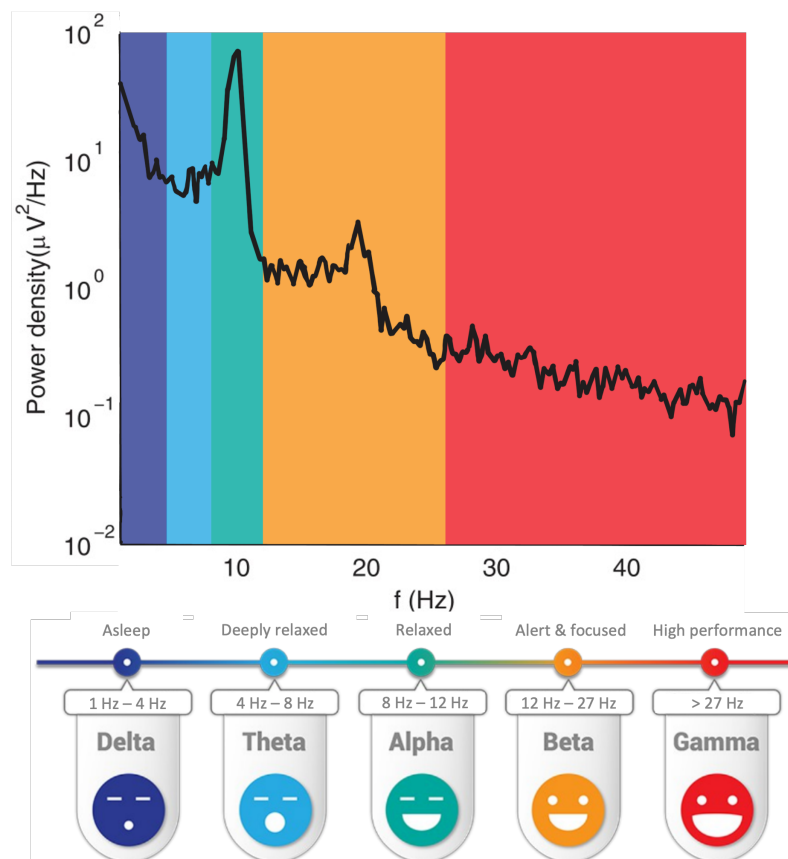


Figure 2-3: In the context of EEG measurements, the frequency spectrum is divided into smaller frequency bandwidths. A peak in a certain bandwidth is typically associated with a particular mental state. For this particular periodogram, the largest peak is in the alpha bandwidth, associated with a relaxed state.

2-3 Eigendecomposition and stability analysis

The behaviour of many dynamic systems is modeled with linear systems, even when the underlying mechanism behaves according to nonlinear dynamics. Linear systems can be applied to a wide range of different physical domains and allow for a uniform set of tools to analyse the system's behaviour. Specifically, the responses of linear *autonomous* systems, dynamic state-space systems without inputs and outputs, can be completely understood using linear algebra.

Eigendecomposition For a state $x \in \mathbb{R}^n$, the *evolution matrix* $A \in \mathbb{R}^{n \times n}$ and time step k , a discrete, autonomous linear system is described as:

$$x(k) = Ax(k-1). \quad (2-4)$$

For an initial condition $x(0)$, we can express the response of the system at time step t in terms of the evolution matrix as:

$$x(k) = A^t x(0). \quad (2-5)$$

An eigenvalue λ of A is a, possibly complex, zero of the *characteristic polynomial* of A ,

$$\det(\lambda I - A) = 0. \quad (2-6)$$

If λ is an eigenvalue of A , then any non-zero vector $e \in \mathbb{C}^n$ is a corresponding *eigenvector* if it satisfies

$$(\lambda I - A)v = 0, \text{ or equivalently } Av = \lambda v. \quad (2-7)$$

Note that eigenvectors are not unique, and that for each eigenvalue there exist at most n linearly independent eigenvectors (a basis of the null space of $\lambda I - A$). For a matrix $A \in \mathbb{R}^{n \times n}$ we can find n eigenvalue-eigenvector pairs that completely characterize the linear system's behaviour, given the initial conditions.

Suppose that A has a complex-valued eigenvalue λ with a corresponding eigenvector v . Then the complex conjugate of λ , $\bar{\lambda}$, is also an eigenvalue of A and the complex conjugate of v , \bar{v} is a corresponding eigenvector. Thus, complex eigenvalues and eigenvectors always exist in pairs.

If the evolution matrix A has n linearly independent eigenvectors, then it can be decomposed as:

$$A = V\Lambda V^T, \quad (2-8)$$

where matrix $\Lambda \in \mathbb{R}^{n \times n}$ is a diagonal matrix containing the eigenvalues of A , the columns of the matrix $V \in \mathbb{R}^{n \times n}$ contain the corresponding eigenvectors, and V^T is the transpose of V . The decomposition of the evolution matrix into Λ and V , or equivalently into eigenvalue-eigenvector pairs, is called the *eigendecomposition* or the eigenvalue decomposition of A .

We can express the state evolution after t time steps, starting at 0, as:

$$x(k) = A^t x(0) = V\Lambda^t V^T x(0). \quad (2-9)$$

Stability We can analyze the stability of the dynamics with the absolute value, or the *magnitude*, of the eigenvalues. The magnitude of the eigenvalue is associated with the exponential growth or decay along the corresponding eigenvector. We can illustrate this idea by considering the magnitude of the linear combination of the original data $z(k) = Vx(k)$. Let $z_i(k)$ denote $v_i^T x(k)$, then its magnitude is expressed as:

$$|z_i(k = t)| = |\lambda_i|^t |z_i(0)|. \quad (2-10)$$

The stability of an autonomous linear system is examined with the asymptotic behaviour of $z_i(k)$ as $t \rightarrow \infty$ [15, 16]. There are three scenarios possible.

- If $|\lambda_i| < 1$ then $|z_i(k)| \rightarrow 0$, meaning any perturbation along the direction of the eigenvector v_i will vanish. We call the process *asymptotically stable*.
- For $|\lambda_i| > 1$ then $|z_i(k)| \rightarrow \infty$. The any perturbation along the corresponding eigenvector tends to explode, and we refer to the process as *unstable*.
- For $|\lambda_i| = 1$ then $|z_i(k)| = |z_i(0)|$. The dynamics of the linear system oscillate between stability and instability. A linearization of a nonlinear system fails to classify the stability of the process when $|\lambda_i| = 1$. In this case, the equilibrium point around which the system is linearized could be asymptotically stable, stable or unstable [22].

Thus, the eigenvalue's magnitude captures the growth or decay of an oscillation, and the eigenvector specifies the direction of the oscillation. Figure 2-4 displays different eigenvalues plotted in a complex plane to visualize the relationship between an eigenvalue's magnitude ($|\lambda|$) and frequency and the corresponding dynamics. The eigenvalue's frequency is proportional to the angle θ . The dynamics in the lower half of the plane mirror the upper half because both eigenvalues in a complex conjugate pair have the same frequency and magnitude.

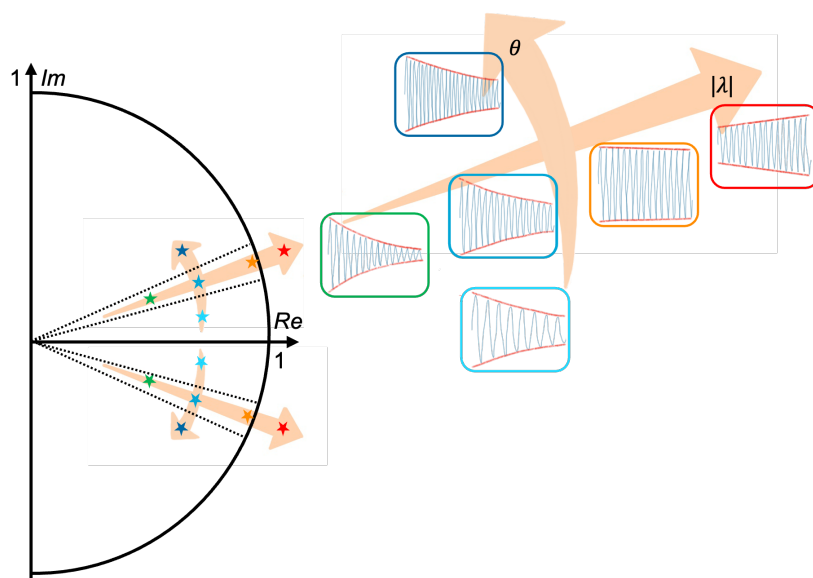


Figure 2-4: The relationship between the complex eigenvalue and its magnitude $|\lambda|$ and its frequency, which is proportional to the angle θ .

Chapter 3

Methodology

Various fields of natural and social science research employ dynamic system models. They can describe oscillatory patterns and predict outcomes in complex systems. In Section 3-1 of this chapter, we describe how dynamic systems modeling can describe the dynamic properties of a complex system. The study to collect *electroencephalogram* (EEG) signals during meditation is described in Section 3-2. Section 3-3 outlines the procedures for processing the data, and Section 3-4 discusses the metrics for determining the statistical significance of the findings.

3-1 Dynamic systems analysis

Dynamic systems can locally approximate the dynamics of a variety of processes as an *autoregressive* (AR) model [22]. Specifically, let $x(k) \in \mathbb{R}^n$ be the measurements at time step k . Then, for time window $K \in \mathbb{Z}$ defined on the interval $[k - \tau, k + \tau]$, where τ is the window size parameter, we obtain the following AR model of order 1, or AR(1), as a function of the evolution matrix $A(K) \in \mathbb{R}^{n \times n}$ and $\varepsilon(k + 1) \in \mathbb{R}^n$ the approximation error:

$$x(k + 1) = A(K)x(k) + \varepsilon(k + 1). \quad (3-1)$$

The local linear approximation relies on the assumption that a linear model can adequately describe the dynamics of the signal over a short time interval. The parameter τ must be selected carefully because it must be small enough to ensure the validity of the linear approximation. On the other hand, the frequency of the dynamics the model captures depends on the time window selection. A time window that is too small will mainly model high-frequency dynamics and noise because it cannot capture low-frequency dynamics. Depending on the objective of the analysis, we must reach a balance for the selection of τ .

It's important to recognize that this model cannot infer any underlying neural mechanisms from the data. Rather, we can assess dynamic properties locally through the eigendecomposition of evolution matrix A [16]. More specifically, the *eigenvalue-eigenvector* pairs capture

linearly independent spatiotemporal dynamics. A complex eigenvalue specifies the oscillatory dynamics for each spatiotemporal process. The eigenvector captures the relative involvement of each EEG electrode for the corresponding dynamics. Thus, the analysis includes both the EEG's temporal and spatial aspects.

We can derive two dynamic features that characterize the EEG from the eigenvalues. Given the sampling frequency f_s in Hz, the angle θ_i corresponding to the i^{th} complex eigenvalue in polar coordinates provides a description of the *frequency* f_i as the following [16]:

$$f_i = \frac{\theta_i}{2\pi} f_s. \quad (3-2)$$

The second feature is the eigenvalue's *magnitude*, or absolute value, associated with an exponential growth or decay of the oscillations. This is also referred to as the *stability* feature, because the magnitude characterizes the stability of the process when it is subject to perturbations [15, 16]. Section 2-3 explains how the eigenvalues characterize different stages of stability and shows the relationship between the magnitude, the frequency, and the corresponding oscillations.

The eigenvectors express the direction of the dynamics of the corresponding eigenvalue. Every entry in the eigenvector relates to an electrode and, accordingly, to a location on the scalp. The eigenvector's standardized values characterize the relative involvement of each electrode per window. The three dynamic features, (i) the eigenvalues' magnitude, (ii) the eigenvalues' frequency, and (iii) the eigenvectors, characterize the dynamics of the EEG over time.

3-2 Experiment protocol

I conducted an experiment involving monitoring various mental states at TNO's Human Performance department. One of the experiment's objectives was to monitor the effects of meditation by physiological and self-reported measures. The participant completed several exercises during the experiment. Figure 3-1 provides a timeline of the experiment. First, the participant watched a selection of videos selected to evoke specific emotions. Next, the Sing-a-Song Stress Test [23] unexpectedly asked subjects to sing a song to induce stress. Then, the participants engaged in an audio-guided meditation session. Finally, following a video's instructions, they performed a set of breathing exercises. Between each section, we conducted baseline measurements. During the experiment, we asked participants to sit still.

This thesis focuses on the meditation session and the surrounding baselines and questionnaires. During the baselines and the meditation, participants kept their eyes closed and followed the audio-guided meditation. We used a loving-kindness meditation recited by Tara Brach for this experiment [24]. The practice asks participants to focus on positive energy within themselves and their surroundings. We monitor the participant's emotional responses on three dimensions using the *Self-Assessment Manikin* (SAM) scale (see Figure 3-2): valence, arousal, and dominance [25]. The test asks participants to rate their current emotions based on the illustrations provided.

Twenty-two people participated in the experiment (8 male and 14 female). Out of all participants only three had previous experience with meditation. Participants ranged in age from 22 to 79 years old. All participants were in generally good health, defined as not

being under medical treatment for an illness or accident, having a physical or mental health diagnosis, smoking, using drugs recreationally, or consuming more than 28 units of alcohol per week.

We collected the EEG data with a 32-channel gel-based BioSemi Active 2 system [26] at a sampling rate of 512 Hz. The electrodes were placed on the scalp according to the standard 10-20 electrode placement. The BioSemi uses one Common Mode Sense active electrode for referencing and one Driven Right Leg passive electrode so that the recordings can be re-referenced offline. During setup, we kept the impedance of each electrode between an offset of -20 and $20 \mu V$ using the BioSemi ActiView software. The participants arrived one hour prior to the start of the experiment to fill out a demographics questionnaire, receive instructions, and have the EEG set up. After the experiment, we interviewed the participants about their experiences.



Figure 3-1: The participants go through an experiment consisting of multiple parts.

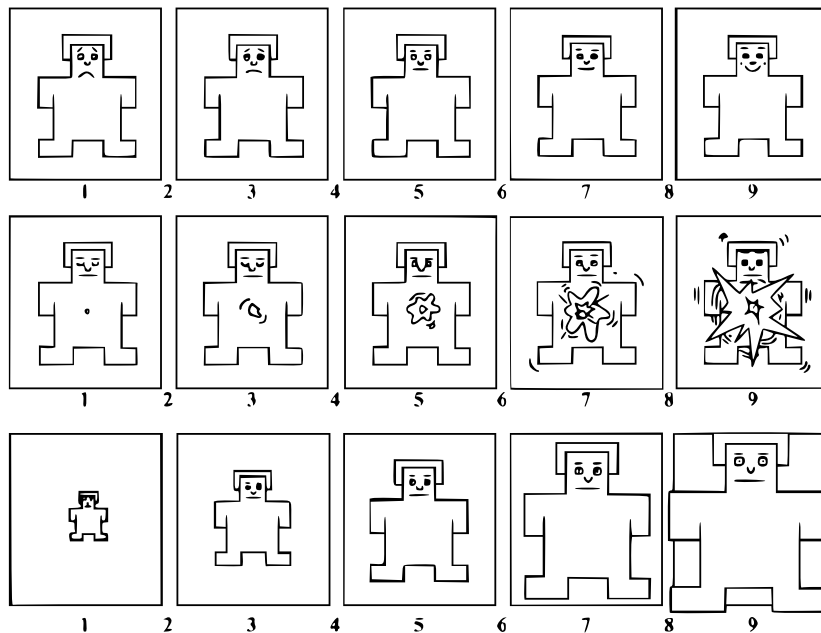


Figure 3-2: The SAM test asks participants to rank their emotion on three dimensions: valence (top), excitement (middle), and dominance (bottom).

3-3 Data processing steps

We processed the data using MATLAB and EEGLAB software [27]. The data was filtered using a high-pass filter at 1 Hz and a low-pass filter at 47 Hz, using a filter of order 1650. The high-pass filter removes sensor drift. Klug *et al.* advise a high-pass filter with a cut-off frequency of 1 Hz [28]. The low-pass filter filters the 50 Hz line noise and high-frequency noise.

The *Clean Rawdata* plug-in in EEGLAB cleans the EEG data [29]. The function removes a channel if it is flat for longer than 5 seconds, is insufficiently correlated to the other channels, or if its standard deviation is too high compared to the other channels. Moreover, *Clean Rawdata* divides the data into short time frames and removes the time frame if the data portion has an unusually large variance. For subsequent analysis, it is convenient if the data maintains its original size. Therefore the bad time frames and the removed channels are reconstructed using *spherical spline interpolation*. Spherical spline interpolation projects all electrodes onto a sphere, similar to the electrode locations on the head, and interpolates the values measured at the good electrodes to the removed channels.

Next, we re-referenced the EEG data to the average of all electrodes. The final pre-processing step is to run the *Extended Infomax Independent Component Analysis* (ICA) [30] to identify and remove particular artifacts in the EEG data. ICA isolates various sources underlying the EEG recordings and returns a number of ICA components equal to the data rank. Finally, the *IC Label* algorithm [31] classifies the components as neural activity or as an artifact, such as eye blinks, eye movement, and muscle activity, based on the source location and spectral density.

We compute the power spectrum of each electrode using Welch's algorithm, with EEGLAB's *spectopo*-function [27]. First, we compute the power spectrum during the baselines and meditation. To find the alpha power per electrode, we compute the average value of the spectral power at frequencies in the 8-12 Hz range. Next, the dynamic systems analysis uses the *ARfit* algorithm [32] to fit the autoregressive model of the first order with a stepwise least squares algorithm. Finally, MATLAB's *eig*-function determines the eigenvalues and eigenvectors for each time window.

3-4 Evaluation metrics

This section explains two methods we use to evaluate the results. First, we use a stationarity test to evaluate the choice of the window size parameter τ . Second, the statistical analysis assesses whether the distributions of the dynamic features during meditation compared to the baseline are statistically significant.

Stationarity test For the dynamic systems approach, we determine the eigenvalues and eigenvectors of the evaluation matrix $A(K) \in \mathbb{R}^{n \times n}$ for each time window $K \in \mathbb{Z}$. Let us define the time interval as $[K - \tau, K + \tau]$, where τ is the parameter that determines the window size. For time step $k \in \mathbb{Z}$ from 0 to N , where N is the total number of time steps per window, and the data per time step $x(k) \in \mathbb{R}^n$, where n is the dimension of the data, we

obtain the following AR(1) model for each time window:

$$x(k+1) = w(K) + A(K)x(k) + \varepsilon(k). \quad (3-3)$$

The vector $w(K) \in \mathbb{R}^n$ allows for a nonzero mean of the time series. The vector $\varepsilon(k) \in \mathbb{R}^n$ is the residual vector per time step. For an AR(1) model for a stationary time series, vectors $\varepsilon(k)$ are uncorrelated random vectors with mean zero and covariance matrix $C \in \mathbb{R}^{n \times n}$ [32]. The window size is the only adjustable parameter; by extension, τ is the only identifiable parameter of this system.

To determine what window size is the most suitable for this application, we evaluate the residuals $\varepsilon(k)$ of the AR model. The assumption that underlies the evaluation metric is that the time series of the residuals are stationary if the AR model completely captures the signal's dynamics. To test whether the residuals are stationary, we test whether the time series has a *unit root* [33]. To illustrate the concept of a unit root, we model the time series as an *autoregressive* (AR) model of order 1. Let y_k be the residual at time step k , $\varepsilon(k)$ an uncorrelated process with zero mean and variance σ^2 , and ϕ the AR(1) coefficient, then we model the time series as:

$$y(k) = \phi y(k-1) + \varepsilon(k). \quad (3-4)$$

If $\phi < 1$, the time series does not contain a unit root, meaning that when a disturbance is present, the time series will revert back to its mean over time. On the other hand, when $\phi \geq 1$, the time series contains a unit root and is thus non-stationary.

We use the *Augmented Dickey-Fuller test* (ADF test) and the *Kwiatkowski-Phillips-Schmidt-Shin test* (KPSS test) to test for the presence of a unit root [33]. The ADF test assesses the null hypothesis that the time series is non-stationary and possesses a unit root ($\phi = 1$), with the alternative hypothesis that the time series is stationary ($\phi < 1$). The KPSS test has the null hypothesis that the time series does not have a unit root and thus is stationary, with the alternative hypothesis that the time series is non-stationary. If the ADF test rejects the null hypothesis and the KPSS test does not, that suggests our residual time series does not have a unit root. Therefore, the tests suggest the residuals are stationary and do not contain any dynamics we wish to capture in our AR model.

Statistical analysis After deciding on the time window parameter, we compute the dynamic features for each time window. Then, we assess the dynamic features during baselines and meditation to determine if their distribution is statistically significantly different. The *Kolmogorov-Smirnov test* (KS test) is a nonparametric test to analyze if two sets of samples are from the same distribution [34, 35]. The advantage of the KS test is that it does not assume any particular underlying distribution.

Let X_1, \dots, X_m and Y_1, \dots, Y_n be independent random samples, respectively, from continuous populations 1 and 2, where n is the number of samples in X , and m is the number of samples in Y . The null hypothesis of the KS test is that there is no difference between continuous populations 1 and 2. The alternative hypothesis is that the samples have a different continuous population. The first step of the test is to find the empirical *cumulative distribution function* (CDF) $F_x(t)$ and $F_y(t)$ for the samples of X and Y over range t , where $F_x(t)$ is the

proportion of X values less than or equal to t and $F_y(t)$ is the proportion of Y values less than or equal to t . Next, we determine the maximum distance D between the empirical distribution functions,

$$D = \max(|F_x(t) - F_y(t)|). \quad (3-5)$$

Then calculate the KS test statistic Z as:

$$Z = D\sqrt{\frac{m \cdot n}{m + n}}. \quad (3-6)$$

We use the test statistic Z to find the two-tailed probability estimate p , which is the probability that we observe a test statistic as extreme as the value we found or more extreme. The *Smirnov formula* or standard tables give the p -value corresponding to a particular test statistic [34]. Afterward, we compare p to a significance level α to determine if the two samples are significantly different.

The research hypothesis is a two-sided, nondirectional hypothesis because we look at a difference in test statistic D , but not in a particular direction. On the other hand, the KS test can also be one-sided by considering the directional difference. Then the alternative hypothesis is that the CDF of X is either larger or smaller than the CDF of Y . The maximum distance D^* between the CDFs is defined as either

$$D_{\text{larger}}^* = \max(F_x(t) - F_y(t)), \quad (3-7)$$

or

$$D_{\text{smaller}}^* = \max(F_y(t) - F_x(t)). \quad (3-8)$$

Chapter 4

Results

4-1 Problem definition

The results in this chapter explore the research question:

Given electroencephalographic (EEG) data recorded during meditation and a baseline, can we determine a dynamic feature to distinguish between meditation and baseline states?

First, Section 4-2 discusses the stationarity of the residuals of the fitted model for different window sizes and determines the time window for further analysis. In Section 4-3-1, I use the *Kolmogorov-Smirnov test* (KS test) to assess whether the eigenvalue's magnitude and frequency distributions change during meditation compared to the baselines. In addition, Section 4-3-2 describes changes in eigenvectors during meditation.

Next, I investigate the sensitivity of the dynamic systems analysis to different subsets of EEG electrodes in Section 4-4. First, I construct a personalized headset based on the electrodes most involved with the changing dynamics. Second, I compare the results to subsets of electrodes based on commercial, wearable EEG headsets.

Finally, Section 4-5 displays the conventional spectral bandwidth analysis results to explore whether it relates to the dynamic system analysis. Moreover, Section 4-6 discusses the results of the SAM questionnaire in order to evaluate the participants' subjective ratings.

4-2 Assessing stationarity of the residuals for different window sizes

To assess the stationarity of the residuals of the fitted *autoregressive* (AR) model, we apply two tests to the residuals for different window sizes. We divide the data into non-overlapping windows of a certain size. Then, for every window we apply the *Augmented Dickey-Fuller test* (ADF test) and the *Kwiatkowski-Phillips-Schmidt-Shin test* (KPSS test) on the residuals of the obtained AR model per channel. Then, we calculate the ratio of rejections of the null

hypothesis over the total number of tests for each window size,

$$r_{H_0} = \frac{\text{nr. of tests that reject } H_0}{\text{total nr. of tests}}.$$

The ADF test has the null hypothesis H_0 : The time series is non-stationary (has a unit root), with the alternative hypothesis that the time series is stationary. The KPSS test has the null hypothesis H_0 : The time series is stationary, with the alternative hypothesis that the time series has a unit root. Therefore, if $r_{H_0} = 1$ for the ADF test and $r_{H_0} = 0$ for the KPSS test, both tests affirm the hypothesis that the time series is stationary in every time window. We determine this ratio for different window sizes. For all time windows, we consider the same number of samples. This means that the shortest time window limits the number of samples we test for the larger time windows.

Figure 4-1a and Figure 4-1b display the results of the stationarity tests. For all participants, the time series of the residuals appears to be stationary for a window size of 0.25 seconds or smaller. For larger time windows, the tests do not affirm the hypothesis that the data is stationary for every time window. The results suggest that for a window size of 0.3 seconds or larger, the residuals contain a trend that the model does not capture.

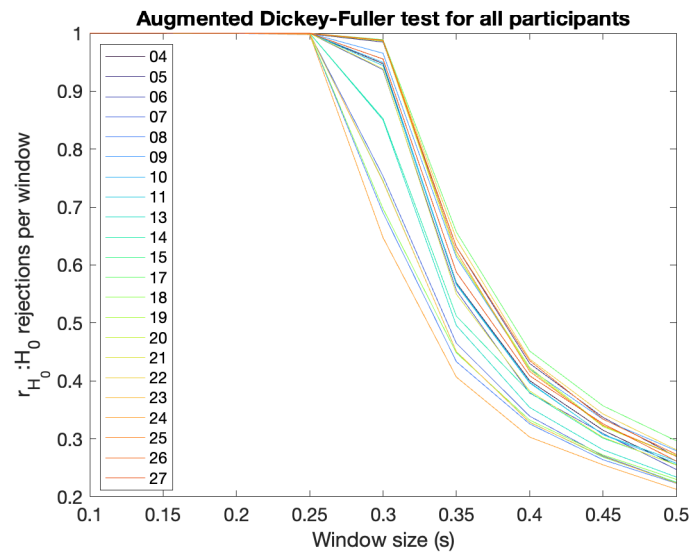
We repeated the same test on a more precise scale to select an appropriate time window. Figure 4-2a and Figure 4-2b show the results. Further results in this thesis use a time window size of 0.24 seconds. We chose the largest window for which the residuals appear to be stationary to prevent overfitting and reduce the computational load by reducing the total number of windows.

4-3 Assessing the dynamic features

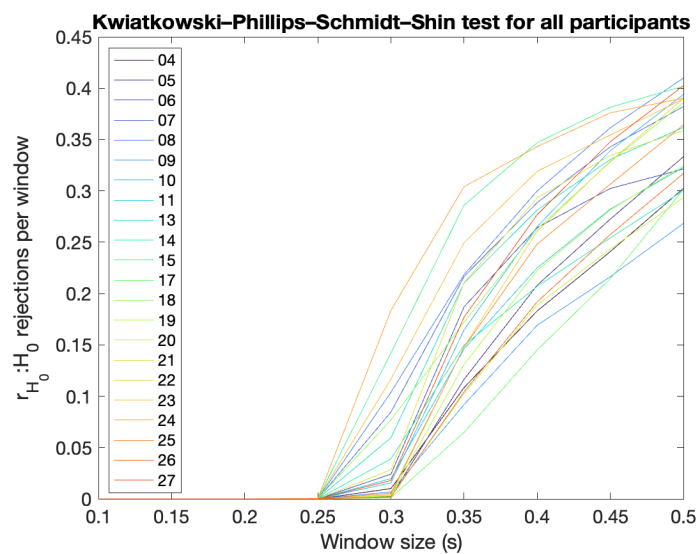
We computed the eigenvalues and eigenvectors for every window during the baselines and meditation. This section assesses the changes in the three dynamic features: (i) the magnitude, (ii) the frequency of the eigenvalues, and (iii) the corresponding eigenvectors.

4-3-1 Eigenvalues: magnitude and frequency

We obtain each participant's eigenvalues and eigenvectors for each time window. For each participant, we can visualize the distribution of the eigenvalues obtained during meditation and the baselines by plotting them on the complex plane. To illustrate the distribution of eigenvalues, Figure 4-3 depicts the eigenvalues of participant 1. Upon visual inspection, the distribution of the eigenvalues appears to be more spread out during meditation compared to the baselines. Moreover, there is a small cluster around the origin. We observe a similar cluster for all other participants. An eigenvalue with a magnitude close to zero signifies an oscillation with a huge dampening factor; thus, the corresponding oscillation dies out very quickly. Furthermore, several eigenvalues lie on the real axis, meaning their frequency equals zero. A zero frequency represents a constant line in the EEG and thus does not describe any oscillatory component of the signals.

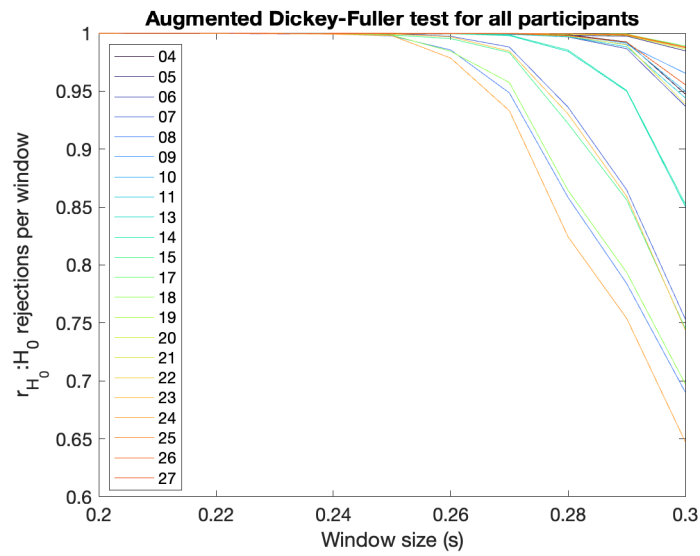


(a) ADF test on a larger time scale

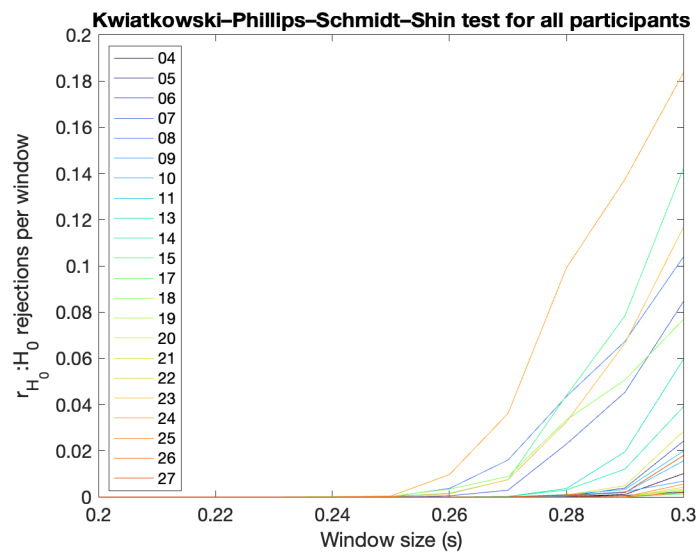


(b) KPSS test on a larger time scale

Figure 4-1: Stationarity tests on a larger time scale for all participants.



(a) ADF test on a smaller time scale



(b) KPSS test on a smaller time scale

Figure 4-2: Stationarity tests on a smaller time scale for all participants.

To statistically verify whether the distribution of the eigenvalues changes during meditation compared to the baseline, we use the two-sample *Kolmogorov-Smirnov test* (KS test). The null hypothesis H_0 is that the meditation eigenvalues are from the same continuous distribution as the baselines'. We performed three KS tests. The first is a two-sided test with the alternative hypothesis H_1 that the underlying continuous distribution of the two samples is unequal. The second and third tests are one-sided, assessing whether the meditation data's empirical *cumulative distribution function* (CDF) is smaller or larger than the baselines' CDF. We evaluate the three tests for the distribution of both the magnitude and the frequency of the eigenvalues. Table 4-1 gives an overview of the six tests. We use *bootstrapping*, random resampling with replacement, to compare the baseline and meditation data sets and run each KS test 100 times. Finally, we compute the average test statistic and test result.

Table 4-2 displays the test results. Note that this test does not include the eigenvalues positioned around the origin and on the real axis since these do capture oscillatory characteristics of the EEG signals. For each test and each participant, the table shows an h and a p -value. The p -value is the probability that the samples from meditation and the baseline are from the same underlying distribution. The h -value is the corresponding hypothesis test result: $h = 1$ indicates a rejection of the null hypothesis at a 0.05 significance level, and $h = 0$ indicates a failure to reject the null hypothesis.

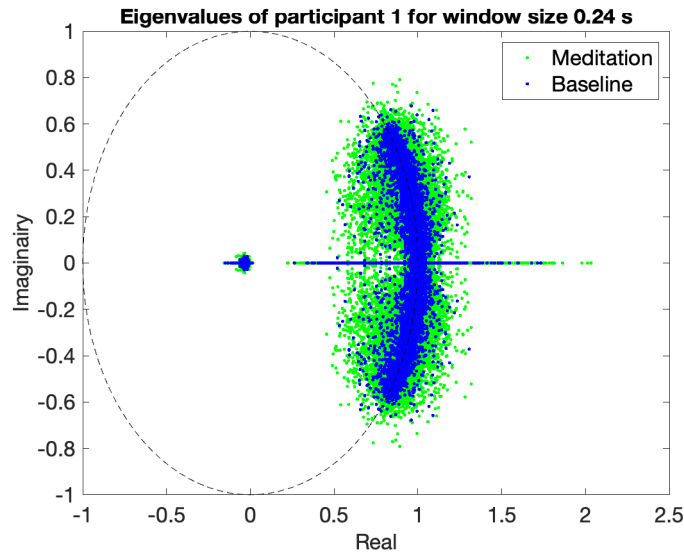


Figure 4-3: Eigenvalues during meditation and the baseline plotted in the complex plane.

| Magnitude tests | | | Frequency tests | | |
|-----------------|--------|---------|-----------------|--------|---------|
| Test 1 | Test 2 | Test 3 | Test 4 | Test 5 | Test 6 |
| Unequal | Larger | Smaller | Unequal | Larger | Smaller |

Table 4-1: An overview of the hypotheses H_1 of every KS test. The null hypothesis H_0 for each test is defined as: The empirical CDF of the magnitude/frequency during meditation is equal to the baselines. The alternative hypothesis H_1 is defined as: The empirical CDF of the magnitude/frequency during meditation is unequal/larger/smaller than the baselines.

The magnitude of the eigenvalues is distributed significantly differently for seven participants, out of whom the CDF of meditation is larger than the baseline CDF for five participants and smaller for one. Participant 9's distribution is significantly different but not consistently smaller or larger. For participant 17, Test 3 suggests that the meditation CDF is larger than the baseline CDF. However, Test 1 cannot reject the null hypothesis that the samples are from the same distribution. Therefore, the tests do not suggest that the magnitude distribution changes significantly for participant 17. The frequency distribution is significantly different for only one participant, for whom the CDF during meditation is larger than the baselines'.

To further inspect the results, we want to assess if certain eigenvalues change significantly over time. Therefore, we group eigenvalues over all time steps by sorting them based on magnitude or frequency. For every time step, the eigenvalue with the highest magnitude or frequency is called *Mode 1*, the second highest *Mode 2*, up until the final mode. Thus, we can assess changes in a particular magnitude or frequency range over time. As an illustration, Figure 4-4 displays the frequency of participant 1's eigenvalues over time, grouped by frequency. Note that the frequency of a complex eigenvalue pair is the same, therefore the total number of modes is 16 rather than 32.

We repeated the six KS tests in Table 4-1 on every mode, both sorted by magnitude and sorted by frequency. This section highlights five groups that showed changes for the most participants. The groups consider eigenvalues with the highest and the lowest magnitude, as well as one group with a magnitude around 1. Moreover, two groups of eigenvalues are included based on the frequency. One group consists of eigenvalues with the lowest and one with the highest frequency, considering modes around 42-50 Hz and 1-8 Hz, respectively.

| | h_1 | p_1 | h_2 | p_2 | h_3 | p_3 | h_4 | p_4 | h_5 | p_5 | h_6 | p_6 |
|----|-------|------------|-------|------------|-------|------------|-------|------------|-------|------------|-------|------------|
| 1 | 0 | 9.1863E-02 | 0 | 1.1984E-01 | 0 | 1.3554E-01 | 0 | 3.0909E-01 | 0 | 3.4017E-01 | 0 | 3.3619E-01 |
| 2 | 0 | 6.6168E-02 | 0 | 1.6888E-01 | 0 | 1.1174E-01 | 0 | 1.8838E-01 | 0 | 1.1626E-01 | 0 | 6.4047E-01 |
| 3 | 1 | 2.5408E-02 | 1 | 1.4517E-02 | 0 | 4.5997E-01 | 0 | 3.0383E-01 | 0 | 2.8368E-01 | 0 | 3.4850E-01 |
| 4 | 1 | 3.1965E-02 | 1 | 3.2769E-02 | 0 | 1.3063E-01 | 0 | 1.3841E-01 | 0 | 5.0601E-01 | 0 | 7.4196E-02 |
| 5 | 0 | 1.0276E-01 | 0 | 1.0484E-01 | 0 | 2.6639E-01 | 0 | 1.9778E-01 | 0 | 1.1845E-01 | 0 | 4.7285E-01 |
| 6 | 0 | 8.3487E-02 | 0 | 6.4439E-02 | 0 | 4.5960E-01 | 0 | 1.8896E-01 | 0 | 2.3163E-01 | 0 | 2.3918E-01 |
| 7 | 0 | 5.5670E-02 | 0 | 5.1168E-02 | 0 | 1.1854E-01 | 0 | 2.3815E-01 | 0 | 2.6652E-01 | 0 | 2.3291E-01 |
| 8 | 0 | 9.3510E-02 | 0 | 3.2859E-01 | 0 | 6.3967E-02 | 0 | 2.3580E-01 | 0 | 3.8247E-01 | 0 | 1.4199E-01 |
| 9 | 1 | 4.4422E-02 | 0 | 9.1303E-02 | 0 | 1.0963E-01 | 0 | 8.1401E-02 | 1 | 4.0704E-02 | 0 | 7.6155E-01 |
| 10 | 0 | 1.1595E-01 | 0 | 3.7844E-01 | 0 | 6.4702E-02 | 0 | 1.4845E-01 | 0 | 1.4090E-01 | 0 | 2.8939E-01 |
| 11 | 0 | 8.3240E-02 | 0 | 1.2934E-01 | 0 | 1.5712E-01 | 0 | 1.7365E-01 | 0 | 2.0123E-01 | 0 | 2.1361E-01 |
| 12 | 1 | 1.7495E-03 | 1 | 8.7477E-04 | 0 | 3.8326E-01 | 0 | 1.9335E-01 | 0 | 2.7107E-01 | 0 | 2.3476E-01 |
| 13 | 0 | 1.3727E-01 | 0 | 3.0084E-01 | 0 | 1.1816E-01 | 0 | 1.9881E-01 | 0 | 2.5614E-01 | 0 | 2.3431E-01 |
| 14 | 1 | 4.7566E-02 | 1 | 3.1190E-02 | 0 | 1.8025E-01 | 1 | 4.6269E-02 | 1 | 3.4903E-02 | 0 | 5.7420E-01 |
| 15 | 0 | 1.0940E-01 | 0 | 9.9477E-02 | 0 | 2.1151E-01 | 0 | 1.8937E-01 | 0 | 1.7690E-01 | 0 | 3.1955E-01 |
| 16 | 0 | 1.2032E-01 | 0 | 1.0956E-01 | 0 | 3.7382E-01 | 0 | 1.5137E-01 | 0 | 7.2639E-01 | 0 | 8.9735E-02 |
| 17 | 0 | 6.5701E-02 | 0 | 5.5778E-01 | 1 | 4.0935E-02 | 0 | 1.4046E-01 | 0 | 3.3091E-01 | 0 | 9.5673E-02 |
| 18 | 1 | 3.7475E-02 | 0 | 5.8028E-01 | 1 | 2.0502E-02 | 0 | 2.1597E-01 | 0 | 1.9469E-01 | 0 | 4.5786E-01 |
| 19 | 0 | 6.4276E-02 | 0 | 2.8846E-01 | 0 | 7.3535E-02 | 0 | 1.2220E-01 | 0 | 1.0251E-01 | 0 | 2.0024E-01 |
| 20 | 0 | 9.7981E-02 | 0 | 6.0603E-02 | 0 | 5.8546E-01 | 0 | 1.6606E-01 | 0 | 1.2084E-01 | 0 | 2.5816E-01 |
| 21 | 1 | 1.6813E-03 | 1 | 9.8799E-04 | 0 | 2.7785E-01 | 0 | 2.1396E-01 | 0 | 1.3764E-01 | 0 | 5.4569E-01 |
| 22 | 0 | 1.0756E-01 | 0 | 2.5228E-01 | 0 | 1.1767E-01 | 0 | 2.5100E-01 | 0 | 1.7654E-01 | 0 | 4.6969E-01 |

Table 4-2: Results of the six KS tests comparing the eigenvalues during meditation with the baselines for each participant.

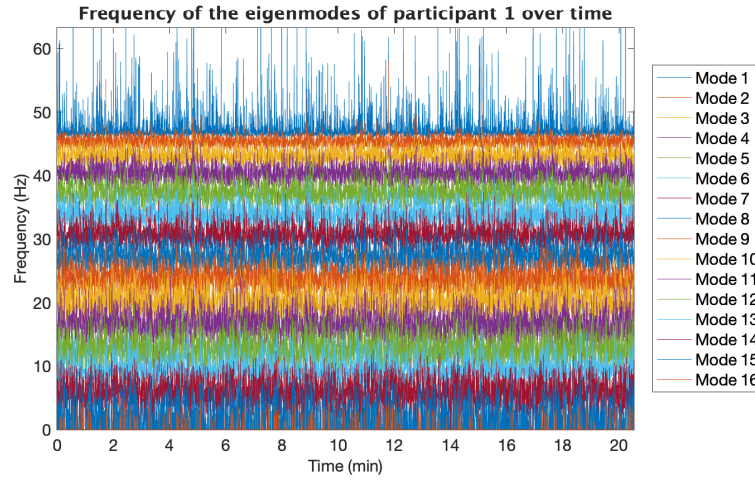


Figure 4-4: Frequency of participant 1's eigenvalues over time, sorted by frequency.

The Appendix A-1 shows the groups of eigenvalues plotted on the complex plane and the tables with the test results per participant. Table 4-3 provides an overview of the test results. The table shows the number of participants for whom each test rejects the null hypothesis. That is the number of participants whose distribution of eigenvalues is significantly different. Moreover, the one-sided test results are only included if the two-sided test rejected the null hypothesis that the distributions are the same.

For each participant at least one of the tests rejected the null hypothesis, suggesting that for each participant the EEG dynamics change during meditation. However, the changes are not consistent across all participants. We observe the largest number of changes in the frequency distribution of the high frequency modes, which changes for eighteen out of the twenty-two participants. The low magnitude modes show the largest number of changes in magnitude distribution, for fifteen out of twenty-two participants.

The low frequency mode shows somewhat consistent changes; the magnitude CDF is larger than the baseline for eight out of eleven participants for whom the magnitude changes. For the seven participants for whom the frequency distribution changes, the CDF is larger for five participants. A larger CDF corresponds to lower values. For example, if CDF A is consistently larger than CDF B, the mean and median value of distribution A are smaller than mean and median B. Therefore, this suggests that the oscillations around 1-8 Hz decrease in magnitude and frequency during meditation.

| | Test 1 | Test 2 | Test 3 | Test 4 | Test 5 | Test 6 |
|-------------------------|--------|--------|--------|--------|--------|--------|
| High magnitude | 10 | 2 | 8 | 7 | 3 | 4 |
| Middle magnitude | 11 | 5 | 6 | 10 | 7 | 3 |
| Low magnitude | 15 | 7 | 8 | 9 | 7 | 2 |
| High frequency | 9 | 5 | 3 | 18 | 10 | 7 |
| Low frequency | 11 | 8 | 3 | 7 | 5 | 2 |

Table 4-3: Overview of the test results for different groups of eigenvalues.

4-3-2 Eigenvectors

For each eigenvalue, one eigenvector corresponds to the same spatiotemporal process and weighs the involvement of each EEG electrode per time step. For example, Figure 4-5 displays the magnitude and the frequency of eigenvalue 14 over time, with the corresponding eigenvector. This mode captures the dynamics with a frequency of around 5 Hz. The eigenvector's entries are normalized to a value between 0 and 1 to indicate the relative involvement of each electrode.

Every row in the plot corresponds to one EEG electrode on the scalp. Figure 4-6 displays the placement of each electrode on the scalp. The figure is a top-down view of the scalp, with the nose pointed towards the top of the page and the left and right ears, respectively, at the left and right side of the illustration. The electrodes that appear to be most active are numbers 14-18, corresponding to the occipital and parietal-occipital regions on the head.

The eigenvectors allow us to investigate whether a particular location is related to the changes we observe in the dynamics. And if so, does this location differ during meditation and the baselines? Moreover, we can explore how the eigenvectors differ across participants. Finally, we can construct a personalized subset of electrodes to monitor changes during meditation for each participant.

First, we assess whether there is a relation between the modes highlighted in Section 4-3-1 and the electrodes' activity. We compute the average eigenvector over time per participant for each mode. Next, we sort the electrodes based on their relative involvement. For each participant, we can assess which electrodes were most active. Notably, there was a difference

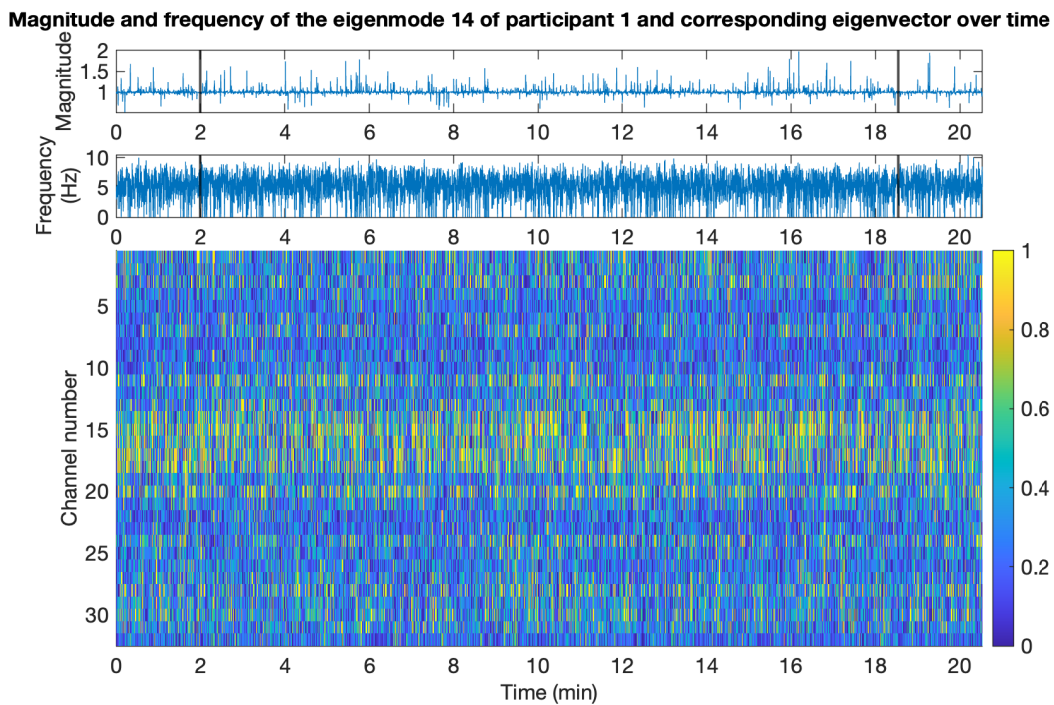


Figure 4-5: Frequency of participant 1's eigenvalues over time, sorted by frequency.

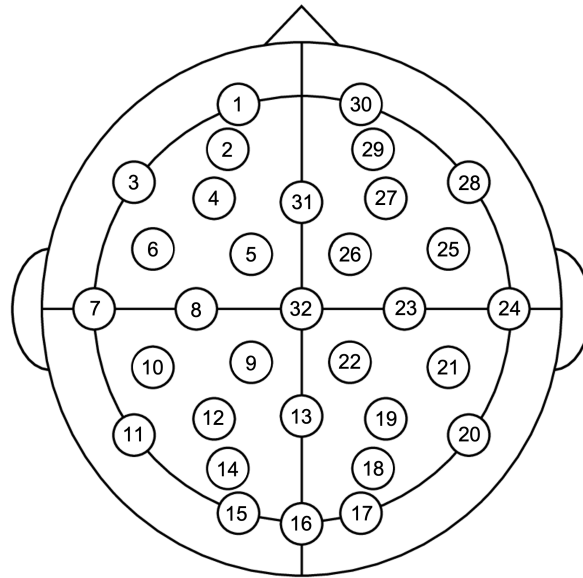


Figure 4-6: Electrode placement of the electrodes according to the 10-20 electrode placement. The figure is a top-down view of the scalp, with the nose pointed towards the top of the page and the left and right ears, respectively, at the left and right side of the illustration.

when comparing the high and low-frequency eigenvectors. To illustrate, Figure 4-7 shows a histogram of how often each electrode occurred in the set of the eight most active electrodes of each participant. The eigenvectors corresponding to modes based on the magnitude of the eigenvalue showed activity in the same regions but did not show clear differences in active regions across the different magnitudes.

Particular regions are most involved during the experiment, and the regions associated with high-frequency EEG oscillations appear to differ from the low-frequency regions. What stands out is that electrodes 11, 14-18, and 20 are more involved in high-frequency than low-frequency dynamics. The corresponding regions are the occipital and parietal-occipital area, located on the back of the head. The occipital lobe is generally associated with visual processing, spatial reasoning, and visual memory, whereas the parietal lobe is linked to sensory perception [36].

On the other hand, other areas are more involved in high-frequency dynamics. The pre-frontal area, the location of electrodes 1 and 30, is often associated with attention, judgement and restrain [37]. Electrodes in the frontal lobe (2, 4, 27, 28, 29) usually involve higher cognitive functions, including emotional expression and regulation [36]. Electrode 3 is linked to language processing [37]. In addition, electrodes 7 and 24, the temporal regions, are more involved. For most people, the left temporal lobe is associated with language processing, whereas the right temporal lobe is linked to emotional memory [36].

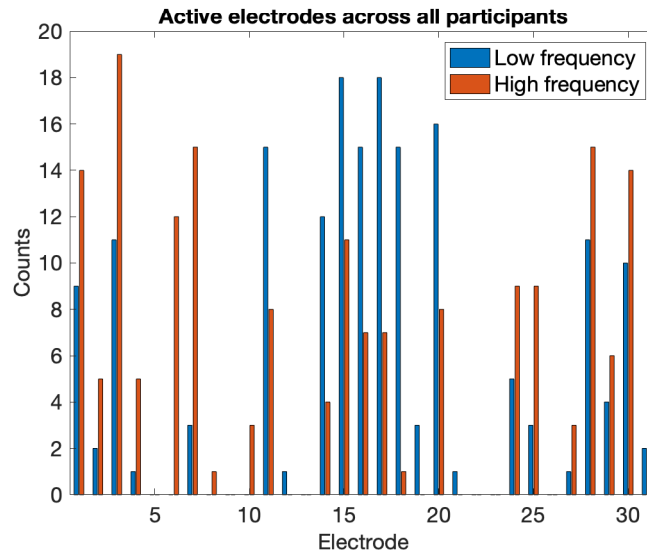


Figure 4-7: Number of times each electrode occurred in the most active electrode sets for the high and low-frequency mode.

We detected the most changes in the eigenvalue distribution of the high-frequency modes. The corresponding eigenvectors suggest that the changes are due to areas associated with language processing, attention, and emotional regulation. To further investigate these changes, we can look at the average eigenvector during the baselines and compare it to meditation. Figure 4-8 shows the most active electrodes for the high-frequency dynamics. Electrode 2 and 29 seem to increase in activity during meditation.

Furthermore, we can investigate changes in involved regions on an individual level. Appendix A-2 shows the eigenvector for each participant, corresponding to the highest frequency eigenvalue for each time step. We can see a shift from one region to another over time for multiple participants. However, the changes do not necessarily occur when transitioning from baseline to meditation. Nevertheless, on a subject-specific level, the eigenvectors could inform us where changes occur during meditation and when. The particular electrodes associated with particular functions suggest what changed in the neural activity.

For example, the pre-frontal electrode 30 is more active during meditation for participants 2, 16, 19, and 22. Since electrode 30 is commonly associated with attention [36], these findings might suggest that the participants were paying attention to the audio-guided meditation or focusing on the task. Similarly, the activity of electrodes 24, 25, or 28 changes throughout the experiment for multiple participants. Studies have linked electrodes 24, 25, and 28 to emotional memory and emotional regulation [36]. Thus, activity changes could suggest emotional changes during the experiment.

Finally, we want to identify each participant's eight most active electrodes to monitor subject-specific changes. Table 4-4 gives the results per participant. The electrodes are ordered from left to right in decreasing order of involvement.

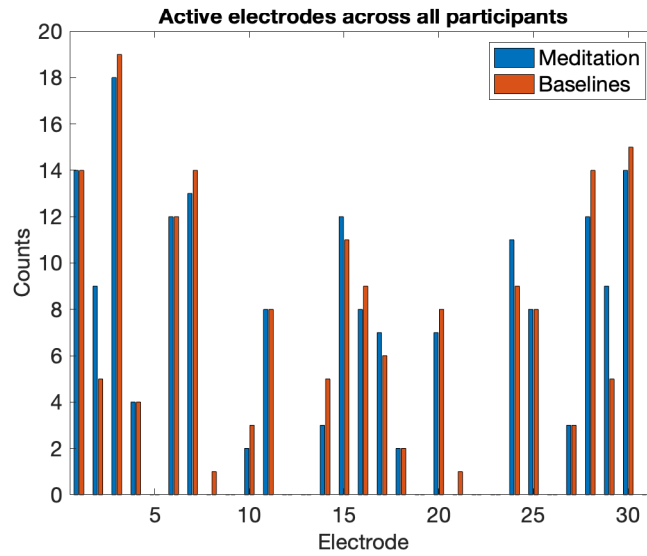


Figure 4-8: Number of times each electrode occurred in the most active electrode sets for the high frequency mode during meditation and baselines.

| | | | | | | | | |
|----|----|----|----|----|----|----|----|----|
| 1 | 3 | 7 | 6 | 28 | 30 | 11 | 1 | 17 |
| 2 | 3 | 1 | 30 | 2 | 24 | 11 | 29 | 4 |
| 3 | 15 | 7 | 16 | 11 | 24 | 17 | 20 | 1 |
| 4 | 3 | 6 | 2 | 7 | 1 | 4 | 28 | 27 |
| 5 | 24 | 3 | 28 | 2 | 25 | 7 | 1 | 4 |
| 6 | 17 | 16 | 15 | 30 | 1 | 18 | 20 | 3 |
| 7 | 3 | 29 | 1 | 24 | 30 | 4 | 6 | 20 |
| 8 | 15 | 11 | 6 | 28 | 14 | 3 | 16 | 25 |
| 9 | 7 | 3 | 6 | 28 | 30 | 10 | 1 | 29 |
| 10 | 25 | 7 | 2 | 6 | 1 | 29 | 30 | 28 |
| 11 | 3 | 24 | 7 | 15 | 16 | 11 | 14 | 10 |
| 12 | 15 | 16 | 7 | 17 | 20 | 30 | 14 | 3 |
| 13 | 17 | 14 | 3 | 15 | 16 | 20 | 11 | 28 |
| 14 | 7 | 6 | 28 | 3 | 24 | 25 | 27 | 8 |
| 15 | 28 | 3 | 30 | 6 | 20 | 7 | 1 | 15 |
| 16 | 11 | 30 | 3 | 15 | 28 | 6 | 20 | 25 |
| 17 | 7 | 2 | 30 | 29 | 3 | 17 | 1 | 28 |
| 18 | 4 | 3 | 24 | 30 | 28 | 7 | 25 | 17 |
| 19 | 3 | 15 | 25 | 30 | 6 | 29 | 16 | 27 |
| 20 | 24 | 1 | 3 | 25 | 15 | 7 | 6 | 28 |
| 21 | 7 | 28 | 30 | 6 | 25 | 15 | 1 | 10 |
| 22 | 24 | 30 | 1 | 11 | 3 | 20 | 28 | 7 |

Table 4-4: Most active electrodes for each participant corresponding to the high frequency mode. The electrodes are ordered from left to right in decreasing order of involvement.

4-4 Dynamic system analysis using a subset of the sensors

The dynamic systems analysis findings suggest that the changes in EEG dynamics are subject-specific. Therefore, we want to investigate whether a personalized subset of electrodes is more sensitive to changes than the standard 32-electrode set. To test the effect of the selection of electrodes, we perform the same analysis as before. However, instead of using all 32 electrodes, we simulate the scenario in which we only have access to specific electrodes. We fit an AR(1) system to the electrodes, which results in a smaller evolution matrix. For example, if we use eight electrodes, $A \in \mathbb{R}^{8 \times 8}$. Consequently, we will have eight eigenvalue-eigenvector pairs for each time step rather than 32. We perform the same tests as before to check for changes in the eigenvalue distribution.

Furthermore, we compare the changes detected by a personalized subset of electrodes to subsets comparable to standard wearable EEG headsets. First, we would like to compare it to Muse [8], a headset designed to monitor meditation. However, Muse does not use electrodes from the standard 10-20 electrode configuration for 32 electrodes but contains sensors from the configuration for 64 electrodes. Therefore, we selected four neighboring sensors to perform the analysis. Second, we compare the analysis to three wearable EEG headsets by Emotiv [38] by selecting the same electrodes used in their configuration. The three headsets contain two, seven, and fourteen electrodes, respectively.

Figure 4-9 shows the four headsets and the electrode selection used in further analysis. For Muse, the positions of the electrodes used in the headset are indicated with green circles. Appendix B shows each subset's eigenvalues distribution for participant 1 and the KS tests' results. Table 4-5 provides an overview of the test results for each subset by indicating the number of participants for whom the KS test recognizes a difference in the distribution for each test.

The personalized headset can detect changes during meditation for nineteen out of the twenty-two participants. Out of all the standard headsets, the electrode selection based on the Muse headset is most sensitive to changes among participants for this particular analysis. Notably, all subsets of electrodes detect changes for more participants than the complete set of 32 electrodes. Each set appears to be more sensitive to the changes in neural activity during meditation.

| | Test 1 | Test 2 | Test 3 | Test 4 | Test 5 | Test 6 |
|-----------------------------|--------|--------|--------|--------|--------|--------|
| Personalized headset | 19 | 11 | 9 | 18 | 7 | 12 |
| Muse | 13 | 2 | 10 | 10 | 4 | 5 |
| Emotiv 1 | 9 | 1 | 8 | 10 | 3 | 6 |
| Emotiv 2 | 10 | 3 | 8 | 8 | 4 | 3 |
| Emotiv 3 | 12 | 7 | 5 | 6 | 3 | 3 |

Table 4-5: Overview of the test results for different subsets of electrodes.

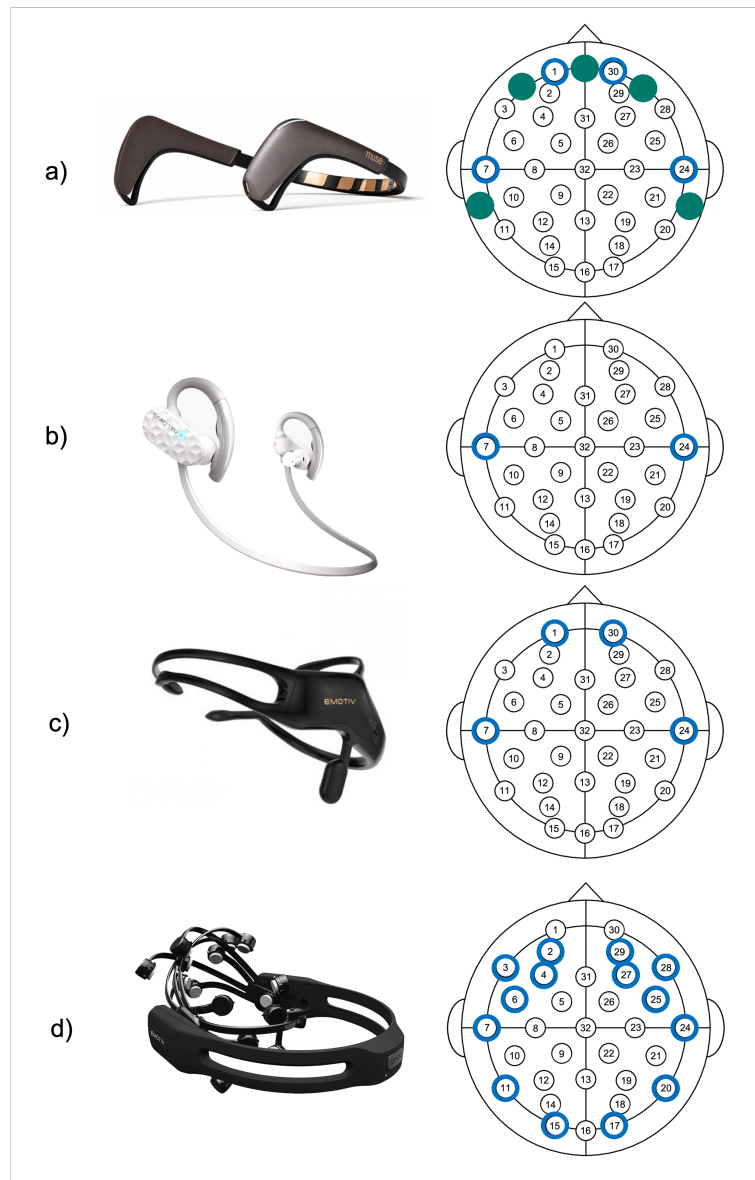


Figure 4-9: The subset of electrodes used for analysis are circled in blue per wearable EEG headset: a) Muse, the green circles indicate the positions of the original electrodes; b) Emotiv 1; c) Emotiv 2; and d) Emotiv 3.

4-5 Alpha power analysis

This section briefly highlights the results of the alpha power analysis. To assess changes during meditation, we calculated the power spectrum for both baselines and the meditation. Then, we determined the average power across the alpha bandwidth (8-12 Hz). Lastly, for each participant, the alpha power is normalized to compare results among participants. Figure 4-10 shows the alpha power difference (baselines - meditation) per electrode and for each participant. The average difference across all participants is close to zero at all locations. That is, the average absolute difference is smaller than 10^{-15}). There is not one region that shows apparent differences in alpha power for all participants.

To visualize the changes per participant, Figure 4-11 shows the same results grouped per participant. For some participants, the alpha power seems to vary during meditation, whereas the changes are minimal for others. For example, participant 21 shows a decrease for nearly all electrodes. However, there are also participants for whom the change is mostly positive, such as participants 13 and 20. Therefore, the alpha power analysis affirms that the changes during meditation are personal and not uniform across all participants. However, groups of participants with an increasing or decreasing alpha power do not necessarily have similar changes in dynamics as assessed with the dynamic systems approach.

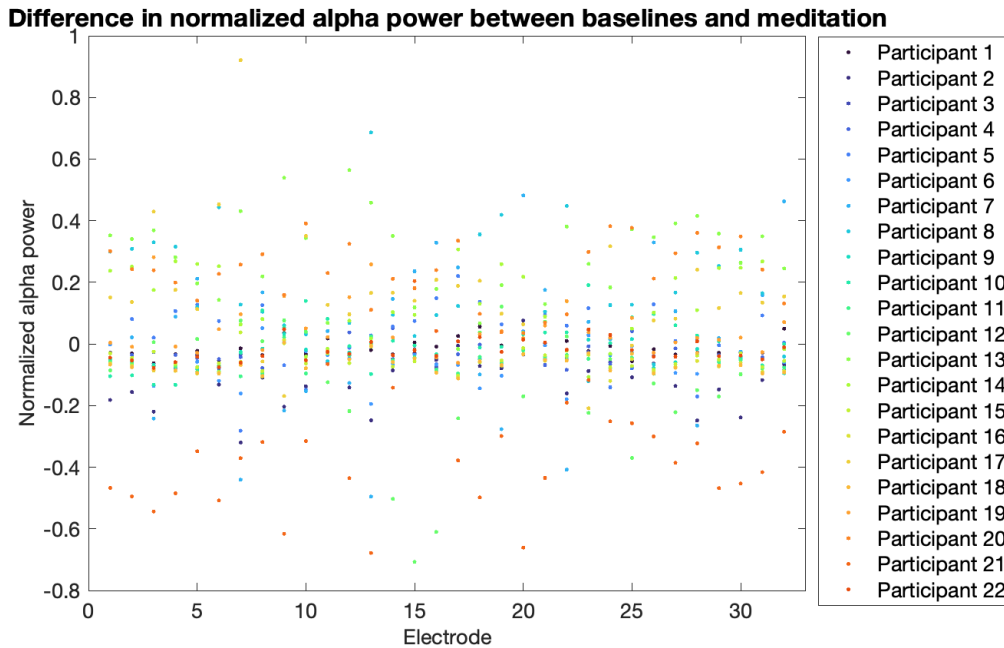


Figure 4-10: Difference in normalized alpha power per participant grouped per electrode.

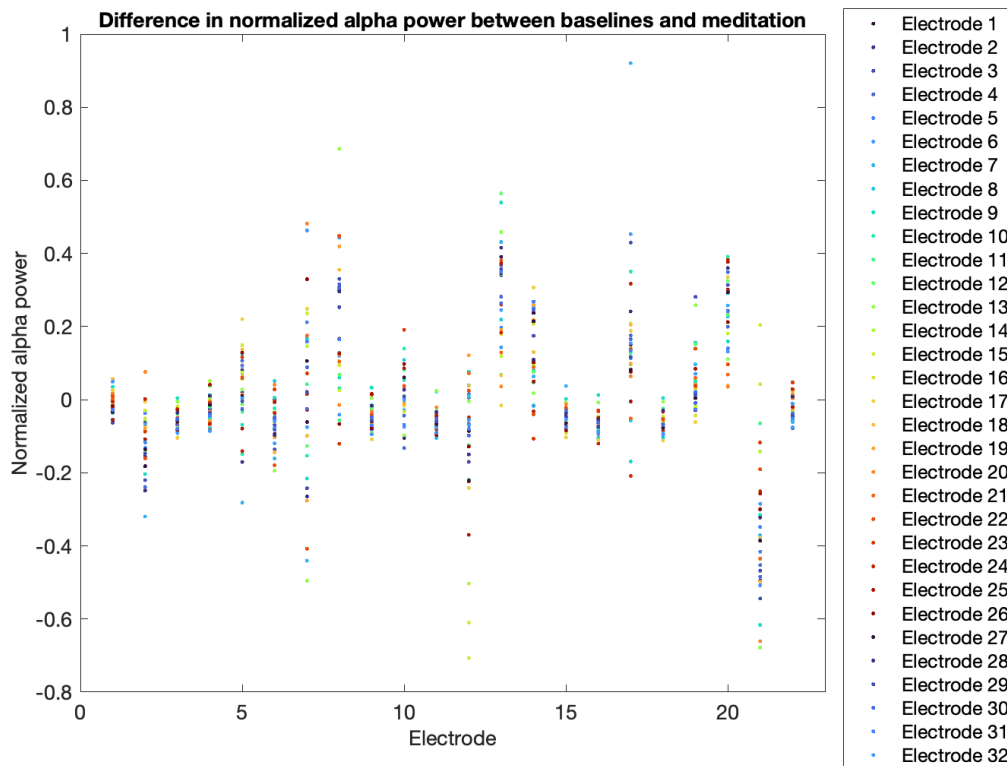


Figure 4-11: Difference in normalized alpha power per electrode grouped per participant.

4-6 SAM questionnaire

The final results section discusses the results of the questionnaires. Participants ranked their emotions on the *Self-Assessment Manikin* (SAM) scale. Table 4-6 shows each participant's valance and arousal scores before and after meditation and the difference. Generally, participants felt calmer after meditation. The majority of participants did not note a difference in their valance scores. However, some participants noted either a positive or a negative difference.

If we define effective meditation as feeling calmer, seventeen people benefited from this meditation session. However, this definition fails to capture people who already felt very calm before meditation and experienced little or no change, such as participants 7, 8, and 12. Additionally, a definition of effective meditation could be an increase in valance score. Six out of twenty-two participants ranked their emotions as more positive after meditation. With either definition, participants 6, 9, and 22 did not appear to benefit from the meditation. Regarding the different definitions, there appears to be no relationship between the meditation's effectiveness and the changes assessed with the dynamic systems approach.

| | Pre-meditation | | Post-meditation | | Difference | |
|-----------|----------------|---------|-----------------|---------|------------|---------|
| | Valance | Arousal | Valance | Arousal | Valance | Arousal |
| 1 | 6 | 4 | 6 | 1 | 0 | -3 |
| 2 | 7 | 3 | 8 | 3 | 1 | 0 |
| 3 | 7 | 4 | 7 | 3 | 0 | -1 |
| 4 | 8 | 3 | 8 | 2 | 0 | -1 |
| 5 | 7 | 3 | 7 | 2 | 0 | -1 |
| 6 | 6 | 3 | 4 | 3 | -2 | 0 |
| 7 | 9 | 1 | 9 | 2 | 0 | 1 |
| 8 | 9 | 1 | 9 | 1 | 0 | 0 |
| 9 | 7 | 3 | 6 | 3 | -1 | 0 |
| 10 | 7 | 7 | 5 | 6 | -2 | -1 |
| 11 | 7 | 2 | 7 | 1 | 0 | -1 |
| 12 | 7 | 1 | 7 | 1 | 0 | 0 |
| 13 | 8 | 2 | 9 | 1 | 1 | -1 |
| 14 | 7 | 3 | 8 | 2 | 1 | -1 |
| 15 | 7 | 6 | 6 | 1 | -1 | -5 |
| 16 | 8 | 3 | 8 | 2 | 0 | -1 |
| 17 | 5 | 2 | 9 | 1 | 4 | -1 |
| 18 | 7 | 3 | 7 | 1 | 0 | -2 |
| 19 | 7 | 3 | 7 | 1 | 0 | -2 |
| 20 | 6 | 4 | 7 | 2 | 1 | -2 |
| 21 | 4 | 6 | 7 | 2 | 3 | -4 |
| 22 | 6 | 5 | 6 | 5 | 0 | 0 |

Table 4-6: Valance and arousal scores from the SAM questionnaire for each participant, pre-meditation, post-meditation, and the difference.

Conclusions & discussion

This section lists the main findings of this thesis and several issues that limited the study, both in the experiment design and data analysis. In addition, I provide recommendations for future studies following this thesis.

Findings This thesis explored the hypothesis that a dynamic feature distinguishes meditation from an eyes-closed resting baseline. The dynamic systems analysis found changes in the eigenvalue distribution for each participant. However, the changes were not consistent among participants. Across all participants, the (pre-)frontal, visual, and temporal regions were the most involved in the changing dynamics. During meditation, activity increased mainly in the (pre-)frontal electrodes 1, 2, 29, and 30. The corresponding area in the brain is associated with attention [36]. Therefore, the changing activity pattern may indicate that the participants were paying attention to the audio guide or focused on the task they had to perform. Regulation of attention and emotion is a central component of meditation [6]. Therefore, the particular frontal activity may be specific to meditation and different from other forms of concentration. On a subject-specific level, the eigenvectors capture shifts in the active regions for some people. The particular electrodes involved might suggest personal changes in neural dynamics, possibly due to the meditation.

Experiment design Several issues limited the experiment design of this thesis. First, the participant group only consisted of twenty-two participants and was not an accurate representation of the population of people who could practice meditation. For example, the number of men and women involved in the study was not balanced. Although the participants varied in age, most participants were older than 60 or younger than 30 years old. In addition, participants may have signed up because they were particularly enthusiastic or skeptical about meditation and may have had previous biases that influenced the results. Therefore, observations from this study might not generalize to other studies on meditation.

Secondly, the changes studied in this thesis were limited to differences between the meditation and baselines. However, it is possible that a participant only meditated for a part of the

meditation session or did not meditate. Inherent to studies concerning meditation is that it is hard for a participant to define what meditation is, especially for people naive to meditation. Instead, this study focussed on the effects of meditation by evaluating the participants' emotions. Throughout the session, the participant could not indicate their emotion or whether they were meditating. Therefore, any mood changes are attributed to changes throughout the entire session.

Third, the observed dynamic changes are not necessarily due to meditation. The meditation was audio-guided, whereas both baseline measurements were silent. Therefore, changes in language processing areas could be due to spoken instructions. Besides, a circumstance we did not monitor could influence the EEG measurements, such as if the participants were right or left-handed. We cannot relate an imbalance in the activity of the left and right hemispheres to left or right-handedness. Moreover, we cannot exclude the possibility that previous activities affected this result, such as the Sing-a-Song stress test before the meditation. Even though the activities did not happen right after each other, it could affect the initial arousal score.

Future studies that build upon this thesis could improve several experimental design factors. First, a future study could design an experiment with a control condition in addition to rest to compare the findings during meditation. For example, the participants could perform a control exercise during which they follow an audio guide to perform a particular task. Such a setting allows for comparing the attention-related changes during meditation and another control task. On the other hand, the study could focus on an unguided meditation to reduce the differences in language processing-related neural activity. Monitoring experienced meditators might be more convenient in the case of unguided meditation.

Furthermore, a future study might explore different subjective ratings. An advantage of the SAM questionnaire is that it is relatively easy to understand and, therefore, suitable for a multifaceted study with participants naive to meditation. However, it does not explicitly monitor meditation. Therefore, a specialized questionnaire might be better suited to capture the effectiveness of meditation. Moreover, a future study might explore shorter meditation sessions where the participant answers the questionnaire more frequently.

Data analysis Besides experimental limitations, the analytical approach affects the results. We approximate the EEG data on a short time frame with a linear model, even though the data is nonlinear. It should be noted that the analysis is purely an analytical tool to monitor changes in a linear approximation of the data and cannot infer any information on underlying neural dynamics. This application is one of the first to apply the dynamic systems analysis to EEG data. To verify the validity of the approach, one could apply it to a more elaborately studied data set. Thus, we could compare the dynamic systems analysis to a more conventional approach with established results.

Finally, comparing different subsets of electrodes should only be regarded as a theoretical experiment. First, the Muse headset does not use the same electrodes, and the algorithm the Muse app uses to analyze the data is unknown. In addition, wearable EEG headsets use different technologies than our experiment. For example, wearable devices use dry EEG technology, whereas our experiment used a saline solution to connect the electrodes to the scalp. Therefore, comparing their performance can only indicate the impact of the location of the electrodes using the dynamic systems analysis. A future study could use the actual headsets to collect the data and compare the results to Muse's performance indicators.

Appendix A

Eigenvalue-eigenvector decomposition

A-1 Eigenvalue distribution test results

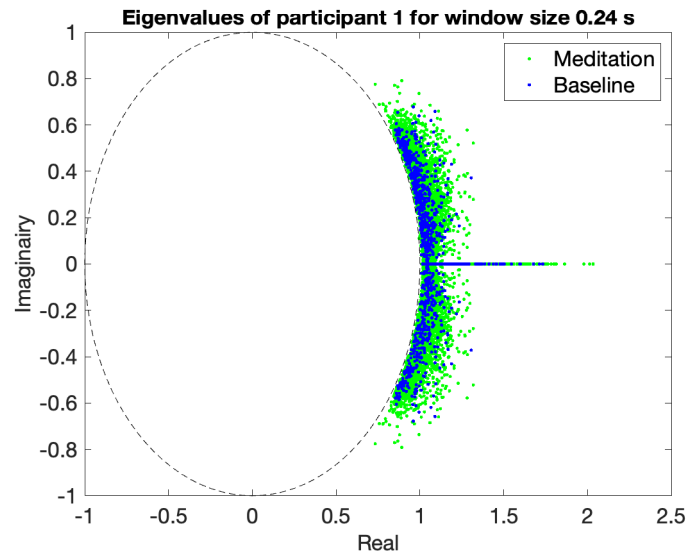


Figure A-1: High magnitude eigenvalues of participant 1 plotted on the complex plane.

| | h_1 | p_1 | h_2 | p_2 | h_3 | p_3 | h_4 | p_4 | h_5 | p_5 | h_6 | p_6 |
|----|-------|------------|-------|------------|-------|------------|-------|------------|-------|------------|-------|------------|
| 1 | 1 | 2.7965E-02 | 0 | 1.5566E-01 | 1 | 2.7881E-02 | 1 | 2.7465E-03 | 0 | 7.7144E-01 | 1 | 1.3732E-03 |
| 2 | 0 | 1.1146E-01 | 0 | 9.2315E-02 | 0 | 4.0430E-01 | 1 | 2.6974E-02 | 0 | 3.8436E-01 | 1 | 1.3487E-02 |
| 3 | 0 | 6.6407E-02 | 0 | 4.4305E-01 | 1 | 3.4034E-02 | 0 | 9.5304E-02 | 0 | 3.7580E-01 | 0 | 6.5292E-02 |
| 4 | 0 | 6.0884E-02 | 0 | 3.8780E-01 | 0 | 5.3393E-02 | 1 | 4.6412E-03 | 0 | 5.9723E-01 | 1 | 2.3206E-03 |
| 5 | 0 | 1.1655E-01 | 0 | 4.6984E-01 | 0 | 5.8289E-02 | 0 | 8.4951E-02 | 0 | 6.7449E-02 | 0 | 3.2891E-01 |
| 6 | 1 | 1.6068E-02 | 1 | 8.0342E-03 | 0 | 3.2136E-01 | 0 | 1.2058E-01 | 0 | 3.5708E-01 | 0 | 7.2051E-02 |
| 7 | 0 | 1.7135E-01 | 0 | 2.3133E-01 | 0 | 1.8996E-01 | 0 | 2.0300E-01 | 0 | 1.2095E-01 | 0 | 6.6668E-01 |
| 8 | 1 | 4.2982E-02 | 0 | 2.9331E-01 | 1 | 2.5473E-02 | 0 | 2.1997E-01 | 0 | 5.7270E-01 | 0 | 1.3032E-01 |
| 9 | 1 | 4.3325E-02 | 0 | 2.5355E-01 | 1 | 2.8009E-02 | 1 | 4.9064E-02 | 1 | 3.1039E-02 | 0 | 5.2963E-01 |
| 10 | 1 | 7.7986E-03 | 0 | 3.5054E-01 | 1 | 3.8993E-03 | 0 | 8.8167E-02 | 0 | 1.9663E-01 | 0 | 8.8404E-02 |
| 11 | 0 | 1.7650E-01 | 0 | 1.9643E-01 | 0 | 2.1749E-01 | 1 | 1.2301E-02 | 1 | 6.1506E-03 | 0 | 3.8594E-01 |
| 12 | 0 | 9.1253E-02 | 0 | 3.6255E-01 | 1 | 4.6504E-02 | 0 | 6.3969E-02 | 0 | 7.8078E-02 | 0 | 1.2561E-01 |
| 13 | 1 | 3.6978E-05 | 0 | 9.0152E-01 | 1 | 1.8489E-05 | 0 | 1.1532E-01 | 0 | 4.7129E-01 | 0 | 8.5643E-02 |
| 14 | 0 | 9.9056E-02 | 0 | 6.3433E-02 | 0 | 3.9121E-01 | 0 | 1.4171E-01 | 0 | 1.1159E-01 | 0 | 2.8014E-01 |
| 15 | 1 | 6.2094E-03 | 0 | 2.4816E-01 | 1 | 3.1047E-03 | 1 | 2.5464E-04 | 0 | 6.6949E-01 | 1 | 1.2732E-04 |
| 16 | 0 | 1.1684E-01 | 0 | 7.7378E-02 | 0 | 4.9280E-01 | 0 | 1.4885E-01 | 0 | 2.1958E-01 | 0 | 1.4470E-01 |
| 17 | 0 | 8.0675E-02 | 1 | 4.4244E-02 | 0 | 4.7923E-01 | 0 | 1.1315E-01 | 0 | 5.8848E-02 | 0 | 2.9201E-01 |
| 18 | 1 | 4.8893E-02 | 1 | 2.6869E-02 | 0 | 6.0924E-01 | 0 | 5.9270E-02 | 0 | 4.3430E-01 | 1 | 2.9636E-02 |
| 19 | 0 | 1.1336E-01 | 0 | 2.2830E-01 | 0 | 8.9249E-02 | 0 | 1.3857E-01 | 0 | 3.0915E-01 | 0 | 1.4961E-01 |
| 20 | 0 | 1.8786E-01 | 0 | 1.0804E-01 | 0 | 4.6849E-01 | 1 | 3.4816E-04 | 1 | 1.8752E-04 | 0 | 1.2325E-01 |
| 21 | 1 | 4.6761E-02 | 0 | 2.9207E-01 | 1 | 2.6556E-02 | 0 | 1.2626E-01 | 0 | 3.9164E-01 | 0 | 1.0369E-01 |
| 22 | 1 | 2.6315E-02 | 0 | 3.0820E-01 | 1 | 1.8164E-02 | 0 | 7.6829E-02 | 0 | 2.0277E-01 | 0 | 1.1948E-01 |

Table A-1: KS test results comparing the CDF of the magnitude and the frequency of the high magnitude eigenvalues during meditation to the baseline eigenvalues.

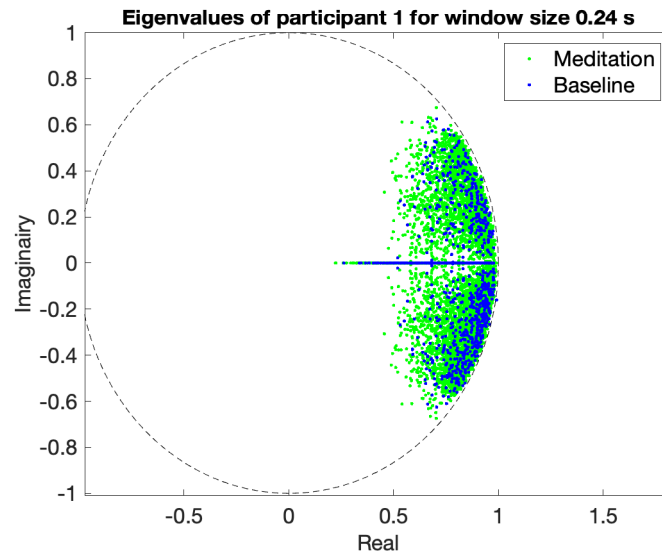


Figure A-2: Low magnitude eigenvalues of participant 1 plotted on the complex plane.

| | h_1 | p_1 | h_2 | p_2 | h_3 | p_3 | h_4 | p_4 | h_5 | p_5 | h_6 | p_6 |
|----|-------|------------|-------|------------|-------|------------|-------|------------|-------|------------|-------|------------|
| 1 | 0 | 9.6118E-02 | 0 | 9.2559E-02 | 0 | 2.5658E-01 | 0 | 1.9319E-01 | 0 | 2.0230E-01 | 0 | 2.5606E-01 |
| 2 | 1 | 1.2471E-02 | 0 | 3.8962E-01 | 1 | 6.2353E-03 | 0 | 7.4864E-02 | 1 | 4.2023E-02 | 0 | 5.0380E-01 |
| 3 | 0 | 5.4673E-02 | 1 | 3.2543E-02 | 0 | 5.6715E-01 | 0 | 1.2335E-01 | 0 | 2.6104E-01 | 0 | 1.0114E-01 |
| 4 | 1 | 2.7876E-02 | 1 | 2.4322E-02 | 0 | 1.3082E-01 | 0 | 1.6406E-01 | 0 | 2.7216E-01 | 0 | 1.9925E-01 |
| 5 | 1 | 9.3121E-03 | 0 | 7.5599E-01 | 1 | 4.6560E-03 | 1 | 5.4783E-03 | 1 | 2.9108E-03 | 0 | 1.2887E-01 |
| 6 | 1 | 2.7853E-02 | 0 | 1.3490E-01 | 1 | 3.7632E-02 | 1 | 4.6757E-03 | 1 | 2.3378E-03 | 0 | 7.7264E-01 |
| 7 | 1 | 6.1462E-03 | 1 | 3.0731E-03 | 0 | 6.1327E-01 | 1 | 2.7371E-03 | 0 | 3.8928E-01 | 1 | 1.5838E-03 |
| 8 | 1 | 2.0433E-03 | 1 | 1.1032E-03 | 0 | 3.7812E-01 | 0 | 1.3636E-01 | 0 | 2.2541E-01 | 0 | 1.9301E-01 |
| 9 | 1 | 1.2213E-02 | 0 | 3.2137E-01 | 1 | 6.7088E-03 | 1 | 9.7919E-03 | 1 | 5.0602E-03 | 0 | 5.1862E-01 |
| 10 | 0 | 1.6645E-01 | 0 | 2.0675E-01 | 0 | 1.8757E-01 | 0 | 9.0381E-02 | 0 | 7.8678E-02 | 0 | 1.6232E-01 |
| 11 | 0 | 2.1093E-01 | 0 | 2.3316E-01 | 0 | 2.2685E-01 | 0 | 1.7346E-01 | 0 | 3.8085E-01 | 0 | 1.6878E-01 |
| 12 | 1 | 1.2534E-02 | 0 | 3.7005E-01 | 1 | 6.7009E-03 | 0 | 5.1382E-02 | 0 | 6.3225E-02 | 0 | 1.8877E-01 |
| 13 | 1 | 3.3205E-02 | 1 | 1.8392E-02 | 0 | 3.9891E-01 | 0 | 1.7059E-01 | 0 | 2.6907E-01 | 0 | 2.2017E-01 |
| 14 | 1 | 2.6862E-02 | 0 | 6.6830E-01 | 1 | 1.3431E-02 | 1 | 1.1881E-02 | 1 | 5.9403E-03 | 0 | 5.0386E-01 |
| 15 | 1 | 2.4322E-02 | 1 | 1.2161E-02 | 0 | 6.0658E-01 | 1 | 4.6137E-02 | 1 | 3.0273E-02 | 0 | 1.5559E-01 |
| 16 | 1 | 4.1956E-02 | 1 | 2.2169E-02 | 0 | 7.5453E-01 | 1 | 2.1574E-02 | 0 | 7.6102E-01 | 1 | 1.2552E-02 |
| 17 | 0 | 2.4267E-01 | 0 | 5.4682E-01 | 0 | 1.8289E-01 | 0 | 6.8776E-02 | 1 | 4.1006E-02 | 0 | 5.0945E-01 |
| 18 | 0 | 7.1329E-02 | 0 | 8.3049E-01 | 1 | 3.5666E-02 | 0 | 1.3293E-01 | 0 | 8.0026E-02 | 0 | 4.4373E-01 |
| 19 | 1 | 1.7612E-02 | 0 | 5.4537E-01 | 1 | 8.8061E-03 | 1 | 1.5539E-02 | 1 | 8.5444E-03 | 0 | 2.7638E-01 |
| 20 | 1 | 4.0483E-02 | 1 | 2.0241E-02 | 0 | 7.3291E-01 | 1 | 1.2884E-03 | 1 | 6.4419E-04 | 0 | 6.0573E-01 |
| 21 | 0 | 7.6240E-02 | 0 | 4.6118E-01 | 0 | 5.0840E-02 | 0 | 1.0947E-01 | 0 | 8.5238E-02 | 0 | 4.1464E-01 |
| 22 | 1 | 5.8963E-03 | 0 | 4.9838E-01 | 1 | 2.9482E-03 | 0 | 1.8435E-01 | 0 | 3.0082E-01 | 0 | 2.9309E-01 |

Table A-2: KS test results comparing the CDF of the magnitude and the frequency of the low magnitude eigenvalues during meditation to the baseline eigenvalues.

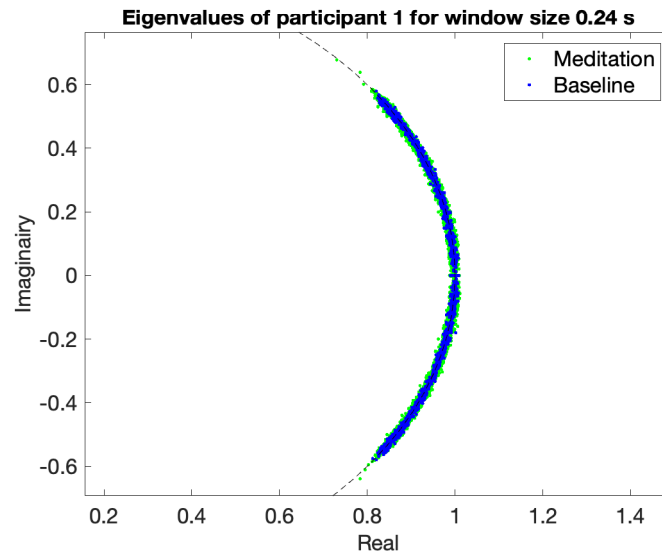


Figure A-3: Middle magnitude eigenvalues of participant 1 plotted on the complex plane.

| | h_1 | p_1 | h_2 | p_2 | h_3 | p_3 | h_4 | p_4 | h_5 | p_5 | h_6 | p_6 |
|----|-------|------------|-------|------------|-------|------------|-------|------------|-------|------------|-------|------------|
| 1 | 1 | 2.7271E-02 | 0 | 4.8794E-01 | 1 | 1.3636E-02 | 1 | 3.9793E-03 | 0 | 4.3471E-01 | 1 | 1.9896E-03 |
| 2 | 0 | 1.4795E-01 | 0 | 2.4533E-01 | 0 | 1.6341E-01 | 0 | 7.7607E-02 | 0 | 2.7013E-01 | 0 | 5.2535E-02 |
| 3 | 1 | 1.6250E-02 | 1 | 1.4546E-02 | 0 | 2.1165E-01 | 1 | 3.2435E-04 | 1 | 1.6218E-04 | 0 | 9.0243E-01 |
| 4 | 1 | 2.4087E-02 | 1 | 1.4797E-02 | 0 | 2.7052E-01 | 0 | 1.3243E-01 | 0 | 1.1304E-01 | 0 | 3.3910E-01 |
| 5 | 1 | 3.2794E-02 | 1 | 1.6397E-02 | 0 | 6.7314E-01 | 0 | 1.8011E-01 | 0 | 1.1814E-01 | 0 | 4.3379E-01 |
| 6 | 0 | 1.9214E-01 | 0 | 2.6316E-01 | 0 | 1.8377E-01 | 1 | 1.8511E-03 | 1 | 9.2556E-04 | 0 | 9.4168E-01 |
| 7 | 0 | 1.1752E-01 | 0 | 9.5656E-02 | 0 | 4.2999E-01 | 0 | 7.0726E-02 | 0 | 6.0609E-02 | 0 | 1.8851E-01 |
| 8 | 1 | 2.0179E-02 | 0 | 8.1817E-01 | 1 | 1.0089E-02 | 0 | 7.4321E-02 | 0 | 5.4038E-01 | 1 | 4.4826E-02 |
| 9 | 0 | 2.1151E-01 | 0 | 3.8637E-01 | 0 | 1.9988E-01 | 0 | 2.0990E-01 | 0 | 1.9083E-01 | 0 | 2.6252E-01 |
| 10 | 1 | 2.7503E-02 | 0 | 5.4477E-01 | 1 | 1.4692E-02 | 1 | 1.1746E-02 | 0 | 3.9308E-01 | 1 | 6.0043E-03 |
| 11 | 0 | 3.1074E-01 | 0 | 3.1524E-01 | 0 | 4.0985E-01 | 1 | 1.5511E-02 | 1 | 7.7556E-03 | 0 | 8.4162E-01 |
| 12 | 0 | 1.3565E-01 | 0 | 8.2651E-02 | 0 | 6.0615E-01 | 1 | 1.3412E-02 | 0 | 6.1229E-01 | 1 | 6.7060E-03 |
| 13 | 0 | 2.2366E-01 | 0 | 4.9120E-01 | 0 | 1.6121E-01 | 1 | 3.6338E-04 | 1 | 1.8169E-04 | 0 | 8.2370E-01 |
| 14 | 1 | 1.4103E-02 | 1 | 1.0334E-02 | 0 | 2.6367E-01 | 0 | 1.5513E-01 | 0 | 4.0844E-01 | 0 | 8.6064E-02 |
| 15 | 0 | 1.2195E-01 | 0 | 5.6911E-01 | 0 | 7.4052E-02 | 0 | 5.5857E-02 | 1 | 3.2577E-02 | 0 | 5.0418E-01 |
| 16 | 0 | 5.6177E-02 | 0 | 1.3019E-01 | 0 | 6.7979E-02 | 1 | 1.4561E-03 | 1 | 8.1039E-04 | 0 | 2.1073E-01 |
| 17 | 1 | 6.5324E-03 | 0 | 5.6711E-01 | 1 | 3.6068E-03 | 0 | 5.5396E-02 | 0 | 1.6853E-01 | 0 | 5.1287E-02 |
| 18 | 1 | 1.3189E-02 | 0 | 1.6226E-01 | 1 | 1.1615E-02 | 1 | 4.3261E-02 | 1 | 2.9291E-02 | 0 | 3.0342E-01 |
| 19 | 1 | 1.7556E-02 | 0 | 7.2625E-01 | 1 | 8.7781E-03 | 1 | 3.8795E-02 | 1 | 4.1099E-02 | 0 | 7.1683E-02 |
| 20 | 0 | 1.0028E-01 | 0 | 7.2546E-02 | 0 | 3.1102E-01 | 0 | 1.3370E-01 | 0 | 3.8228E-01 | 0 | 9.2012E-02 |
| 21 | 1 | 4.1441E-04 | 1 | 2.0720E-04 | 0 | 8.5642E-01 | 0 | 2.9230E-01 | 0 | 2.1016E-01 | 0 | 5.3581E-01 |
| 22 | 0 | 1.6405E-01 | 0 | 3.0231E-01 | 0 | 2.2340E-01 | 0 | 8.3318E-02 | 0 | 2.2008E-01 | 0 | 5.9833E-02 |

Table A-3: KS test results comparing the CDF of the magnitude and the frequency of the middle magnitude eigenvalues during meditation to the baseline eigenvalues.

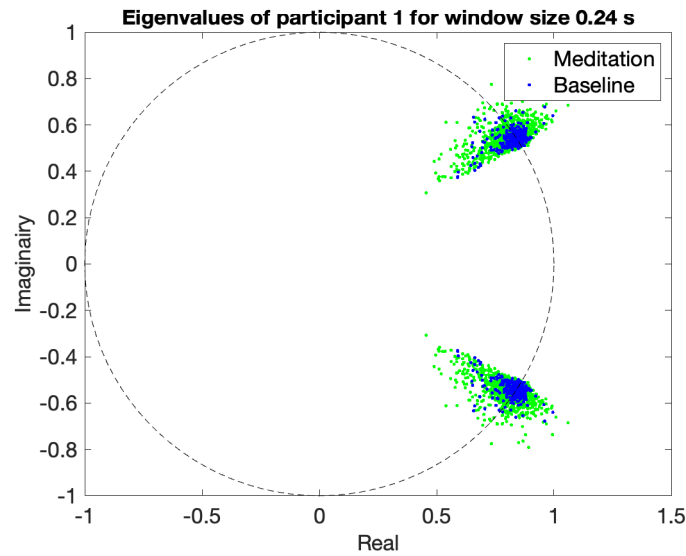


Figure A-4: High frequency eigenvalues of participant 1 plotted on the complex plane.

| | h_1 | p_1 | h_2 | p_2 | h_3 | p_3 | h_4 | p_4 | h_5 | p_5 | h_6 | p_6 |
|----|-------|------------|-------|------------|-------|------------|-------|------------|-------|------------|-------|------------|
| 1 | 0 | 7.6133E-02 | 0 | 7.3424E-01 | 1 | 3.9926E-02 | 1 | 3.4764E-02 | 0 | 1.3486E-01 | 0 | 5.2034E-02 |
| 2 | 1 | 2.1306E-02 | 1 | 1.2433E-02 | 0 | 2.5957E-01 | 1 | 7.7177E-03 | 1 | 3.8589E-03 | 0 | 9.3951E-01 |
| 3 | 1 | 2.1486E-02 | 1 | 1.2888E-02 | 0 | 4.6784E-01 | 1 | 2.4827E-02 | 1 | 1.8260E-02 | 0 | 3.0417E-01 |
| 4 | 0 | 8.4763E-02 | 0 | 1.2485E-01 | 0 | 1.5597E-01 | 0 | 1.4236E-01 | 0 | 1.0511E-01 | 0 | 3.0738E-01 |
| 5 | 1 | 6.5032E-03 | 1 | 3.2516E-03 | 0 | 6.1602E-01 | 1 | 5.0284E-03 | 1 | 2.5142E-03 | 0 | 4.9825E-01 |
| 6 | 0 | 1.4029E-01 | 0 | 1.2474E-01 | 0 | 3.7754E-01 | 1 | 1.7228E-02 | 0 | 1.3977E-01 | 1 | 1.2740E-02 |
| 7 | 1 | 2.9622E-02 | 1 | 1.5762E-02 | 0 | 4.2774E-01 | 0 | 1.5441E-01 | 0 | 2.6917E-01 | 0 | 1.9980E-01 |
| 8 | 0 | 1.3182E-01 | 0 | 3.2727E-01 | 0 | 9.1244E-02 | 1 | 2.4353E-03 | 0 | 4.1587E-01 | 1 | 1.2177E-03 |
| 9 | 1 | 1.0779E-04 | 0 | 3.8801E-01 | 1 | 5.3896E-05 | 1 | 3.2433E-02 | 0 | 6.9074E-02 | 0 | 1.1030E-01 |
| 10 | 1 | 2.1054E-04 | 1 | 1.0527E-04 | 0 | 3.8843E-01 | 0 | 7.1500E-02 | 0 | 2.6186E-01 | 1 | 3.7368E-02 |
| 11 | 0 | 1.5404E-01 | 0 | 1.5825E-01 | 0 | 2.9530E-01 | 1 | 2.8391E-04 | 1 | 1.4195E-04 | 0 | 5.0733E-01 |
| 12 | 0 | 1.0812E-01 | 0 | 8.2075E-02 | 0 | 2.6093E-01 | 0 | 8.7459E-02 | 0 | 3.1869E-01 | 1 | 4.6834E-02 |
| 13 | 1 | 5.9281E-03 | 0 | 5.4755E-01 | 1 | 2.9641E-03 | 1 | 4.8541E-02 | 0 | 4.1313E-01 | 1 | 3.6461E-02 |
| 14 | 1 | 4.9056E-02 | 0 | 3.9231E-01 | 1 | 2.5211E-02 | 1 | 3.3514E-03 | 1 | 1.6757E-03 | 0 | 9.0491E-01 |
| 15 | 0 | 1.1137E-01 | 0 | 7.1530E-02 | 0 | 5.1694E-01 | 1 | 1.3500E-03 | 1 | 6.7502E-04 | 0 | 2.8482E-01 |
| 16 | 0 | 7.1996E-02 | 1 | 4.0798E-02 | 0 | 6.9461E-01 | 1 | 3.3848E-02 | 0 | 8.4420E-01 | 1 | 1.6924E-02 |
| 17 | 0 | 1.0336E-01 | 0 | 1.1577E-01 | 0 | 2.1018E-01 | 1 | 1.6516E-02 | 1 | 8.4799E-03 | 0 | 3.0091E-01 |
| 18 | 0 | 5.1011E-02 | 1 | 2.5506E-02 | 0 | 4.1420E-01 | 1 | 1.0971E-03 | 1 | 5.4854E-04 | 0 | 5.3042E-01 |
| 19 | 1 | 3.0468E-02 | 0 | 7.9191E-02 | 0 | 5.7458E-02 | 1 | 2.2903E-05 | 1 | 1.1451E-05 | 0 | 2.5577E-01 |
| 20 | 0 | 6.6822E-02 | 1 | 3.7511E-02 | 0 | 6.1769E-01 | 1 | 6.0057E-05 | 0 | 1.3116E-01 | 1 | 3.0029E-05 |
| 21 | 0 | 1.5232E-01 | 0 | 2.4370E-01 | 0 | 3.2317E-01 | 1 | 2.0373E-02 | 0 | 3.3877E-01 | 1 | 1.4923E-02 |
| 22 | 0 | 8.5709E-02 | 0 | 6.7246E-02 | 0 | 3.1587E-01 | 1 | 1.1360E-02 | 1 | 1.2455E-02 | 1 | 4.7709E-02 |

Table A-4: K-S test results comparing the CDF of the magnitude and the frequency of the eigenvalues during meditation to the baseline eigenvalues.

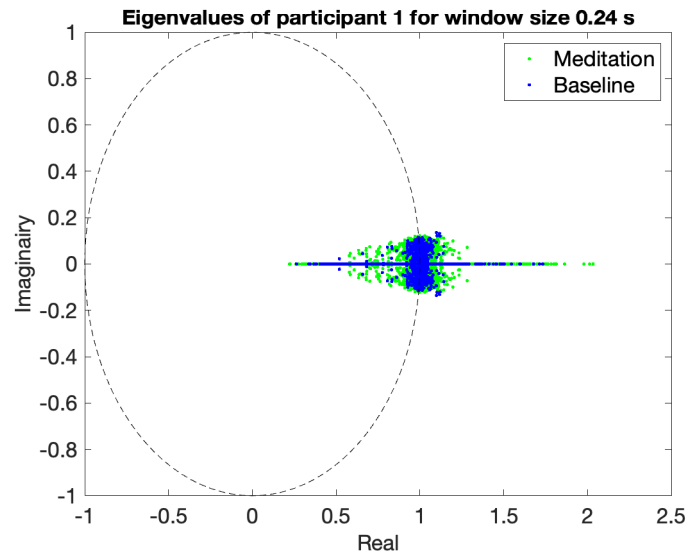


Figure A-5: Low frequency eigenvalues of participant 1 plotted on the complex plane.

| | h_1 | p_1 | h_2 | p_2 | h_3 | p_3 | h_4 | p_4 | h_5 | p_5 | h_6 | p_6 |
|----|-------|------------|-------|------------|-------|------------|-------|------------|-------|------------|-------|------------|
| 1 | 1 | 3.4234E-02 | 1 | 1.7117E-02 | 0 | 4.1324E-01 | 0 | 1.3708E-01 | 0 | 5.0293E-01 | 0 | 9.0313E-02 |
| 2 | 1 | 1.5891E-05 | 1 | 7.9457E-06 | 0 | 9.7745E-01 | 0 | 1.7038E-01 | 0 | 5.5883E-01 | 0 | 9.7332E-02 |
| 3 | 1 | 2.2602E-02 | 1 | 3.5455E-02 | 0 | 5.3656E-02 | 0 | 8.8858E-02 | 0 | 5.3638E-02 | 0 | 3.8101E-01 |
| 4 | 1 | 4.9680E-02 | 1 | 3.9177E-02 | 0 | 4.9583E-01 | 0 | 6.1855E-02 | 0 | 1.8371E-01 | 0 | 1.0596E-01 |
| 5 | 1 | 2.0097E-02 | 0 | 1.2310E-01 | 1 | 1.4495E-02 | 1 | 1.1342E-04 | 1 | 5.6710E-05 | 0 | 8.5804E-01 |
| 6 | 1 | 6.4191E-03 | 1 | 3.2095E-03 | 0 | 4.4095E-01 | 0 | 2.5292E-01 | 0 | 1.7158E-01 | 0 | 4.3224E-01 |
| 7 | 0 | 1.3086E-01 | 0 | 2.6014E-01 | 0 | 2.1622E-01 | 0 | 5.0277E-02 | 0 | 3.3483E-01 | 1 | 4.6579E-02 |
| 8 | 0 | 1.0415E-01 | 0 | 2.4931E-01 | 0 | 1.4142E-01 | 0 | 1.6357E-01 | 0 | 2.8823E-01 | 0 | 1.7971E-01 |
| 9 | 0 | 5.8738E-02 | 0 | 2.8015E-01 | 1 | 4.3395E-02 | 0 | 7.7226E-02 | 0 | 1.8227E-01 | 0 | 9.0416E-02 |
| 10 | 0 | 7.8055E-02 | 0 | 1.0065E-01 | 0 | 1.2783E-01 | 1 | 9.8914E-04 | 1 | 4.9457E-04 | 0 | 8.0052E-01 |
| 11 | 0 | 1.0204E-01 | 0 | 4.0430E-01 | 0 | 7.0008E-02 | 0 | 1.4269E-01 | 0 | 4.7805E-01 | 0 | 9.1002E-02 |
| 12 | 0 | 1.2033E-01 | 0 | 1.1008E-01 | 0 | 2.9402E-01 | 0 | 7.1259E-02 | 1 | 4.9001E-02 | 0 | 3.4779E-01 |
| 13 | 1 | 1.5627E-02 | 0 | 4.6718E-01 | 1 | 9.4288E-03 | 0 | 9.2784E-02 | 0 | 1.0127E-01 | 0 | 2.2864E-01 |
| 14 | 0 | 1.3738E-01 | 0 | 9.2707E-02 | 0 | 5.4896E-01 | 0 | 1.0298E-01 | 0 | 6.3158E-02 | 0 | 4.2253E-01 |
| 15 | 0 | 1.0499E-01 | 0 | 1.0970E-01 | 0 | 3.6551E-01 | 1 | 3.8853E-02 | 0 | 2.8463E-01 | 1 | 1.9934E-02 |
| 16 | 0 | 6.0304E-02 | 0 | 7.3620E-02 | 0 | 1.7421E-01 | 0 | 1.2791E-01 | 0 | 3.4229E-01 | 0 | 1.3249E-01 |
| 17 | 1 | 2.5632E-02 | 1 | 1.2816E-02 | 0 | 6.3664E-01 | 1 | 1.1854E-02 | 0 | 1.8161E-01 | 1 | 8.8361E-03 |
| 18 | 1 | 2.5729E-03 | 0 | 8.0682E-01 | 1 | 1.2864E-03 | 1 | 4.6108E-02 | 1 | 2.3054E-02 | 0 | 8.1106E-01 |
| 19 | 1 | 4.2142E-02 | 1 | 2.1873E-02 | 0 | 4.2224E-01 | 0 | 8.7560E-02 | 1 | 4.7020E-02 | 0 | 6.2885E-01 |
| 20 | 0 | 1.0873E-01 | 0 | 2.0399E-01 | 0 | 9.0547E-02 | 1 | 4.0944E-02 | 1 | 4.3926E-02 | 0 | 2.1267E-01 |
| 21 | 1 | 2.8819E-04 | 1 | 1.4409E-04 | 0 | 7.7231E-01 | 1 | 8.7060E-03 | 1 | 4.3530E-03 | 0 | 3.1975E-01 |
| 22 | 0 | 8.1462E-02 | 1 | 4.0884E-02 | 0 | 5.3881E-01 | 0 | 6.6512E-02 | 1 | 3.9138E-02 | 0 | 3.1403E-01 |

Table A-5: K-S test results comparing the CDF of the magnitude and the frequency of the eigenvalues during meditation to the baseline eigenvalues.

A-2 Eigenvectors

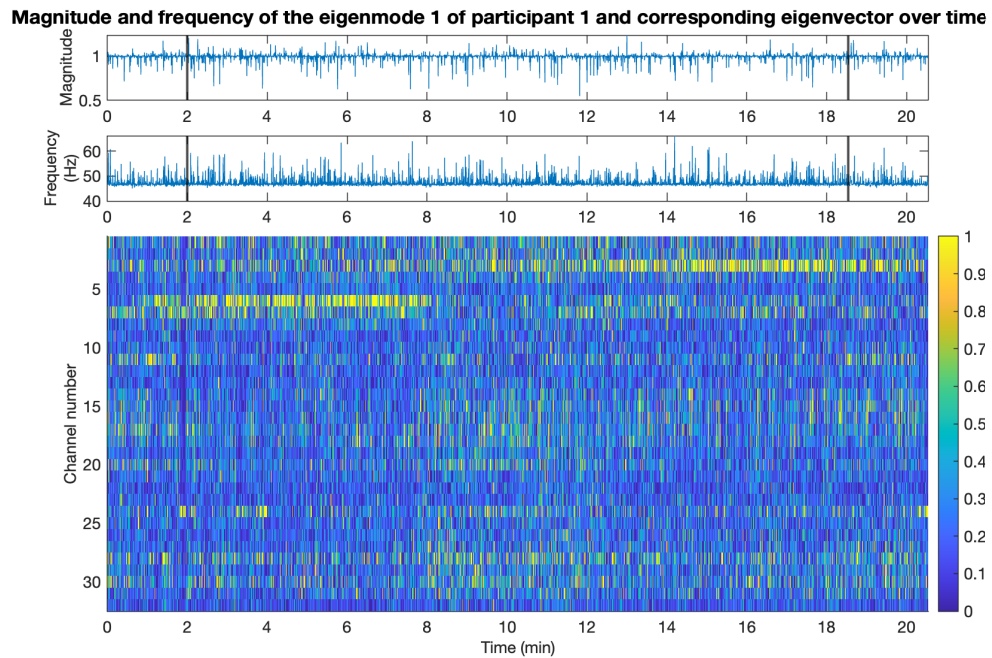


Figure A-6: Evolution of an eigenvector corresponding to a high frequency eigenvalue for participant 1.

Magnitude and frequency of the eigenmode 1 of participant 2 and corresponding eigenvector over time

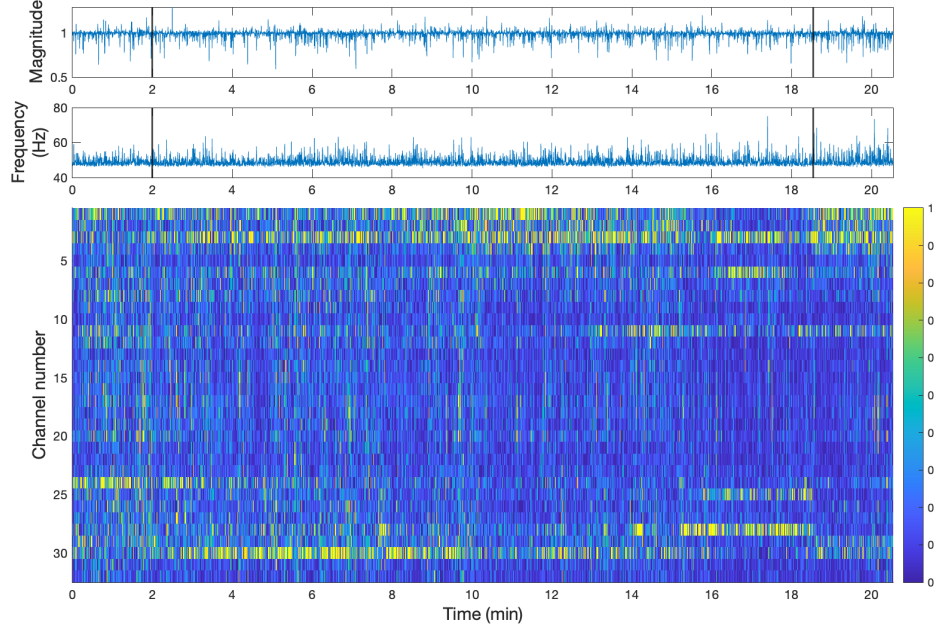


Figure A-7: Evolution of an eigenvector corresponding to a high frequency eigenvalue for participant 2.

Magnitude and frequency of the eigenmode 1 of participant 3 and corresponding eigenvector over time

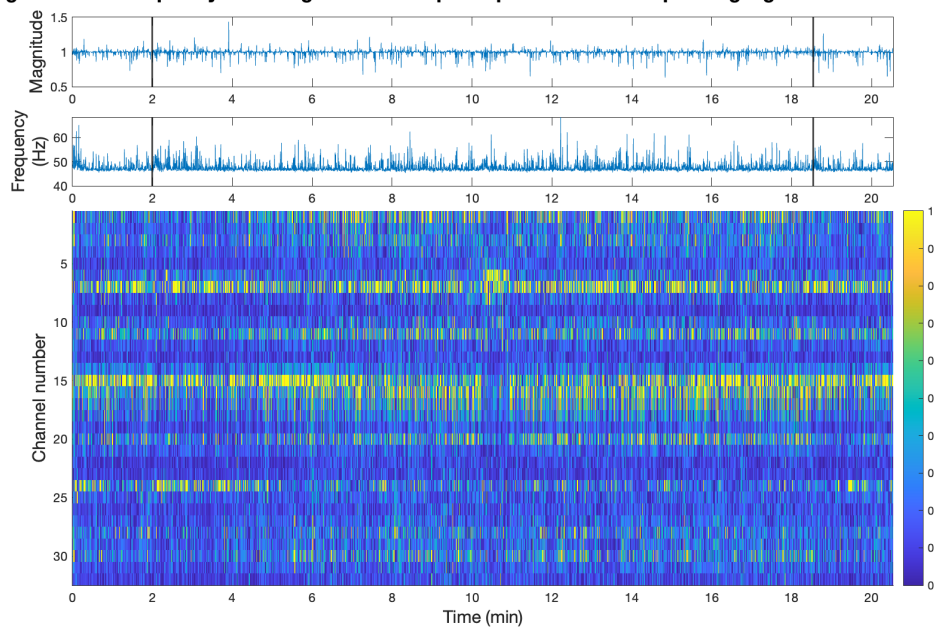
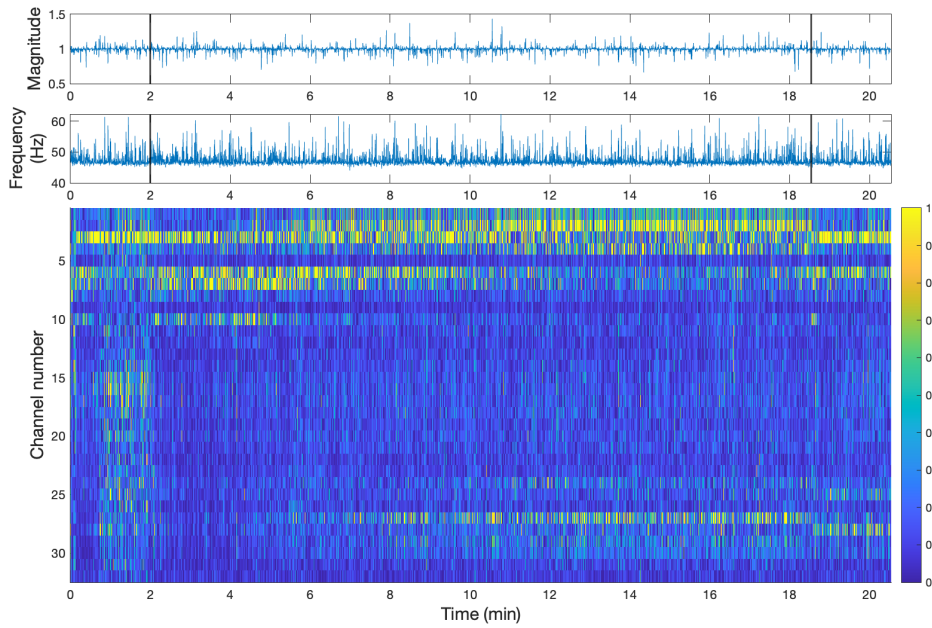
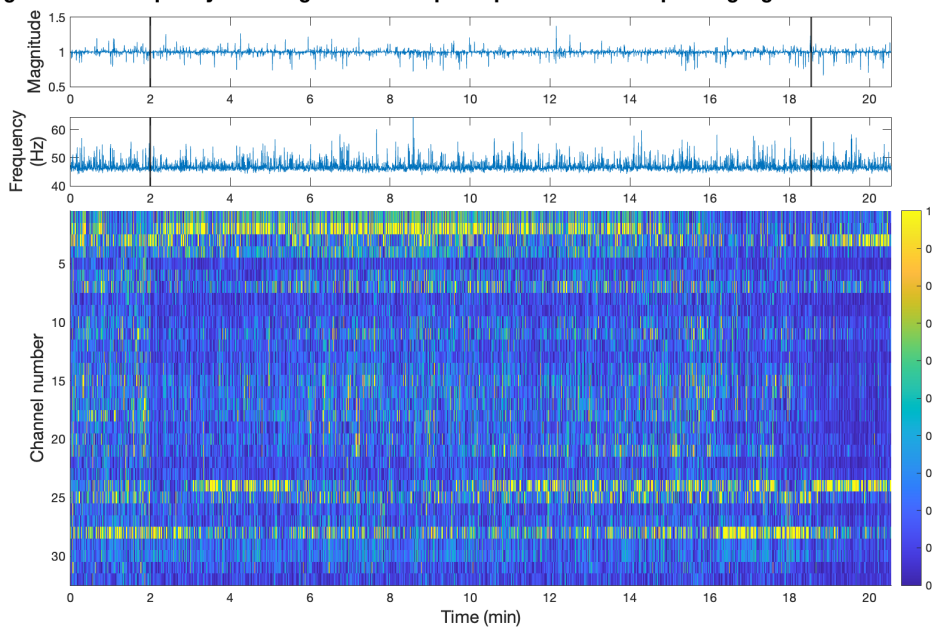
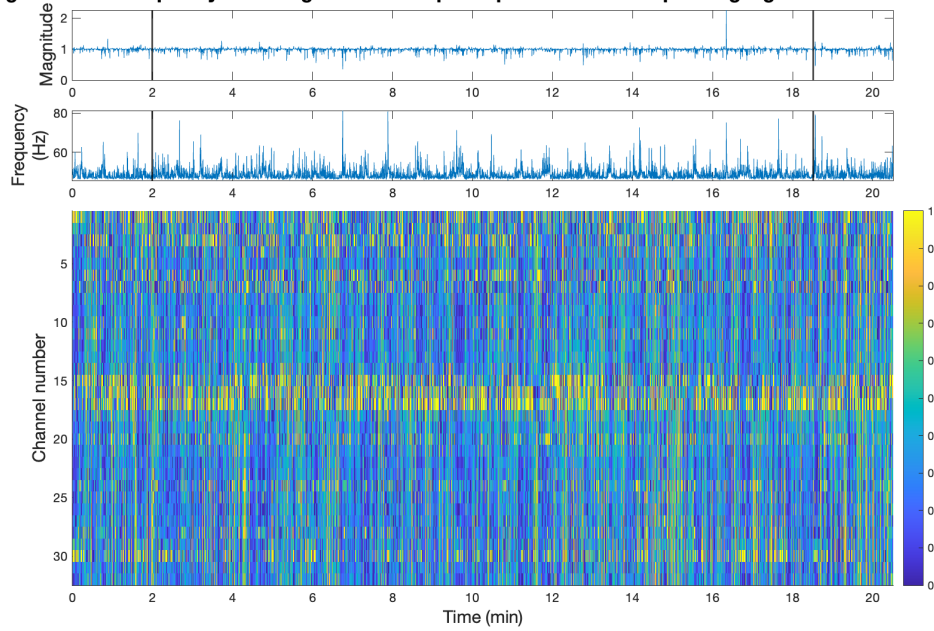
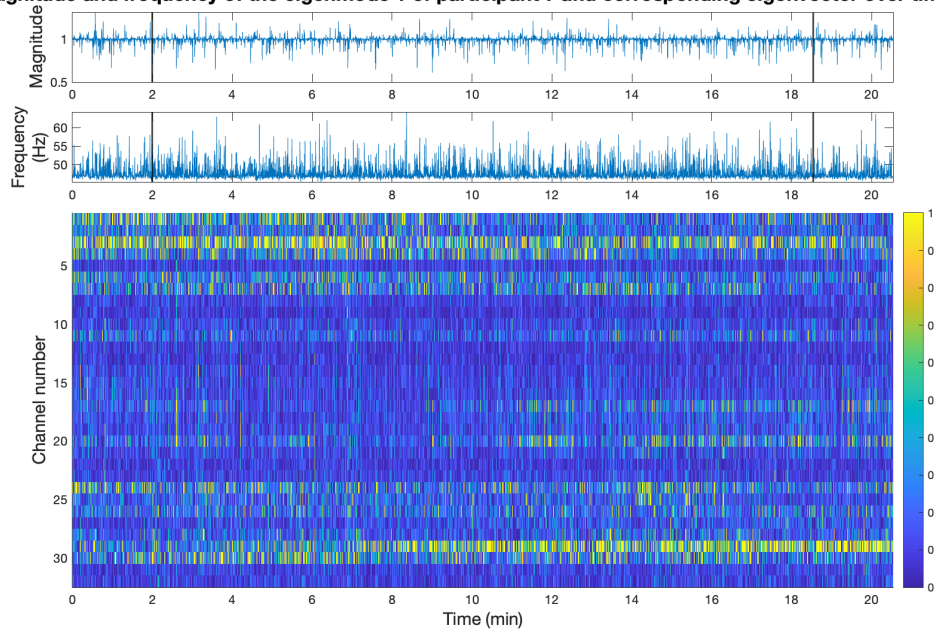
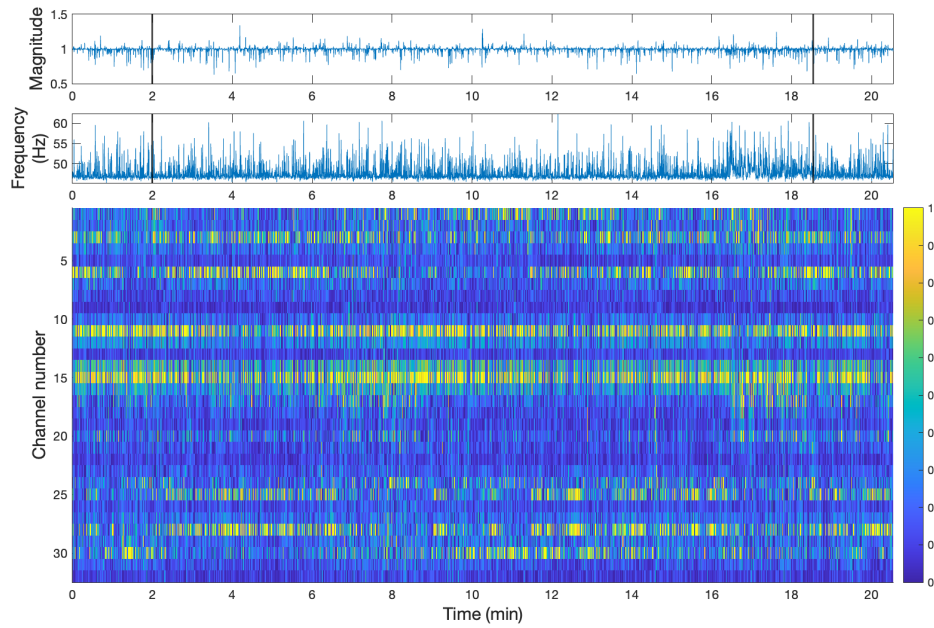
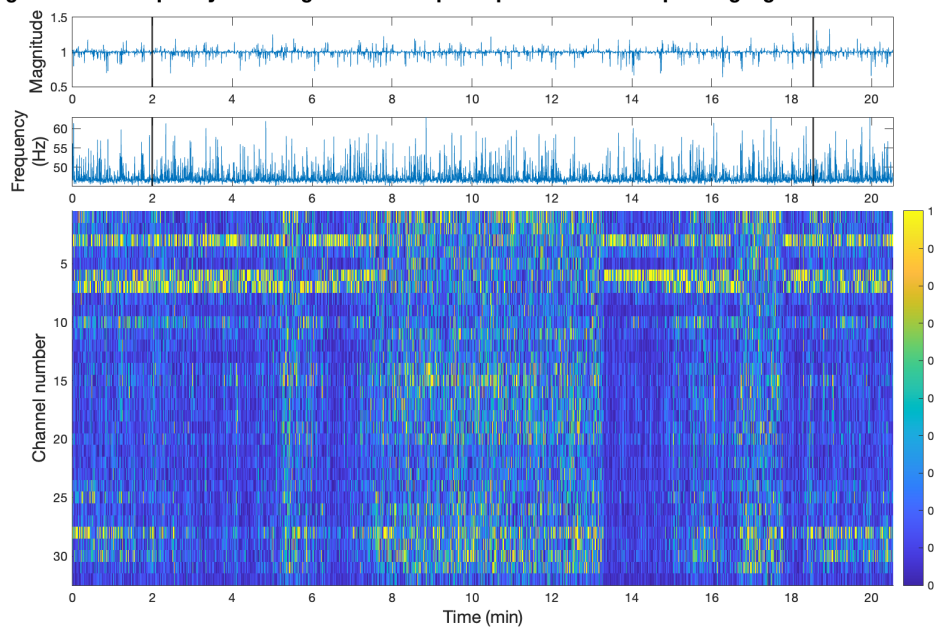
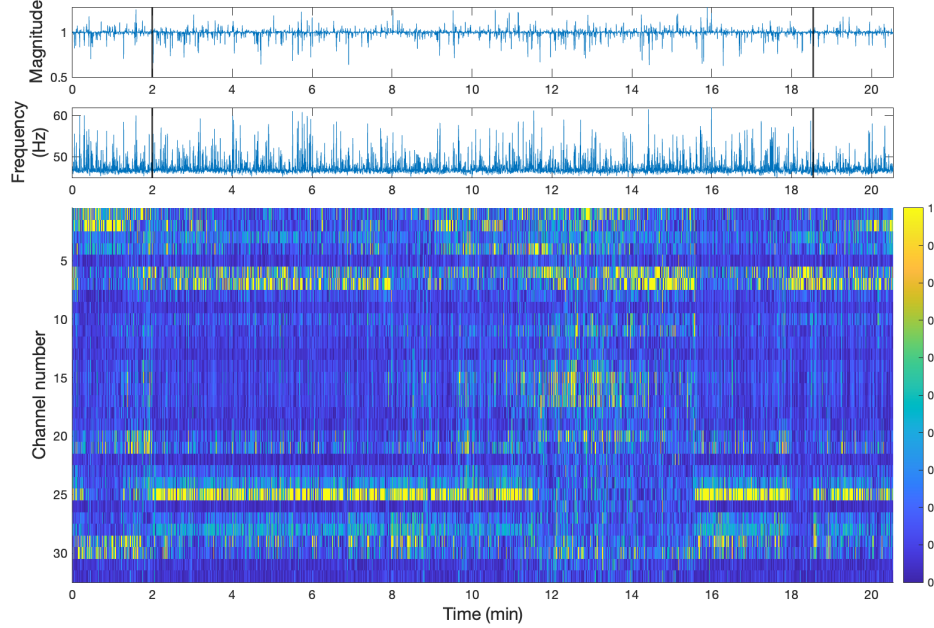
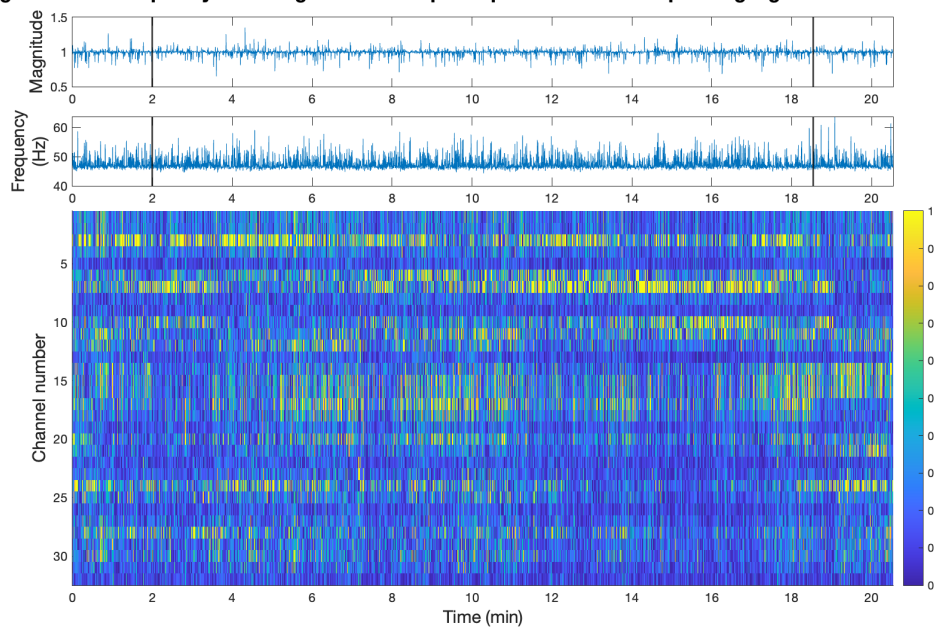


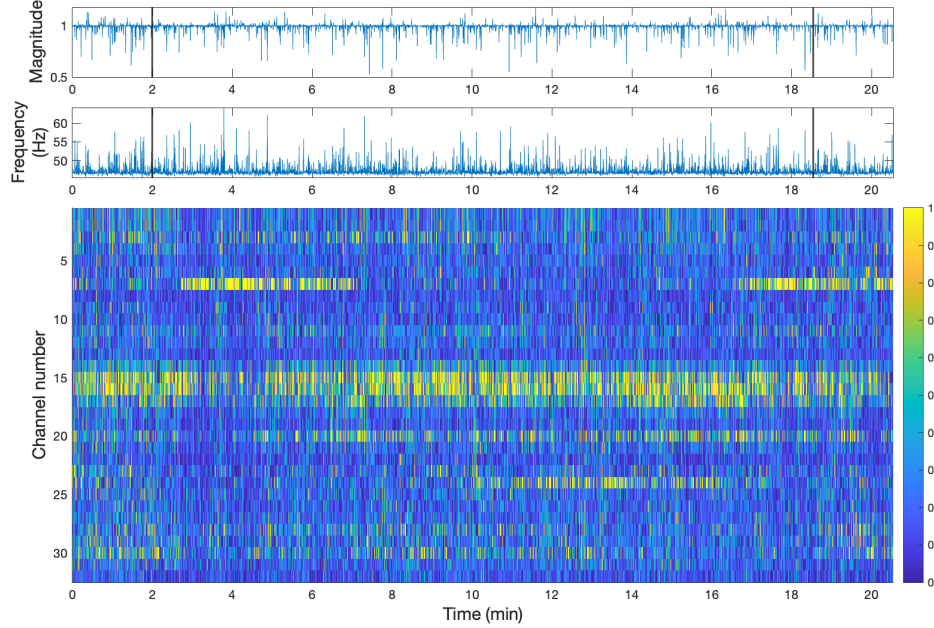
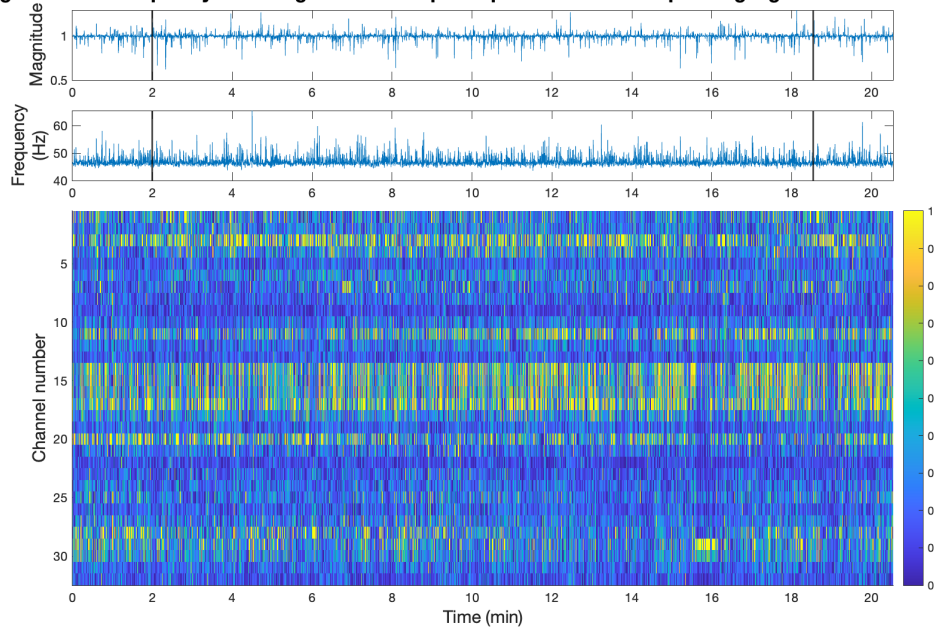
Figure A-8: Evolution of an eigenvector corresponding to a high frequency eigenvalue for participant 3.

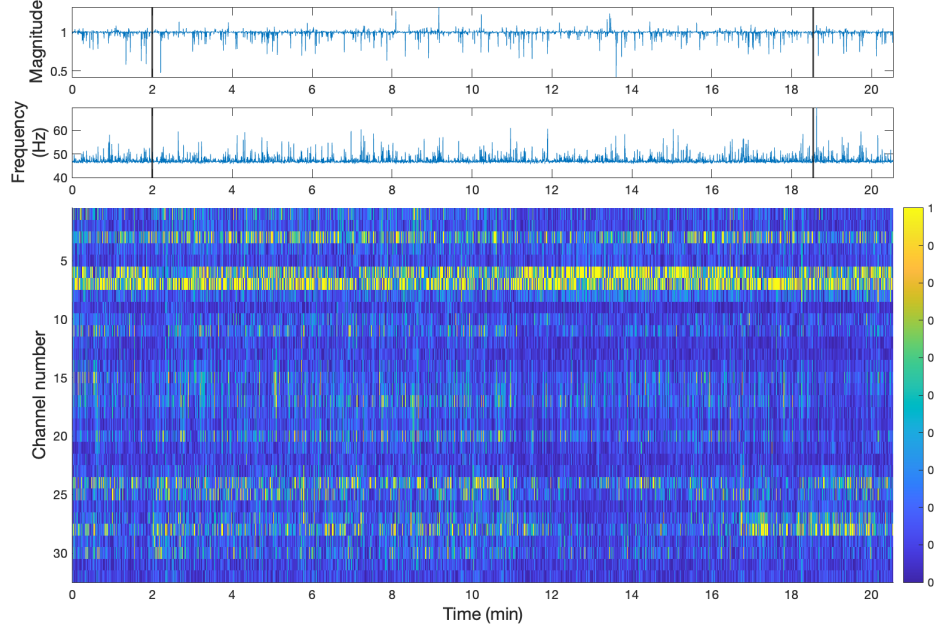
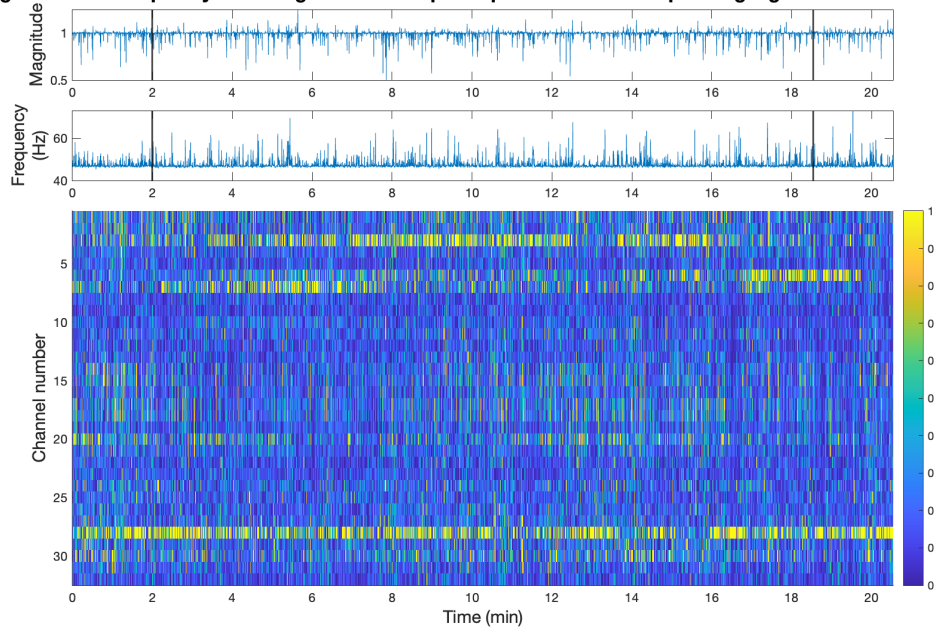
Magnitude and frequency of the eigenmode 1 of participant 4 and corresponding eigenvector over time**Figure A-9:** Evolution of an eigenvector corresponding to a high frequency eigenvalue for participant 4.**Magnitude and frequency of the eigenmode 1 of participant 5 and corresponding eigenvector over time****Figure A-10:** Evolution of an eigenvector corresponding to a high frequency eigenvalue for participant 5.

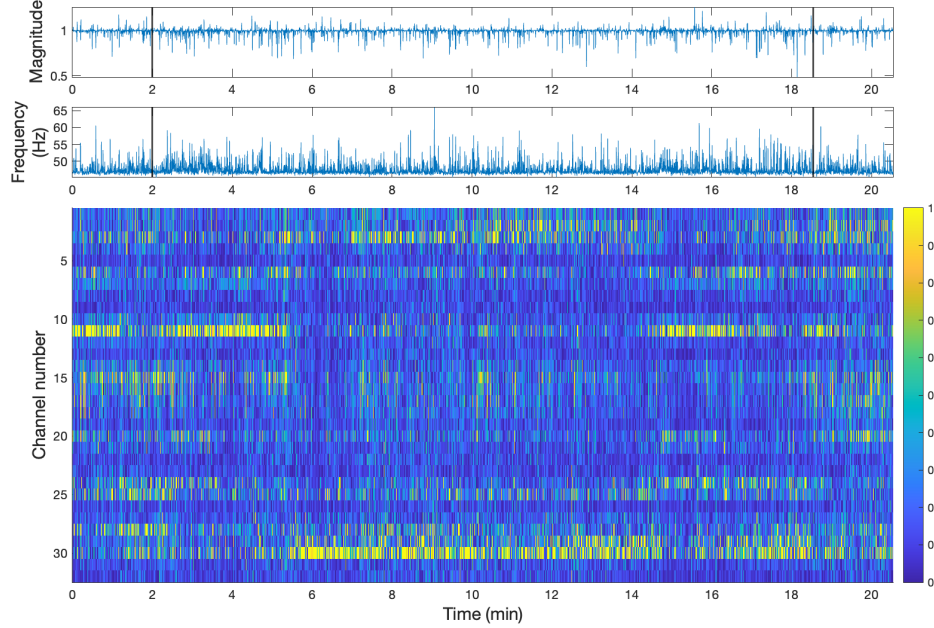
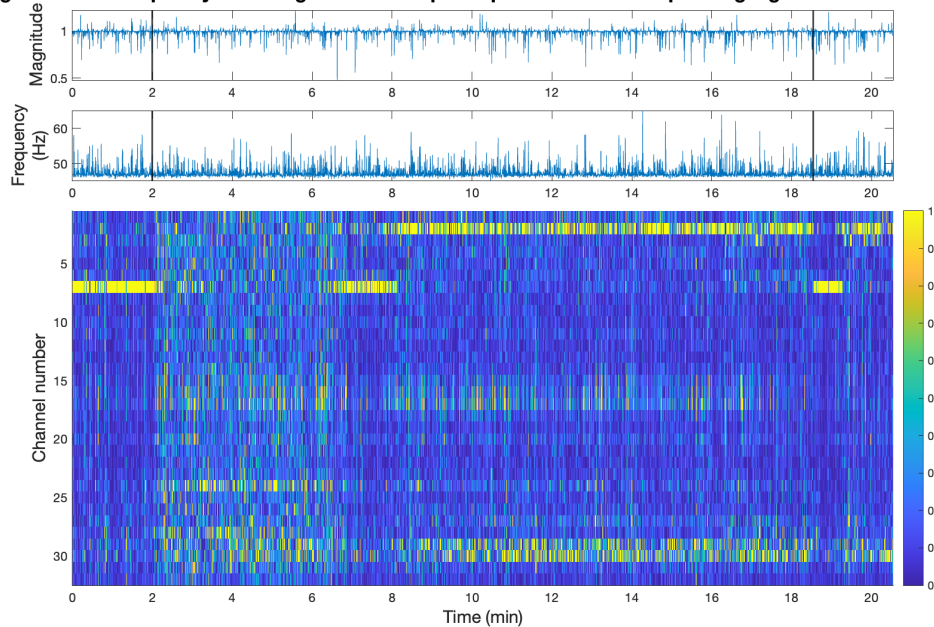
Magnitude and frequency of the eigenmode 1 of participant 6 and corresponding eigenvector over time**Figure A-11:** Evolution of an eigenvector corresponding to a high frequency eigenvalue for participant 6.**Magnitude and frequency of the eigenmode 1 of participant 7 and corresponding eigenvector over time****Figure A-12:** Evolution of an eigenvector corresponding to a high frequency eigenvalue for participant 7.

Magnitude and frequency of the eigenmode 1 of participant 8 and corresponding eigenvector over time**Figure A-13:** Evolution of an eigenvector corresponding to a high frequency eigenvalue for participant 8.**Magnitude and frequency of the eigenmode 1 of participant 9 and corresponding eigenvector over time****Figure A-14:** Evolution of an eigenvector corresponding to a high frequency eigenvalue for participant 9.

Magnitude and frequency of the eigenmode 1 of participant 10 and corresponding eigenvector over time**Figure A-15:** Evolution of an eigenvector corresponding to a high frequency eigenvalue for participant 10.**Magnitude and frequency of the eigenmode 1 of participant 11 and corresponding eigenvector over time****Figure A-16:** Evolution of an eigenvector corresponding to a high frequency eigenvalue for participant 11.

Magnitude and frequency of the eigenmode 1 of participant 12 and corresponding eigenvector over time**Figure A-17:** Evolution of an eigenvector corresponding to a high frequency eigenvalue for participant 12.**Magnitude and frequency of the eigenmode 1 of participant 13 and corresponding eigenvector over time****Figure A-18:** Evolution of an eigenvector corresponding to a high frequency eigenvalue for participant 13.

Magnitude and frequency of the eigenmode 1 of participant 14 and corresponding eigenvector over time**Figure A-19:** Evolution of an eigenvector corresponding to a high frequency eigenvalue for participant 14.**Magnitude and frequency of the eigenmode 1 of participant 15 and corresponding eigenvector over time****Figure A-20:** Evolution of an eigenvector corresponding to a high frequency eigenvalue for participant 15.

Magnitude and frequency of the eigenmode 1 of participant 16 and corresponding eigenvector over time**Figure A-21:** Evolution of an eigenvector corresponding to a high frequency eigenvalue for participant 16.**Magnitude and frequency of the eigenmode 1 of participant 17 and corresponding eigenvector over time****Figure A-22:** Evolution of an eigenvector corresponding to a high frequency eigenvalue for participant 17.

Magnitude and frequency of the eigenmode 1 of participant 18 and corresponding eigenvector over time

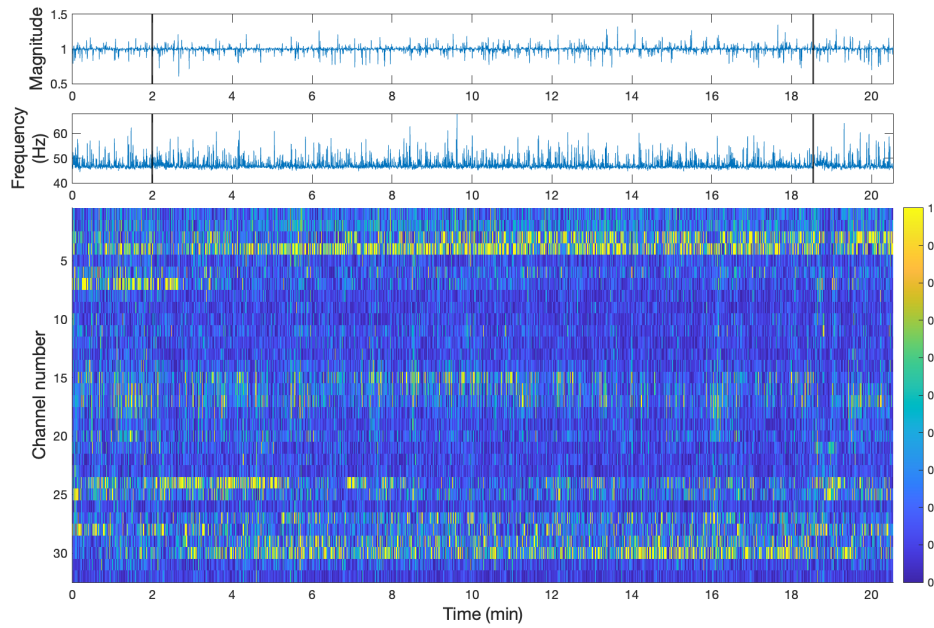


Figure A-23: Evolution of an eigenvector corresponding to a high frequency eigenvalue for participant 18.

Magnitude and frequency of the eigenmode 1 of participant 19 and corresponding eigenvector over time

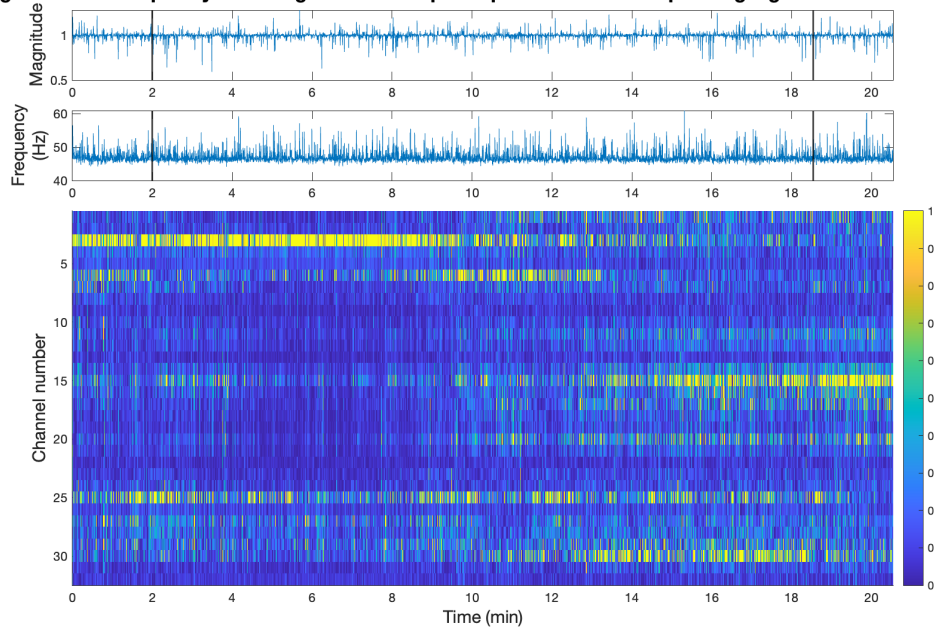
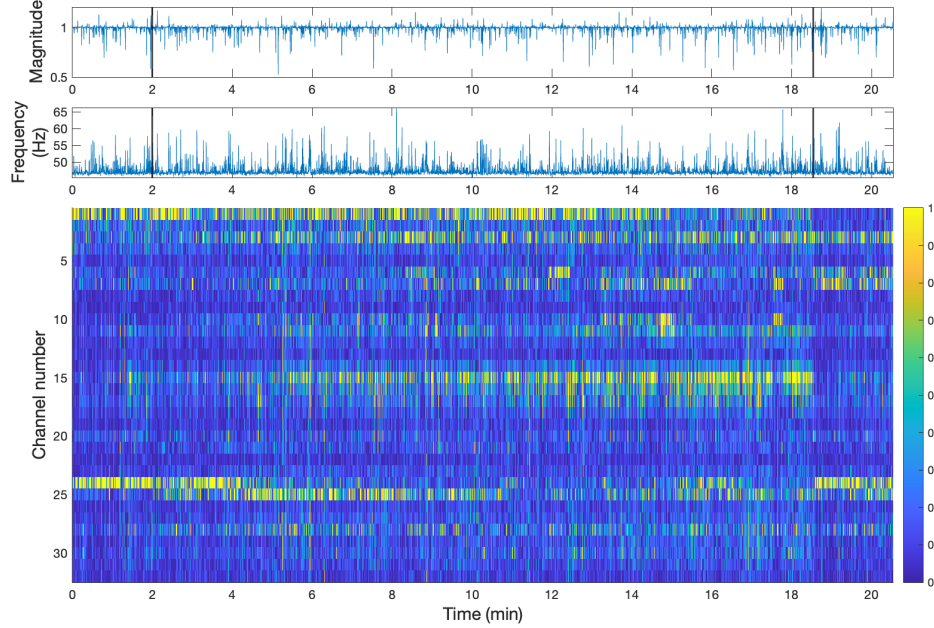
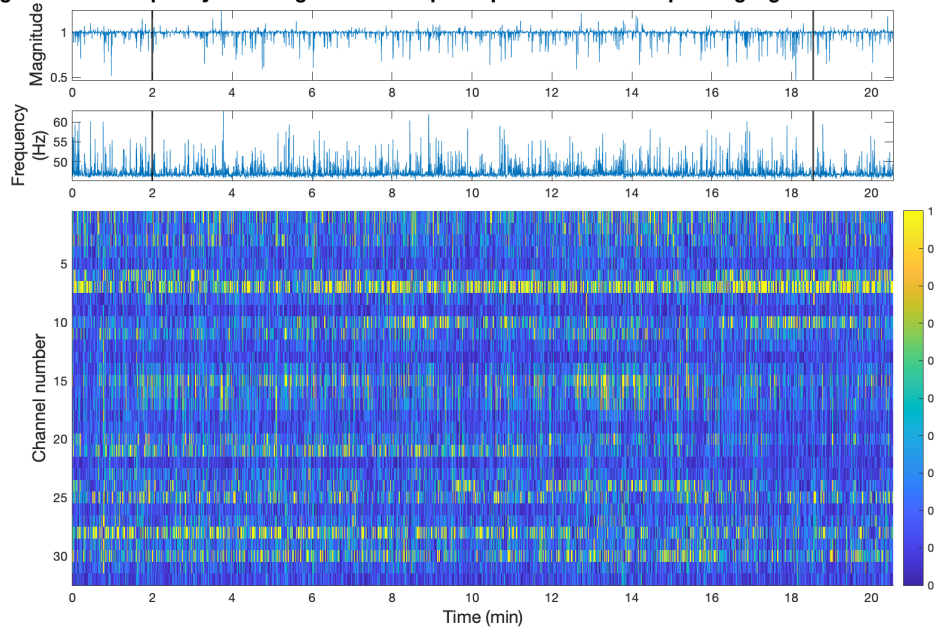


Figure A-24: Evolution of an eigenvector corresponding to a high frequency eigenvalue for participant 19.

Magnitude and frequency of the eigenmode 1 of participant 20 and corresponding eigenvector over time**Figure A-25:** Evolution of an eigenvector corresponding to a high frequency eigenvalue for participant 20.**Magnitude and frequency of the eigenmode 1 of participant 21 and corresponding eigenvector over time****Figure A-26:** Evolution of an eigenvector corresponding to a high frequency eigenvalue for participant 21.

Magnitude and frequency of the eigenmode 1 of participant 22 and corresponding eigenvector over time

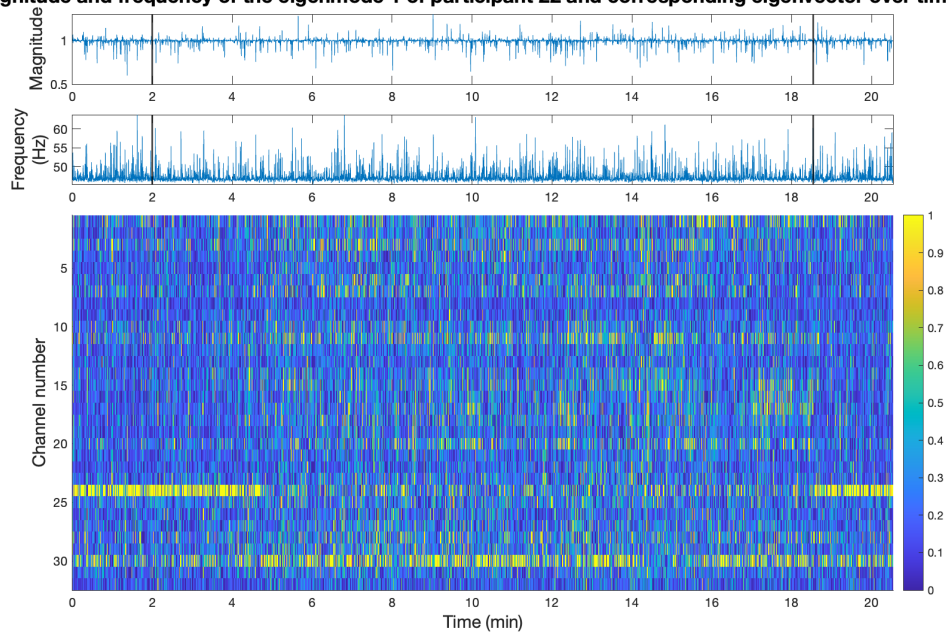


Figure A-27: Evolution of an eigenvector corresponding to a high frequency eigenvalue for participant 22.

Appendix B

Subsets of electrodes

B-1 Personalized subset

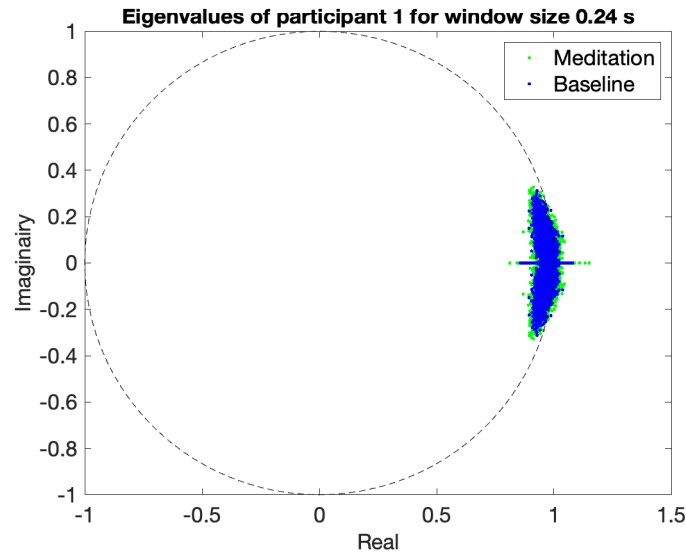


Figure B-1: Eigenvalues of participant 1 for the personal subset of electrodes plotted on the complex plane.

| | h_1 | p_1 | h_2 | p_2 | h_3 | p_3 | h_4 | p_4 | h_5 | p_5 | h_6 | p_6 |
|----|-------|------------|-------|------------|-------|------------|-------|------------|-------|------------|-------|------------|
| 1 | 1 | 1.2741E-10 | 0 | 9.6789E-01 | 1 | 6.3703E-11 | 1 | 1.0095E-04 | 1 | 5.0473E-05 | 0 | 5.8965E-01 |
| 2 | 1 | 1.7086E-21 | 1 | 8.5431E-22 | 0 | 9.9791E-01 | 1 | 1.1355E-07 | 0 | 8.7435E-01 | 1 | 5.6775E-08 |
| 3 | 1 | 5.1342E-08 | 0 | 9.8436E-01 | 1 | 2.5671E-08 | 1 | 2.9548E-06 | 1 | 1.4774E-06 | 0 | 8.6989E-01 |
| 4 | 1 | 6.7855E-59 | 1 | 3.3928E-59 | 0 | 9.9964E-01 | 1 | 4.9185E-39 | 0 | 9.9688E-01 | 1 | 2.4593E-39 |
| 5 | 1 | 3.5870E-68 | 1 | 1.7935E-68 | 0 | 9.8979E-01 | 1 | 1.4648E-05 | 0 | 3.8985E-01 | 1 | 7.3238E-06 |
| 6 | 0 | 7.7287E-02 | 0 | 6.0727E-02 | 0 | 1.6142E-01 | 1 | 1.3276E-02 | 0 | 1.9596E-01 | 1 | 8.0487E-03 |
| 7 | 1 | 1.6922E-08 | 0 | 8.5304E-01 | 1 | 8.4610E-09 | 1 | 4.1673E-05 | 1 | 2.0837E-05 | 0 | 7.4036E-01 |
| 8 | 1 | 2.4341E-22 | 1 | 1.2171E-22 | 0 | 9.9286E-01 | 1 | 1.3342E-14 | 0 | 9.1028E-01 | 1 | 6.6711E-15 |
| 9 | 1 | 3.1845E-52 | 0 | 9.9763E-01 | 1 | 1.5922E-52 | 1 | 9.4656E-23 | 1 | 4.7328E-23 | 0 | 3.9587E-01 |
| 10 | 0 | 7.5746E-02 | 0 | 5.9716E-02 | 0 | 3.0687E-01 | 1 | 1.9245E-03 | 0 | 1.1036E-01 | 1 | 9.6422E-04 |
| 11 | 1 | 7.4777E-05 | 0 | 5.8997E-01 | 1 | 3.7388E-05 | 0 | 8.2894E-02 | 0 | 9.4060E-02 | 0 | 1.5779E-01 |
| 12 | 1 | 5.6129E-03 | 1 | 1.1792E-02 | 1 | 3.8312E-02 | 1 | 1.3337E-02 | 1 | 1.9489E-02 | 1 | 2.8838E-02 |
| 13 | 1 | 3.3428E-07 | 1 | 1.6714E-07 | 0 | 8.2408E-01 | 1 | 7.4656E-03 | 0 | 7.5327E-01 | 1 | 3.7328E-03 |
| 14 | 1 | 3.6897E-02 | 1 | 1.9513E-02 | 0 | 5.6286E-01 | 0 | 1.2296E-01 | 0 | 1.3388E-01 | 0 | 1.6235E-01 |
| 15 | 1 | 1.5485E-19 | 1 | 7.7426E-20 | 0 | 9.9092E-01 | 1 | 2.5809E-09 | 0 | 8.7499E-01 | 1 | 1.2904E-09 |
| 16 | 1 | 1.7161E-03 | 0 | 8.5586E-01 | 1 | 8.5803E-04 | 1 | 9.3020E-03 | 0 | 8.1699E-01 | 1 | 4.6510E-03 |
| 17 | 1 | 5.4223E-15 | 1 | 2.7111E-15 | 0 | 9.9021E-01 | 1 | 4.2474E-04 | 0 | 1.9643E-01 | 1 | 2.1584E-04 |
| 18 | 1 | 6.9785E-07 | 1 | 3.4892E-07 | 0 | 8.7413E-01 | 1 | 2.1124E-05 | 0 | 9.1211E-01 | 1 | 1.0562E-05 |
| 19 | 1 | 1.9017E-08 | 0 | 9.2324E-01 | 1 | 9.5084E-09 | 1 | 2.5332E-05 | 1 | 1.2666E-05 | 0 | 8.6287E-01 |
| 20 | 1 | 3.4455E-07 | 1 | 1.7228E-07 | 0 | 9.9568E-01 | 1 | 1.7667E-13 | 1 | 8.8336E-14 | 0 | 7.2231E-01 |
| 21 | 0 | 1.3294E-01 | 0 | 3.7955E-01 | 0 | 9.7937E-02 | 0 | 1.0778E-01 | 0 | 7.7047E-02 | 0 | 4.5233E-01 |
| 22 | 1 | 6.3870E-05 | 0 | 7.4802E-01 | 1 | 3.1935E-05 | 0 | 6.0980E-02 | 1 | 3.0641E-02 | 0 | 6.2413E-01 |

Table B-1: KS test results for the personalized subset comparing the CDF of the magnitude and the frequency of the eigenvalues during meditation to the baseline eigenvalues.

B-2 Wearable EEG subsets

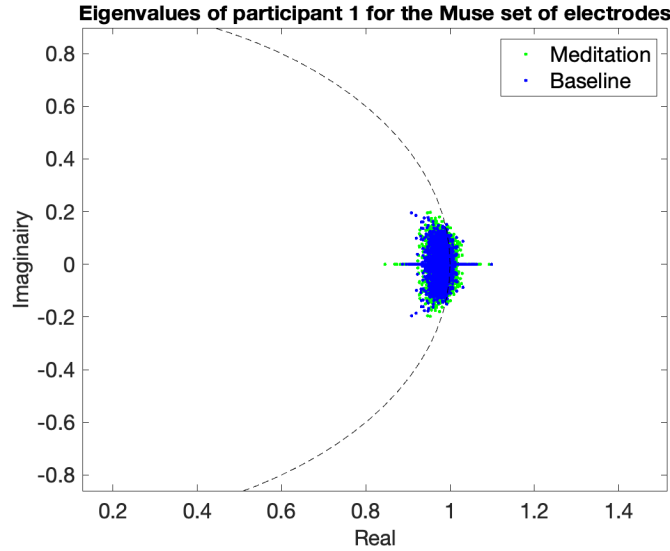


Figure B-2: Eigenvalues of participant 1 for the Muse headset plotted on the complex plane.

| | h_1 | p_1 | h_2 | p_2 | h_3 | p_3 | h_4 | p_4 | h_5 | p_5 | h_6 | p_6 |
|----|-------|------------|-------|------------|-------|------------|-------|------------|-------|------------|-------|------------|
| 1 | 1 | 2.0921E-02 | 0 | 7.0306E-02 | 0 | 7.9961E-02 | 1 | 2.4259E-02 | 0 | 5.2428E-01 | 1 | 1.3996E-02 |
| 2 | 0 | 5.5144E-02 | 0 | 1.0244E-01 | 0 | 2.3532E-01 | 1 | 3.3916E-04 | 0 | 4.4655E-01 | 1 | 1.6958E-04 |
| 3 | 1 | 3.6913E-02 | 0 | 3.4804E-01 | 1 | 3.1174E-02 | 0 | 6.5044E-02 | 0 | 2.6399E-01 | 0 | 5.0686E-02 |
| 4 | 1 | 4.4807E-03 | 0 | 5.9379E-01 | 1 | 2.2403E-03 | 0 | 9.0740E-02 | 0 | 1.3054E-01 | 0 | 1.2147E-01 |
| 5 | 0 | 1.4493E-01 | 0 | 3.0891E-01 | 0 | 1.4365E-01 | 0 | 1.2779E-01 | 0 | 2.1204E-01 | 0 | 1.1489E-01 |
| 6 | 0 | 9.3047E-02 | 0 | 8.3646E-02 | 0 | 3.0039E-01 | 0 | 1.6322E-01 | 0 | 4.8534E-01 | 0 | 9.1650E-02 |
| 7 | 1 | 3.4622E-02 | 0 | 4.1986E-01 | 1 | 2.0326E-02 | 0 | 8.0133E-02 | 0 | 4.3172E-01 | 0 | 5.0475E-02 |
| 8 | 1 | 2.6695E-02 | 0 | 6.2134E-01 | 1 | 1.3347E-02 | 1 | 4.1113E-02 | 0 | 1.8656E-01 | 1 | 4.1932E-02 |
| 9 | 1 | 1.9479E-02 | 1 | 2.6258E-02 | 0 | 5.1031E-02 | 1 | 3.6240E-02 | 1 | 1.8120E-02 | 0 | 5.4141E-01 |
| 10 | 1 | 4.3723E-03 | 0 | 1.6807E-01 | 1 | 3.5927E-03 | 0 | 1.6877E-01 | 0 | 1.0050E-01 | 0 | 4.3363E-01 |
| 11 | 0 | 6.7099E-02 | 1 | 4.2572E-02 | 0 | 4.2292E-01 | 1 | 3.6227E-03 | 1 | 1.8114E-03 | 0 | 1.8541E-01 |
| 12 | 1 | 1.4779E-02 | 0 | 5.3587E-02 | 1 | 1.6597E-02 | 0 | 1.5142E-01 | 0 | 3.8192E-01 | 0 | 1.3509E-01 |
| 13 | 1 | 2.1174E-03 | 0 | 9.1246E-01 | 1 | 1.0587E-03 | 0 | 1.2415E-01 | 0 | 3.9564E-01 | 0 | 7.1440E-02 |
| 14 | 0 | 1.4420E-01 | 0 | 1.0686E-01 | 0 | 3.9442E-01 | 1 | 3.6934E-02 | 0 | 7.3087E-02 | 0 | 7.8729E-02 |
| 15 | 1 | 7.7167E-03 | 0 | 4.5329E-01 | 1 | 4.1234E-03 | 1 | 3.6981E-02 | 0 | 7.5616E-02 | 1 | 4.8083E-02 |
| 16 | 0 | 1.0616E-01 | 0 | 1.0565E-01 | 0 | 3.0984E-01 | 0 | 8.4665E-02 | 0 | 1.6212E-01 | 0 | 1.3326E-01 |
| 17 | 0 | 5.1803E-02 | 0 | 1.0488E-01 | 0 | 6.8323E-02 | 0 | 8.0976E-02 | 1 | 4.4733E-02 | 0 | 4.7627E-01 |
| 18 | 1 | 3.1944E-02 | 0 | 1.1521E-01 | 1 | 3.1039E-02 | 0 | 1.3180E-01 | 0 | 7.1121E-02 | 0 | 4.6791E-01 |
| 19 | 0 | 8.9856E-02 | 0 | 1.8229E-01 | 0 | 1.5471E-01 | 0 | 1.1231E-01 | 0 | 1.9852E-01 | 0 | 7.2511E-02 |
| 20 | 1 | 2.8689E-02 | 1 | 1.4345E-02 | 0 | 6.8900E-01 | 1 | 7.3097E-05 | 1 | 3.6549E-05 | 0 | 4.0176E-01 |
| 21 | 0 | 8.0546E-02 | 0 | 8.5543E-02 | 0 | 1.2387E-01 | 1 | 2.6418E-02 | 1 | 2.0624E-02 | 0 | 2.0393E-01 |
| 22 | 1 | 4.3869E-02 | 0 | 2.2264E-01 | 1 | 2.3725E-02 | 1 | 4.4552E-02 | 0 | 4.5109E-01 | 1 | 2.6267E-02 |

Table B-2: KS test results for the Muse subset comparing the CDF of the magnitude and the frequency of the eigenvalues during meditation to the baseline eigenvalues.

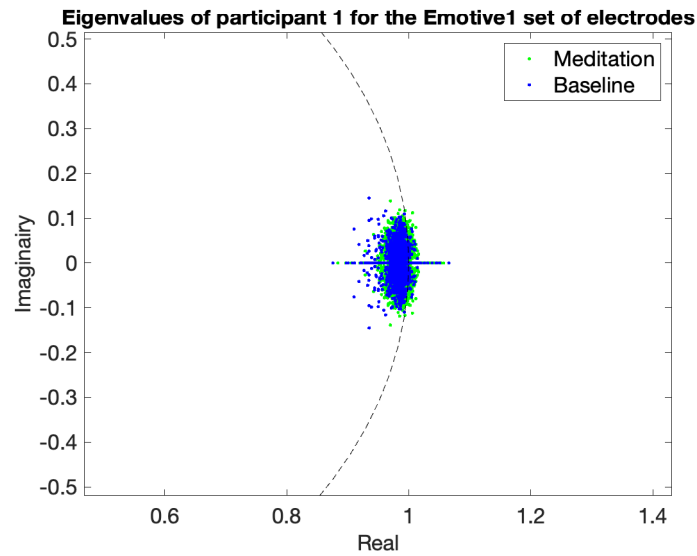


Figure B-3: Eigenvalues of participant 1 for the Emotiv 1 headset plotted on the complex plane.

| | h_1 | p_1 | h_2 | p_2 | h_3 | p_3 | h_4 | p_4 | h_5 | p_5 | h_6 | p_6 |
|----|-------|------------|-------|------------|-------|------------|-------|------------|-------|------------|-------|------------|
| 1 | 1 | 3.6499E-02 | 0 | 1.3131E-01 | 1 | 3.3719E-02 | 1 | 5.4180E-03 | 0 | 5.8037E-01 | 1 | 3.0766E-03 |
| 2 | 0 | 1.3798E-01 | 0 | 1.3526E-01 | 0 | 2.1901E-01 | 1 | 1.5293E-02 | 0 | 5.1123E-01 | 1 | 7.6465E-03 |
| 3 | 1 | 2.4064E-02 | 0 | 5.5343E-01 | 1 | 1.2415E-02 | 0 | 1.1171E-01 | 0 | 4.0434E-01 | 0 | 7.7392E-02 |
| 4 | 0 | 9.9739E-02 | 0 | 2.7487E-01 | 0 | 7.0782E-02 | 1 | 3.0068E-03 | 0 | 7.2310E-01 | 1 | 1.5034E-03 |
| 5 | 0 | 8.0071E-02 | 0 | 3.8663E-01 | 1 | 4.5671E-02 | 0 | 9.0972E-02 | 0 | 8.9020E-02 | 0 | 2.4051E-01 |
| 6 | 1 | 3.5844E-02 | 1 | 2.0923E-02 | 0 | 4.0613E-01 | 1 | 4.6012E-02 | 0 | 6.8375E-01 | 1 | 2.3472E-02 |
| 7 | 0 | 2.1085E-01 | 0 | 3.8506E-01 | 0 | 1.6381E-01 | 0 | 2.9065E-01 | 0 | 2.1789E-01 | 0 | 4.0075E-01 |
| 8 | 0 | 5.1879E-02 | 0 | 2.0687E-01 | 1 | 3.8681E-02 | 0 | 2.9181E-01 | 0 | 4.4761E-01 | 0 | 1.7142E-01 |
| 9 | 1 | 3.8350E-02 | 0 | 2.4782E-01 | 1 | 2.9440E-02 | 1 | 2.0120E-02 | 1 | 1.0060E-02 | 0 | 6.2247E-01 |
| 10 | 1 | 6.3330E-03 | 0 | 3.1562E-01 | 1 | 3.4808E-03 | 0 | 5.9528E-02 | 0 | 2.1397E-01 | 1 | 3.7161E-02 |
| 11 | 0 | 1.1268E-01 | 0 | 2.2307E-01 | 0 | 1.1993E-01 | 1 | 9.3948E-03 | 1 | 4.6974E-03 | 0 | 4.5082E-01 |
| 12 | 1 | 4.3509E-02 | 0 | 4.0241E-01 | 1 | 2.1755E-02 | 1 | 4.9228E-02 | 0 | 7.3658E-02 | 0 | 9.6625E-02 |
| 13 | 1 | 3.5492E-05 | 0 | 8.9877E-01 | 1 | 1.7746E-05 | 0 | 1.2530E-01 | 0 | 4.1951E-01 | 0 | 8.1266E-02 |
| 14 | 0 | 1.5418E-01 | 0 | 8.8275E-02 | 0 | 3.2641E-01 | 0 | 1.0593E-01 | 0 | 8.7071E-02 | 0 | 3.2949E-01 |
| 15 | 1 | 5.6198E-03 | 0 | 3.8382E-01 | 1 | 2.8099E-03 | 1 | 4.9435E-04 | 0 | 5.4323E-01 | 1 | 2.4717E-04 |
| 16 | 0 | 1.0349E-01 | 0 | 6.0679E-02 | 0 | 4.7552E-01 | 0 | 1.1586E-01 | 0 | 4.3371E-01 | 0 | 9.7984E-02 |
| 17 | 0 | 9.9869E-02 | 0 | 5.6581E-02 | 0 | 4.3531E-01 | 0 | 1.1700E-01 | 0 | 6.8921E-02 | 0 | 3.9504E-01 |
| 18 | 0 | 5.6107E-02 | 1 | 3.6704E-02 | 0 | 5.6979E-01 | 1 | 4.4663E-02 | 0 | 3.8879E-01 | 1 | 2.2332E-02 |
| 19 | 0 | 1.4105E-01 | 0 | 2.8642E-01 | 0 | 9.8918E-02 | 0 | 1.2801E-01 | 0 | 2.9450E-01 | 0 | 1.7494E-01 |
| 20 | 0 | 1.4147E-01 | 0 | 8.6426E-02 | 0 | 4.4190E-01 | 1 | 2.3838E-04 | 1 | 1.1919E-04 | 0 | 1.4667E-01 |
| 21 | 0 | 5.6996E-02 | 0 | 2.7568E-01 | 1 | 3.8788E-02 | 0 | 1.6119E-01 | 0 | 4.2696E-01 | 0 | 1.1853E-01 |
| 22 | 1 | 2.3604E-02 | 0 | 2.8723E-01 | 1 | 1.3558E-02 | 0 | 7.9952E-02 | 0 | 2.2396E-01 | 0 | 1.1604E-01 |

Table B-3: KS test results for the Emotiv 1 subset comparing the CDF of the magnitude and the frequency of the eigenvalues during meditation to the baseline eigenvalues.

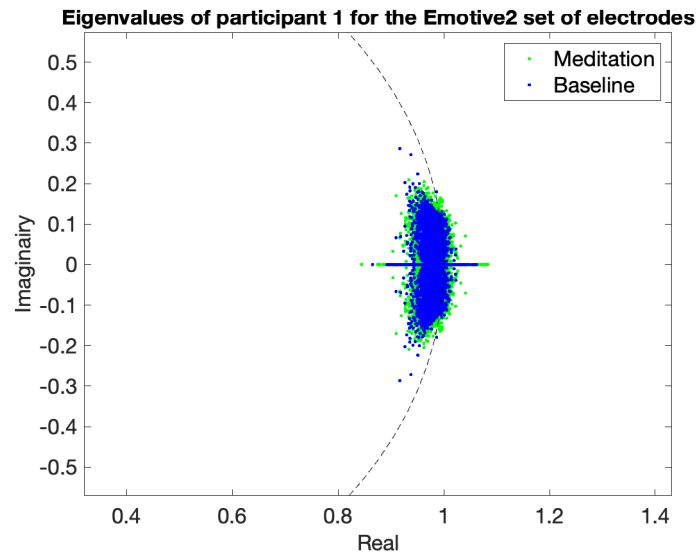


Figure B-4: Eigenvalues of participant 1 for the Emotiv 2 headset plotted on the complex plane.

| | h_1 | p_1 | h_2 | p_2 | h_3 | p_3 | h_4 | p_4 | h_5 | p_5 | h_6 | p_6 |
|----|-------|------------|-------|------------|-------|------------|-------|------------|-------|------------|-------|------------|
| 1 | 0 | 6.4238E-02 | 0 | 6.7511E-02 | 0 | 1.2097E-01 | 0 | 6.4663E-02 | 0 | 4.6008E-01 | 1 | 3.5015E-02 |
| 2 | 0 | 8.5873E-02 | 0 | 1.6349E-01 | 0 | 1.6320E-01 | 1 | 5.8372E-03 | 0 | 3.9556E-01 | 1 | 2.9186E-03 |
| 3 | 0 | 5.2831E-02 | 0 | 2.0463E-01 | 1 | 4.7027E-02 | 0 | 1.0713E-01 | 0 | 1.7531E-01 | 0 | 1.4216E-01 |
| 4 | 1 | 5.7895E-03 | 0 | 6.4200E-01 | 1 | 2.8947E-03 | 0 | 9.1733E-02 | 0 | 2.1938E-01 | 0 | 1.2068E-01 |
| 5 | 0 | 1.1051E-01 | 0 | 1.7998E-01 | 0 | 1.9426E-01 | 0 | 1.5172E-01 | 0 | 1.0563E-01 | 0 | 3.2537E-01 |
| 6 | 0 | 1.3452E-01 | 0 | 8.7073E-02 | 0 | 4.4165E-01 | 0 | 6.7542E-02 | 0 | 7.1490E-01 | 1 | 3.4208E-02 |
| 7 | 1 | 1.3859E-02 | 0 | 5.6613E-01 | 1 | 6.9294E-03 | 0 | 1.3545E-01 | 0 | 3.8396E-01 | 0 | 1.0200E-01 |
| 8 | 1 | 4.3968E-02 | 0 | 7.5560E-01 | 1 | 2.1984E-02 | 1 | 3.9398E-02 | 0 | 1.3607E-01 | 0 | 6.7290E-02 |
| 9 | 1 | 2.2551E-02 | 1 | 2.6140E-02 | 0 | 7.1319E-02 | 1 | 9.7616E-03 | 1 | 4.8808E-03 | 0 | 7.2948E-01 |
| 10 | 1 | 2.2354E-02 | 0 | 6.3964E-02 | 1 | 1.8371E-02 | 0 | 7.1382E-02 | 1 | 3.8445E-02 | 0 | 5.5734E-01 |
| 11 | 0 | 1.3233E-01 | 0 | 7.9152E-02 | 0 | 4.6395E-01 | 1 | 4.6951E-02 | 1 | 4.2772E-02 | 0 | 1.5250E-01 |
| 12 | 1 | 9.3571E-03 | 1 | 3.7580E-02 | 1 | 1.7968E-02 | 0 | 1.8654E-01 | 0 | 3.6866E-01 | 0 | 1.7624E-01 |
| 13 | 1 | 1.6095E-03 | 0 | 9.5095E-01 | 1 | 8.0477E-04 | 0 | 1.2952E-01 | 0 | 2.8771E-01 | 0 | 8.4007E-02 |
| 14 | 0 | 1.1189E-01 | 0 | 5.8614E-02 | 0 | 5.3645E-01 | 0 | 6.3134E-02 | 0 | 7.9354E-02 | 0 | 1.3410E-01 |
| 15 | 1 | 2.6833E-02 | 0 | 3.6621E-01 | 1 | 1.7361E-02 | 1 | 4.1566E-02 | 0 | 8.0406E-02 | 1 | 4.1187E-02 |
| 16 | 0 | 8.0855E-02 | 1 | 4.6946E-02 | 0 | 4.3471E-01 | 0 | 9.6381E-02 | 0 | 2.2485E-01 | 0 | 1.0523E-01 |
| 17 | 0 | 6.4095E-02 | 0 | 1.6481E-01 | 0 | 6.3807E-02 | 0 | 2.1275E-01 | 0 | 2.7480E-01 | 0 | 2.6946E-01 |
| 18 | 0 | 6.3108E-02 | 0 | 1.9735E-01 | 0 | 6.7149E-02 | 0 | 9.1310E-02 | 0 | 5.0634E-02 | 0 | 3.6325E-01 |
| 19 | 0 | 1.0399E-01 | 0 | 1.8688E-01 | 0 | 1.3420E-01 | 1 | 1.7447E-02 | 0 | 1.9652E-01 | 1 | 1.0388E-02 |
| 20 | 1 | 3.8130E-02 | 1 | 1.9065E-02 | 0 | 5.9293E-01 | 1 | 1.6342E-04 | 1 | 8.1709E-05 | 0 | 4.5304E-01 |
| 21 | 0 | 9.7692E-02 | 0 | 9.6984E-02 | 0 | 1.9198E-01 | 1 | 1.9260E-02 | 1 | 1.0129E-02 | 0 | 2.8164E-01 |
| 22 | 1 | 2.6385E-02 | 0 | 3.4416E-01 | 1 | 1.7162E-02 | 0 | 8.7953E-02 | 0 | 4.6623E-01 | 0 | 5.2815E-02 |

Table B-4: KS test results for the Emotiv 2 subset comparing the CDF of the magnitude and the frequency of the eigenvalues during meditation to the baseline eigenvalues.

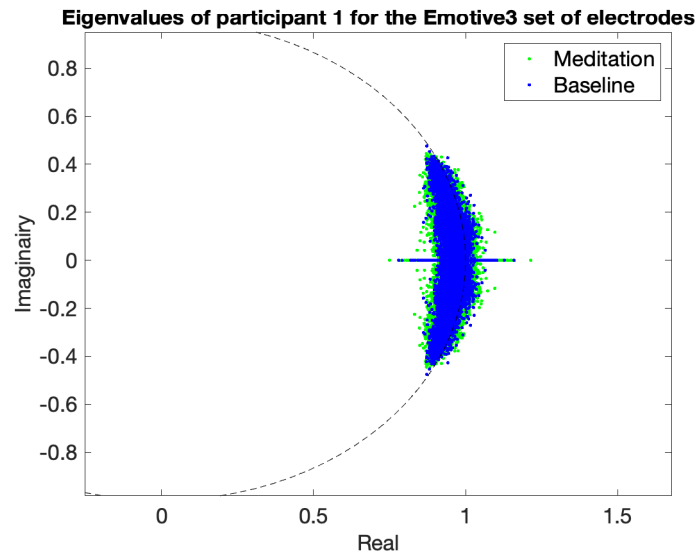


Figure B-5: Eigenvalues of participant 1 for the Emotiv 3 headset plotted on the complex plane.

| | h_1 | p_1 | h_2 | p_2 | h_3 | p_3 | h_4 | p_4 | h_5 | p_5 | h_6 | p_6 |
|----|-------|------------|-------|------------|-------|------------|-------|------------|-------|------------|-------|------------|
| 1 | 0 | 7.0265E-02 | 0 | 5.8088E-02 | 0 | 1.0634E-01 | 0 | 1.0373E-01 | 0 | 1.1173E-01 | 0 | 2.7953E-01 |
| 2 | 1 | 1.9222E-02 | 1 | 4.6163E-02 | 0 | 5.4484E-02 | 0 | 1.3659E-01 | 0 | 1.5039E-01 | 0 | 1.1701E-01 |
| 3 | 1 | 6.4849E-03 | 1 | 3.2425E-03 | 0 | 4.0725E-01 | 0 | 9.3901E-02 | 0 | 1.0534E-01 | 0 | 2.6804E-01 |
| 4 | 0 | 1.1407E-01 | 0 | 2.4824E-01 | 0 | 9.8168E-02 | 0 | 7.0127E-02 | 0 | 3.2098E-01 | 1 | 4.6639E-02 |
| 5 | 0 | 9.8186E-02 | 0 | 1.3913E-01 | 0 | 2.1660E-01 | 0 | 1.9865E-01 | 0 | 1.9935E-01 | 0 | 2.8924E-01 |
| 6 | 0 | 8.5264E-02 | 0 | 6.8012E-02 | 0 | 2.6635E-01 | 0 | 9.6066E-02 | 0 | 4.7620E-01 | 0 | 5.8402E-02 |
| 7 | 1 | 1.2653E-02 | 0 | 5.9192E-01 | 1 | 7.0219E-03 | 0 | 2.4814E-01 | 0 | 3.9257E-01 | 0 | 1.7208E-01 |
| 8 | 1 | 3.4204E-02 | 0 | 6.3869E-01 | 1 | 1.7102E-02 | 0 | 1.1051E-01 | 0 | 3.2051E-01 | 0 | 9.2040E-02 |
| 9 | 1 | 1.3783E-02 | 0 | 1.6915E-01 | 1 | 1.0848E-02 | 1 | 2.4765E-02 | 1 | 1.2382E-02 | 0 | 3.1235E-01 |
| 10 | 0 | 1.3791E-01 | 0 | 2.9010E-01 | 0 | 1.2390E-01 | 1 | 2.3439E-02 | 1 | 1.9118E-02 | 0 | 2.1407E-01 |
| 11 | 0 | 7.1454E-02 | 1 | 3.5728E-02 | 0 | 5.8499E-01 | 0 | 1.9983E-01 | 0 | 2.0268E-01 | 0 | 2.8620E-01 |
| 12 | 1 | 3.8501E-05 | 1 | 1.9250E-05 | 0 | 2.9463E-01 | 0 | 1.2475E-01 | 0 | 6.2389E-02 | 0 | 4.7595E-01 |
| 13 | 0 | 5.2506E-02 | 0 | 2.5803E-01 | 1 | 3.4525E-02 | 1 | 3.4560E-02 | 0 | 5.5045E-01 | 1 | 1.7807E-02 |
| 14 | 1 | 7.5630E-03 | 1 | 3.7815E-03 | 0 | 3.2927E-01 | 0 | 1.0068E-01 | 0 | 8.5980E-02 | 0 | 4.5351E-01 |
| 15 | 0 | 1.4340E-01 | 0 | 1.4041E-01 | 0 | 2.0786E-01 | 0 | 5.7266E-02 | 0 | 3.6118E-01 | 1 | 3.8720E-02 |
| 16 | 1 | 3.5296E-02 | 1 | 4.0790E-02 | 0 | 1.5239E-01 | 1 | 2.5108E-02 | 0 | 8.2795E-01 | 1 | 1.2554E-02 |
| 17 | 1 | 5.6685E-03 | 0 | 5.4049E-01 | 1 | 2.8343E-03 | 0 | 1.9938E-01 | 0 | 2.2827E-01 | 0 | 2.4770E-01 |
| 18 | 0 | 5.4593E-02 | 0 | 3.5665E-01 | 1 | 4.5214E-02 | 0 | 7.2938E-02 | 0 | 1.7955E-01 | 1 | 4.6054E-02 |
| 19 | 0 | 2.1317E-01 | 0 | 1.7144E-01 | 0 | 3.2487E-01 | 1 | 1.2291E-02 | 0 | 1.7164E-01 | 1 | 6.2281E-03 |
| 20 | 1 | 3.7022E-02 | 1 | 2.1691E-02 | 0 | 4.6003E-01 | 1 | 2.5685E-02 | 1 | 1.5184E-02 | 0 | 2.3801E-01 |
| 21 | 1 | 1.6744E-03 | 1 | 8.3720E-04 | 0 | 5.7919E-01 | 0 | 1.8749E-01 | 0 | 5.7236E-01 | 0 | 1.3339E-01 |
| 22 | 1 | 3.1589E-02 | 0 | 1.7206E-01 | 1 | 2.1625E-02 | 0 | 1.8220E-01 | 0 | 3.4142E-01 | 0 | 1.4354E-01 |

Table B-5: KS test results for the Emotiv 3 subset comparing the CDF of the magnitude and the frequency of the eigenvalues during meditation to the baseline eigenvalues.

Bibliography

- [1] A. Lutz, H. A. Slagter, J. D. Dunne, and R. J. Davidson, “Attention regulation and monitoring in meditation,” *Trends in Cognitive Sciences*, vol. 12, pp. 163–169, April 2008.
- [2] K. B. Bærentsen, H. Stødkilde-Jørgensen, B. Sommerlund, T. Hartmann, J. Damsgaard-Madsen, M. Fosnaes, and A. C. Green, “An investigation of brain processes supporting meditation,” *Cognitive Processing*, vol. 11, pp. 57–84, February 2010.
- [3] N. T. van Dam, M. K. van Vugt, D. R. Vago, L. Schmalzl, C. D. Saron, A. Olendzki, T. Meissner, S. W. Lazar, C. E. Kerr, J. Gorchov, K. C. Fox, B. A. Field, W. B. Britton, J. A. Brefczynski-Lewis, and D. E. Meyer, “Mind the hype: A critical evaluation and prescriptive agenda for research on mindfulness and meditation,” *Perspectives on Psychological Science*, vol. 13, pp. 36–61, January 2018.
- [4] D. Y. Kim, S. H. Hong, S. H. Jang, S. H. Park, J. H. Noh, J. M. Seok, H. J. Jo, C. G. Son, and E. J. Lee, “Systematic review for the medical applications of meditation in randomized controlled trials,” *International Journal of Environmental Research and Public Health*, vol. 19, February 2022.
- [5] P. Grossman, L. Niemann, S. Schmidt, and H. Walach, “Mindfulness-based stress reduction and health benefits: A meta-analysis,” *Journal of Psychosomatic Research*, vol. 57, pp. 35–43, July 2004.
- [6] B. R. Cahn and J. Polich, “Meditation states and traits: EEG, ERP, and neuroimaging studies,” *Psychological Bulletin*, vol. 132, pp. 180–211, March 2006.
- [7] L. Hu and Z. Zhang, *EEG Signal Processing and Feature Extraction*. Springer, 2019.
- [8] Muse, InteraXon Inc., “Muse, the brain sensing headband.” Retrieved on December 1st 2022 from <https://choosemuse.com>.
- [9] C. S. Deolindo, M. W. Ribeiro, M. A. Aratanha, R. F. Afonso, M. Irrmischer, and E. H. Kozasa, “A critical analysis on characterizing the meditation experience through the electroencephalogram,” *Frontiers in Systems Neuroscience*, vol. 14, August 2020.

- [10] T. Lomas, I. Ivtzan, and C. H. Fu, “A systematic review of the neurophysiology of mindfulness on EEG oscillations,” *Neuroscience and Biobehavioral Reviews*, vol. 57, pp. 401–410, October 2015.
- [11] D. J. Lee, E. Kulubya, P. Goldin, A. Goodarzi, and F. Girgis, “Review of the neural oscillations underlying meditation,” *Frontiers in Neuroscience*, vol. 12, March 2018.
- [12] B. R. Dunn, J. A. Hartigan, and W. L. Mikulas, “Concentration and mindfulness meditations: Unique forms of consciousness?,” *Applied Psychophysiology and Biofeedback*, vol. 24, September 1999.
- [13] J. H. Medicine, “Brain anatomy and how the brain works.” Retrieved on December 1st 2022 from <https://www.hopkinsmedicine.org/health/conditions-and-diseases/anatomy-of-the-brain>.
- [14] K. C. Fox, M. L. Dixon, S. Nijeboer, M. Girn, J. L. Floman, M. Lifshitz, M. Ellamil, P. Sedlmeier, and K. Christoff, “Functional neuroanatomy of meditation: A review and meta-analysis of 78 functional neuroimaging investigations,” *Neuroscience and Biobehavioral Reviews*, vol. 65, pp. 208–228, June 2016.
- [15] G. Solovey, L. M. Alonso, T. Yanagawa, N. Fujii, M. O. Magnasco, G. A. Cecchi, and A. Proekt, “Loss of consciousness is associated with stabilization of cortical activity,” *Journal of Neuroscience*, vol. 35, pp. 10866–10877, July 2015.
- [16] A. Ashourvan, S. Pequito, A. N. Khambhati, S. N. Baldassano, K. A. Davis, T. Lucas, J. M. Vettel, B. Litt, G. J. Pappas, and D. S. Bassett, “Parsing spatiotemporal dynamical stability in ECoG during seizure onset, propagation, and termination,” *Society for Neuroscience*, November 2017.
- [17] K. Xie, S. Zhang, S. Dong, S. Li, C. Yu, K. Xu, W. Chen, W. Guo, J. Luo, and Z. Wu, “Portable wireless electrocorticography system with a flexible microelectrodes array for epilepsy treatment,” *Scientific Reports*, vol. 7, December 2017.
- [18] H. Aurlien, I. O. Gjerde, J. H. Aarseth, G. Eldøen, B. Karlsen, H. Skeidsvoll, and N. E. Gilhus, “EEG background activity described by a large computerized database,” *Clinical Neurophysiology*, vol. 115, pp. 665–673, March 2004.
- [19] C. Rye, R. Wise, V. Jurukovski, J. DeSaix, J. Choi, and Y. Avissar, “Biology: How neurons communicate.” Retrieved on June 20th 2022 from <https://openstax.org/books/biology/pages/35-2-how-neurons-communicate>.
- [20] M. Verhaegen and V. Verdult, *Filtering and System Identification: A Least Squares Approach*. Cambridge University Press, 2007.
- [21] P. D. Welch, “The use of Fast Fourier Transform for the estimation of power spectra: A method based on time averaging over short, modified periodograms,” *IEEE Transactions on Audio and Electroacoustics*, vol. 15, pp. 70–73, June 1967.
- [22] H. K. Khalil, *Nonlinear Control, Global Edition*. Pearson, 2015.
- [23] A. M. Brouwer and M. A. Hogervorst, “A new paradigm to induce mental stress: The Sing-a-Song Stress Test (SSST),” *Frontiers in Neuroscience*, vol. 8, July 2014.

-
- [24] T. Brach, “Guided meditation loving this life, happiness metta practise.” Retrieved on December 1st 2022 from <https://www.tarabrach.com/guided-meditation-loving-this-life-happiness-metta-practice/>.
- [25] M. M. Bradley and P. J. Lang, “Measuring emotion: the Self-Assessment Manikin and the Semantic Differential,” *Journal of behavior therapy and experimental psychiatry*, vol. 25, pp. 49–59, March 1994.
- [26] BioSemi. B.V., “BioSemi.” Retrieved on June 20th 2022 from <https://www.biosemi.com>.
- [27] A. Delorme and S. Makeig, “EEGLAB: An open source toolbox for analysis of single-trial EEG dynamics including independent component analysis,” *Journal of Neuroscience Methods*, vol. 134, pp. 9–21, March 2004.
- [28] M. Klug and K. Gramann, “Identifying key factors for improving ICA-based decomposition of EEG data in mobile and stationary experiments,” *European Journal of Neuroscience*, vol. 54, pp. 8406–8420, December 2021.
- [29] C. Kothe, M. Makoto, and A. Delorme, “Clean Rawdata version 2.7.” Retrieved on December 7th 2022 from https://github.com/sccn/clean_rawdata.
- [30] A. Hyvärinen and E. Oja, “Independent component analysis: algorithms and applications,” *Neural networks*, vol. 13, pp. 411–430, March 2000.
- [31] L. Pion-Tonachini, K. Kreutz-Delgado, and S. Makeig, “ICLabel: An automated electroencephalographic independent component classifier, dataset, and website,” *NeuroImage*, vol. 198, pp. 181–197, September 2019.
- [32] A. Neumaier and T. Schneider, “Estimation of parameters and eigenmodes of multivariate autoregressive models,” *CM Transactions on Mathematical Software*, vol. 27, pp. 27–58, March 2001.
- [33] H. Bonakdari and M. Zeynoddin, *Stochastic Modeling, Chapter 2: Preparation & stationarizing*. Elsevier, 2022.
- [34] G. W. Corder, *Nonparametric Statistics : A Step-By-Step Approach*. John Wiley & Sons, Incorporated., 2014.
- [35] F. J. Massey, “The Kolmogorov-Smirnov test for goodness of fit,” *Source: Journal of the American Statistical Association*, vol. 46, pp. 68–78, March 1951.
- [36] B. Kolb and I. Q. Whishaw, *Fundamentals of human neuropsychology*. Worth Publishers, 7th ed., 2015.
- [37] M. Agarwal and R. Sivakumar, “Cerebro: A wearable solution to detect and track user preferences using brainwaves,” *WearSys 19: The 5th ACM Workshop on Wearable Systems and Applications*, pp. 47–52, June 2019.
- [38] Emotiv, “Emotiv.” Retrieved on December 7th 2022 from <https://www.emotiv.com>.

Glossary

List of Acronyms

| | |
|------------------|---|
| ADF test | <i>Augmented Dickey-Fuller test</i> |
| AR | <i>autoregressive</i> |
| CDF | <i>cumulative distribution function</i> |
| DFT | <i>Discrete Fourier Transform</i> |
| DTFT | <i>Discrete-Time Fourier Transform</i> |
| ECoG | <i>electrocochleography</i> |
| EEG | <i>electroencephalogram</i> |
| fMRI | <i>functional magnetic resonance imaging</i> |
| KPSS test | <i>Kwiatkowski-Phillips-Schmidt-Shin test</i> |
| KS test | <i>Kolmogorov-Smirnov test</i> |
| PET | <i>positron emission tomography</i> |
| SAM | <i>Self-Assessment Manikin</i> |